Reports of the Department of Geodetic Science

Report No. 218

DIRECT RECOVERY OF MEAN GRAVITY ANOMALIES FROM SATELLITE TO SATELLITE TRACKING

by

D. P. Hajela

Prepared for

National Aeronautics and Space Administration
Goddard Space Flight Center
Greenbelt, Maryland 20770

Grant No. NGR 36-008-161
OSURF Project No. 3210

The Ohio State University
Research Foundation
Columbus, Ohio 43212

December, 1974

Reports of the Department of Geodetic Science

Report No. 218

Direct Recovery of Mean Gravity Anomalies From Satellite to Satellite Tracking

by

D. P. Hajela

Prepared for

National Aeronautics and Space Administration
Goddard Space Flight Center
Greenbelt, Maryland 20770

Grant No. NGR 36-008-161
OSURF Project No. 3210

The Ohio State University
Research Foundation
Columbus, Ohio 43212

December, 1974

FOREWORD

This report was prepared by Dr. D. P. Hajela, Research Associate, Department of Geodetic Science, The Ohio State University, under NASA Grant NGR 36-008-161, The Ohio State University Research Foundation Project No. 3210. The contract covering this research is administered through the Goddard Space Flight Center, Greenbelt, Maryland, Mr. James Marsh, Technical Officer.

This report has been slightly condensed from a dissertation presented to the Graduate School of The Ohio State University in partial fulfillment of the requirements for the Ph. D. degree.

ACKNOWLEDGEMENTS

I am grateful to my Adviser, Professor Richard H. Rapp for suggesting this study and for his guidance and support throughout this work. His continued interest ensured timely clarifications and a steady progress of work. I also thank Professor Rapp for the opportunity of associating me with some of his research projects, which helped to prepare me for this study.

I thank the Faculty of the Department of Geodetic Science of The Ohio State University, particularly Professor Urho A. Uotila and Professor Ivan I. Mueller, for the education I have received here. My thanks are also due to the Department of the Survey of India for permitting me leave to undertake these studies.

I wish to acknowledge the availability in this study of the Geodyn program prepared by Mr. T.V. Martin and his colleagues at the Wolf Research and Development Corporation. The credit for incorporating the gravity anomalies as parameters in this program largely goes to Mr. Pentti A. Karki, and I wish to acknowledge this contribution. I also recognize the earlier studies (1970) by Dr. C.R. Schwarz on the Gravity Field Refinement by Satellite to Satellite Doppler Tracking. I am also grateful to Professor W. M. Kaula for kindly supplying the computer programs used in his Error Analysis of Earth Physics Satellite Systems.

Extensive computer support was provided for this study by the Instruction and Research Computer Center of The Ohio State University. The get-up of this report has been greatly improved by the careful typing of Miss Janet I. Wancho. She painstakingly rearranged the material for a better presentation.

Finally, I am deeply indebted to my family for their understanding and fortitude.

ABSTRACT

This study investigates the direct recovery of mean gravity anomalies from summed range rate ($\dot{R}_s$) observations, the signal path being ground station to a geosynchronous relay satellite to a close satellite significantly perturbed by the short wave features of the earth's gravitational field. To ensure realistic observations, these were simulated with the nominal orbital elements for the relay satellite corresponding to ATS-6, and for two different close satellites one at about 250 km height, and the other at about 900 km height corresponding to the nominal values for Geos-C. The earth's gravitational field was represented by a reference set of potential coefficients up to degree and order 12, considered as known values, and by residual gravity anomalies obtained by subtracting the anomalies, implied by the potential coefficients, from their terrestrial estimates. The Geodyn orbit generation and parameter estimation program was used after modifying it to accept gravity anomalies as parameters. The standard deviation (std. devn.) of $\dot{R}_s$ observations was assumed as 0.08 cm/sec. based on an integration interval of 10 seconds.

The recovery of mean gravity anomalies over 10° and 5° equal area blocks from $\dot{R}_s$ observations to close satellites at heights of about 900 and 250 km respectively were classified as recovery from strong signal. The recovery of 5° and $2^\circ.5$ equal area mean anomalies using the same close satellites were classified as recovery from weak signal. The anomaly recovery was considered over local or regional areas. The satellite state vectors could not be recovered from short individual arcs of 4 to 20 minutes duration, and were held fixed in this study to a-priori known values.

It was found that gravity anomalies could be recovered from strong signal without using any a-priori terrestrial information, i.e. considering their initial values as zero and also assigning them a zero weight matrix. However, while recovering them from weak signal, it was necessary to use the a-priori estimate of the std. devn. of the anomalies to form their a-priori diagonal weight matrix. Without this a-priori information, the solutions from weak signal were unstable and not meaningful.

The optimum density of observations was achieved by considering ascending and descending satellite arcs with spacing between adjacent arcs roughly half the size of anomaly block being recovered. If the observations along an arc were more closely spaced than the spacing between adjacent arcs, the std. devn. of the recovered anomalies was required to be multiplied by a scaling factor.

The density of observations should be nearly uniform over the area. If the orbital inclination of the close satellite is about 45°, the area of investigation needs to be located in the form of a rhombus with its diagonals in the

east-west and the north-south directions. A latitudinal extent up to 40° is advisable, and the area should lie either in the mid-latitudes or the equatorial region. The observations should not extend beyond the limits of the area of investigation, and one anomaly block all around the area should be included in the estimation process. These latter anomalies not covered by observations cannot be recovered but these ensure the optimum recovery of the gravity anomalies inside the area of investigation. For small mean anomaly blocks like $2^{\circ}.5$, anomalies in two blocks all around the area need to be included in the estimation process.

The criteria for examining the 'goodness' of anomaly recovery have been described. The std. devn. of recovered anomalies from strong signal was found to be about 2 mgals for 10° and about 6 mgals for 5° equal area mean anomalies. These results have been compared with those obtained by Schwarz in 1970.

TABLE OF CONTENTS

LIST OF TABLES

LIST OF FIGURES

LIST OF NOTATIONS

		First Used in Equation
a_e	Semi-major axis of reference ellipsoid	(2.20)
a, $(\bar{a})$	Semi-major axis of satellite orbit, (optimized value)	(1.2) (2.53)
a	Subscript for adjusted value	(2.37)
a	Subscript for arc parameters	(2.43)
$\overline{a_{nm}}$, a_{nm}	Fully normalized and conventional coefficients in the spherical harmonic expansion of gravity anomaly, (residual gravity anomaly)	(3.10)
$(\overline{a_{nm}}')$		(2.50)
A	Partial derivatives matrix	(2.1)
A	Area of anomaly block	(3.2)
α	Azimuth	(2.29)
$\overline{b_{nm}}$, b_{nm}	Fully normalized and conventional coefficients in the spherical harmonic expansion of gravity anomaly, (residual gravity anomaly)	(3.10)
$(\overline{b_{nm}}')$		(2.50)
B	Partial derivatives matrix	(2.39)
β	Unknown parameters	(2.10)
$C(\psi)$	Covariance function of gravity anomalies	(3.15)
$C'(\psi)$	Covariance function of residual gravity anomalies	(3.19)
C	Covariance matrix of residual gravity anomalies	(3.13)
c_n	Degree variances of gravity anomalies	(3.15)
$\overline{C_{nm}}$, C_{nm}	Fully normalized and conventional coefficients in the spherical harmonic expansion of earth's gravitational potential	(2.20)
$\overline{C}_{n,o}^{*}$	Fully normalized coefficients, after subtraction of $C_{2,o}$, $C_{4,o}$ for the reference ellipsoid	(3.3)
$\overline{C_{nm}}'$	Fully normalized coefficients developed from residual gravity anomalies	(2.50)
d	Subscript for downward, down-link	(2.3)
D	Diagonal matrix of (std. devn.)^2 of residual gravity anomalies	(3.13)
Δg, (Δg_T)	Gravity anomalies, (terrestrial gravity anomalies)	(2.22)
Δg_0	Average value of gravity anomaly over the earth	(3.3)
$\Delta g'$	Residual gravity anomalies	(2.21)
$\Delta g'_s$, $\Delta g'_T$	Recovered and expected value of residual gravity anomalies	(4.1)

Δg^*	Predicted value of residual gravity anomaly	(3.13)
Δg_{pc}	Gravity anomaly implied by potential coefficients	(2.22)
e	First eccentricity of satellite orbit	(1.2)
f	Flattening of reference ellipsoid	(3.7)
F, G	Functions	(2.37), (2.38)
γ, γ_e	Average value of gravity over earth sphere, equatorial value of gravity	(2.50) (3.7)
i	Inclination of satellite orbit	(1.2)
I	Identity matrix	(4.2)
$(\ )^{-1}$	Inverse of matrix in parentheses	(2.1)
k	Subscript for gravity anomaly parameters	(2.43)
K	Lagrange multipliers	(2.40)
kM	Gravitational constant times earth's mass	(2.20)
L	Vector of misclosures	(2.1)
L_F, L_X	Vector of observations	(2.37)
λ	Geodetic longitude	(2.20)
m	Order of harmonic coefficients	(2.20)
M	Mean anomaly of satellite	(2.54)
n	Mean motion of satellite	(2.53)
n	Degree of harmonic coefficients	(2.20)
N_{max}	Maximum degree	(2.20)
N	Normals matrix	(2.1)
ω	Rotational velocity of earth	(3.6)
ω	Argument of perigee of satellite orbit	(2.51)
Ω	Right ascension of the ascending node of satellite orbit	(2.52)
P	Weight matrix	(2.1)
$\overline{P_{nm}}$, P_{nm}	Associated Legendre functions; fully normalized, conventional	(2.20)
φ	Geodetic latitude	(2.51)
φ'	Geocentric latitude	(2.20)
r	Geocentric radius vector (magnitude)	(2.20)
$\vec{R}$	Geocentric radius vector	(2.4)
R	Radius of earth sphere	(2.21)
R_s	Summed range	(2.3)
$\dot{R}_s$	Summed range rate	(2.8)
ρ	Correlation coefficient	(4.1)

s	Size of anomaly block	(2.52)
S, $S(\psi)$	Stokes' function	(2.24)
$S(r, \psi)$	Extended Stokes' function	(2.21)
$\overline{S_{nm}}$, S_{nm}	Fully normalized and conventional coefficients in the spherical harmonic expansion of earth's gravitational potential	(2.20)
$\overline{S_{nm}}'$	Fully normalized coefficients developed from residual gravity anomalies	(2.50)
ψ	Spherical distance	(2.21)
σ	Earth's surface	(2.21)
σ, σ^2, σ_0^2	Standard deviation, variance; variance of unit weight	Sec. 2.2.2
$\sum$	Summation	(2.20)
Σ	Variance-covariance matrix	(2.43)
t	Time	(2.4)
T	Earth's anomalous potential	(2.19)
$'$	Superscript for transpose of matrix	(2.1)
θ	Greenwich siderial time	(2.52)
u	Subscript for upward, up-link	(2.3)
U	Earth's normal potential	(2.19)
U	Constant vector in normal equations	(2.1)
V	Earth's gravitational potential	(2.19)
V	Correction vector, residual vector	(2.39)
W	Vector of misclosures	(2.39)
X	Solution vector	(2.1)
X_i, $\dot{X}_i$, $\ddot{X}_i$	Inertial position and velocity coordinates, acceleration components	(2.10) (2.19)
X, Y, Z	Inertial position coordinates	(1.1)
$\dot{X}, \dot{Y}, \dot{Z}$	Inertial velocity coordinates	(1.1)

LIST OF ABBREVIATIONS

Anom.	Anomaly
Anom. Discrep.	Anomaly Discrepancy
Approx.	Approximately
Appx.	Appendix
cm	centimeter
col.	Column
Correln. coeff.	Correlation coefficient
E.	East
e.g.	exempli gratia, for instance
hr.	hour
ibid.	ibidem, in the same place
i.e.	id est, that is
Inter-se	Among, or between, themselves
km	kilometer
m	meter
max.	maximum
min.	minimum
min.	minute
N.	North
NE	north-east
NW	north-west
No.	number
Obsns.	Observations
P.C.	Potential Coefficients
pts.	points
p., pp.	page, pages
rad	radians
R.M.S.	Root Mean Square
S.	South
SE	south-east
SW	south-west
Sat	Satellite
sec	seconds
Sec.	Section
Soln.	Solution
Std. Devn.	Standard Deviation(s)

vs.	versus
viz.	videlicet, namely
Vol.	Volume
W.	West
w/o	without
YYMMDD	Year, Month, Day

1. INTRODUCTION

The concept of a geostationary satellite tracking a close satellite, significantly perturbed by the short wave features of the earth's gravitational field, was discussed at the Williamstown concerence (Kaula, 1969). The measurement of the range rate of the close satellite from the geostationary satellite, relayed to a ground tracking station, would then permit the evaluation of those short wave features of the earth's gravitational field, whose effect is discernible at the altitude of the close satellite. Schwarz (1970) considered the short wave features of the earth's gravitational field represented by a surface density layer residual to spherical harmonic potential coefficients field up to degree 12. He studied the size of blocks $2^\circ \times 2^\circ$ and $5^\circ \times 5^\circ$ on the earth's surface, over which the density of surface layer was assumed constant, which could be resolved in local areas from satellite to satellite range rate measurements. Kaula (1972) considered these measurements for determining the local variations in the earth's gravitational field in terms of point masses over various sized blocks, $2^\circ.5 \times 2^\circ.5$, $5^\circ \times 5^\circ$ and $10^\circ \times 10^\circ$, residual to spherical harmonic potential coefficients field up to degree 12.

Several global solutions for the short wave features of the earth's gravitational field have also been made using other types of satellite data. Koch and Morrison (1970) determined 48 surface density values in $30^\circ \times 30^\circ$ blocks, residual to potential coefficients field up to degree 4 using optical satellite observations. Koch and Witte (1971) extended this determination to 104, $20^\circ \times 20^\circ$ surface density elements, using range rate measurements from ground stations to satellites. Arnold (1972) describes the solution of 52 gravity anomalies in 20° blocks in selected areas using optical satellite observations. Obenson (1970) proposed a method for the recovery of 184 gravity anomalies in 15° blocks from opitcal satellite data. Rapp (1971a) described another approach for the recovery of gravity anomalies from such data; and elaborated on the procedures (1971c) for their determination, and the combination with existing gravity material.

The Geodyn program (Martin, February 1972b) performs numerical integration of the equations of motion of the satellites; and simultaneously evaluates the variational partials by the numerical integration of the variational equations. This program was modified by Karki (1973) to accept gravity anomalies as unknown parameters. Rapp (1973b) describes the recovery of 184 15° equal area gravity anomalies, utilizing the modified Geodyn program, from optical satellite observations, and in combination with terrestrial gravity observations.

Vonbun (1971), Kahn et al (1972) have described the Geos-C/ATS-F satellite to satellite tracking and gravimetry experiment. With the launch of ATS-6 in May, 1974 and the proposed launch of Geos-C in March, 1975, it was timely to study the recovery of gravity anomalies from satellite to satellite tracking data. Similar data may also be available during Apollo-Soyuz-Link flight in July, 1975.

The Geodyn program was enlarged (Martin, February, 1972a) to accept satellite to satellite range and range rate measurements. This revised version (November, 1972) of Geodyn program was accordingly modified by Hajela (1974) to accept gravity anomalies as unknown parameters, generally following Karki (1973). The purpose of the present study is to investigate the recovery of mean gravity anomalies over $2^\circ.5$, 5° and 10° equal area blocks in regional or local areas, from 60° by 60° down to 20° by 20° or less. To explore the capability of satellite to satellite range rate, and range, observations in recovering gravity anomalies, utilizing close satellites at height of 900 km, or 250 km, combination solutions were not attempted. No use was thus made of a-priori information about gravity anomalies from terrestrial observations, except in Sec. 5.2 and 5.3, where the value of a-priori variance of anomalies in $2^\circ.5$ and 5° blocks was utilized to form their weight matrix. The present study otherwise follows the approach outlined by Rapp (1971a, 1971c).

1.1 Satellite to Satellite Tracking

This term will be used in this study to indicate a geostationary satellite of the ATS-6 type, generally referred to as the relay satellite, tracking a satellite close to earth. The close satellite would either be the Geos-C type satellite at a height of about 900 km, or a lower drag-free type satellite (Lange, DeBra, Kaula, 1969) or any other satellite, e.g. Apollo-Soyuz-Link flight, at a height of about 250 km. The case of one close satellite tracking another close satellite in the same nominal orbit (Comfort, 1973; Schwarz, 1970) will not be considered in this study.

The cartesian position and velocity coordinates of the relay satellite used in this study, were kindly supplied by Mr. J.G. Marsh of NASA, and were as follows:

$$\begin{aligned} X &= 13{,}848.503\ldots\text{km} & \dot{X} &= 2.905\ldots\text{km/sec} \\ Y &= -39{,}803.422\ldots\text{km} & \dot{Y} &= 1.006\ldots\text{km/sec} \\ Z &= 380.053\ldots\text{km} & \dot{Z} &= 7.928\ldots\text{km/sec}, \end{aligned} \tag{1.1}$$

at time 20 Sep. 1969 23 hour 55 min. 0 sec. This however, gave a nominal geostationary longitude of $63^\circ.2$ W. The coordinates of the relay satellite in equation (1.1) were then assumed to refer to time 21 Sep. 1969 01 hour 33 min. 36.3 sec., which gave a nominal geostationary longitude of $93^\circ.95$ W., which was close to the planned value of 94° W. for ATS-6. The inertial coordinate system used in this study was assumed to be the true of date coordinate system at 690921.0 (YYMMDD), with the Z axis defined by the instantaneous rotation axis of the earth, X axis by the true equinox of date and Y axis forming a right handed orthogonal system. The velocity coordinates in the same directions were defined by $\dot{Z}$, $\dot{X}$, $\dot{Y}$. The inertial position and velocity coordinates of the relay satellite were then defined to be in this sytem, and expressed by equation (1.1) at the time 690921 (YYMMDD) 01 hour 33 min. 36.3 sec. The coordinates of the close satellite were then also referred to this initial epoch (see Sec. 2.3.1).

The nominal value of the Keplerian elements for the Geos-C type of satellite was taken from Kahn et al (1972) as:

$$\begin{aligned} a &= 7214\,\text{km} \\ e &= 0.006 \\ i &= 115^\circ \end{aligned} \tag{1.2}$$

The nominal value of the Keplerian elements of the close satellite at height of about 250 km was taken as:

$$\begin{aligned} a &= 6626\,\text{km} \\ e &= 0.0005 \\ i &= 115^\circ \end{aligned} \tag{1.3}$$

The inclination of the 250 km high satellite was kept the same as that of the Geos-C type satellite, so that the pattern of satellite arcs would have the same geometry over the area of investigation. The actual orbital parameters of the close satellites were optimized, as described in Sec. 2.3.1, so that the subsatellite points, in subsequent passes of the close satellite, cover the area of investigation in an optimum manner. The optimized values of the Keplerian elements for the two satellites will be given in equations (2.54) and (2.56).

The satellite to satellite observations considered were the range from the ground tracking station to the relay satellite, plus the range from the relay satellite to the close satellite. This will be referred to as the summed range. The summed range rate would be the time derivative of the summed range, i.e. the time rate change of the range from the ground station to the relay satellite to the close satellite. The anticipated standard deviation (NASA, 1974, p. 4-65) of the summed range rate observations in the proposed Geos-C/ATS-6 tracking experiment is .07 cm/sec. with an integration interval of 10 seconds. This is expected to improve to .04 cm/sec. and .03 cm/sec., if the integration interval for determining summed range rate is 30 seconds and 1 minute respectively. As the time interval of observations in most of the investigations in the present study was kept as 10 seconds, a slightly conservative estimate of .08 cm/sec. was used for the standard deviation of the summed range rate observations not only for the close satellite at height of 900 km, but also for the close satellite at height of 250 km.

1.2 Gravity Anomalies

Mean gravity anomalies were considered in this study over 10° equal area blocks, according to the generalized division proposed by Rapp (1971b). Further subdivision into 5° equal area blocks was according to Hajela (1973). These, and the further subdivision into $2^\circ.5$ equal area blocks, will be described in Sec. 3.1. The limits of all blocks were in integer number of degrees, to enable the determination of mean gravity anomalies over large size blocks from the available free air gravity anomalies in $1^\circ \times 1^\circ$ equiangular blocks. This led to

the $2^{\circ}.5$ blocks being considerably unequal in area, but the word 'equal area' was retained to differentiate it from equiangular blocks.

The initial values for the free air mean gravity anomalies over 10° equal area blocks were taken from Hajela (1973). The gravity formula and the constants used for the reference ellipsoid will be given in Sec. 3.2, equations (3.7) and (3.8). The gravity anomalies actually used, however, referred to a set of spherical harmonic potential coefficients up to degree and order 12, i.e. from the free air terrestrial gravity anomalies, the gravity anomaly implied by the set of potential coefficients, was subtracted out, as described in Sec. 3.2. The resulting value will be referred to as the residual gravity anomalies.

The set of potential coefficients used as a reference to describe the earth's gravitational field were those obtained by least squares collocation by Rapp (1973a). As their value was considered to be known and held fixed, the anomaly implied by these potential coefficients was also a fixed constant value. After the residual anomaly is recovered from the adjustment procedure described in Chapter 2, the anomaly implied by the potential coefficients may be added to it, to get the recovered gravity anomaly referred to the specified gravity formula. We thus concern ourselves in this study with the recovery of residual anomalies. These will, in general, be referred to as anomalies, unless it is necessary to specifically distinguish between terrestrial anomalies, anomalies implied by the potential coefficients, and residual anomalies. The residual anomalies recovered from the adjustment scheme would be referred to as the 'recovered anomalies'; and the residual anomalies used to simulate satellite to satellite observations would be referred to as the 'expected anomalies'. The difference of recovered anomaly minus the expected anomaly would be referred to as the 'anomaly discrepancy' and would be used as one of the measures to examine the recovery model.

The formation of the mean residual anomalies over $2^{\circ}.5$, 5° and 10° equal area blocks will be described in Chapter 3.

1.3 Brief Description of Study

The investigations in this study have been grouped under four main problems. These are firstly, the recovery of 10° equal area mean anomalies from close satellite at height of about 900 km, and the recovery of 5° equal area mean anomalies from close satellite at height of about 250 km. These two problems will be discussed in Chapter 4. As the effect of anomalies over 10° blocks would be felt more strongly on the summed range rate, and range, observations at the height of close satellite of 900 km, as compared to the effect of anomalies over 5° blocks; and similarly, the 5° anomalies would be more discernible at the height of close satellite of 250 km as compared to $2^{\circ}.5$ anomalies, the discussion in Chapter 4 is categorized as the recovery of gravity anomalies from strong signal. This also enables us to test various considerations, which may then be applied with greater confidence to the recovery of gravity anomalies from weak signal. The latter category comprises of the investigations for the recovery

of 5° equal area mean anomalies from close satellite at height of 900 km, and the recovery of $2^{\circ}.5$ equal area mean anomalies from close satellite at height of 250 km; and these have been grouped in Chapter 5.

As already mentioned, we will consider in this study only the satellite to satellite tracking observations. Preliminary investigations showed that summed range observations were not very sensitive for the recovery of gravity anomalies. This has been discussed in Sec. 4.1.5. In all subsequent investigations, only the summed range rate observations were utilized. The gravity anomalies were the only unknowns considered. The only arc parameters considered were the constants of integration, i.e. the position and velocity coordinates at the start of integrating the orbits, which were eliminated from the normals, as the observations in that arc were processed, according to Sec. 2.2.1. A satellite arc consisted of a single pass of the close satellite, as the trajectory of the subsatellite point of the close satellite moved over the area of investigation from one edge to the other. The word 'satellite arc', or 'arc', has been used to indicate both the trajectory of the subsatellite points, as well as the summed range rate observations along that arc, and the usage is clear according to the context. As the duration of individual satellite arcs was short, from 4 to 20 minutes depending upon the area of investigation, the arc parameters were not recovered in this study, and were held fixed, as discussed in Sec. 2.2.1.

The geodetic coordinates of the ground tracking station were taken as:

$$\begin{array}{lll} \text{Latitude} & 35^{\circ} - 12' - 7''.28\,\text{N.}, & \\ \text{Longitude} & 277^{\circ} - 07' - 41''.16\,\text{E.}, & (1.4) \\ \text{Height} & 850 \text{ meters.} & \end{array}$$

The ground tracking station was intended to be Rosman, North Carolina, but as the reference ellipsoid (equation 3.7) used in this study was different from the reference ellipsoid on which the coordinates in equation (1.4) were given, these coordinates now refer to a hypothetical station in its vicinity.

We begin by discussing in Chapter 2 the mathematical model and the procedure of recovery. The gravity anomalies for data simulation will be described in Chapter 3. The main investigations of this study will be reported in Chapters 4 and 5. Discussion about the use of real data, a summary of main results, and suggestions for further study will be presented in Chapter 6. The results obtained by Schwarz (1970) will also be compared with the results of this study at the end of Sec. 6.3.

The standard deviation of range rate observations of .05 mm/sec. assumed by Schwarz was about 16 times more optimistic than what is likely to be achieved in currently proposed satellite to satellite tracking experiments like ATS-6/Geos-C and Apollo/Soyuz flight. The results of the present study are more realistic in terms of the precision of observations and the height of close satellites. We have

now also the advantage of better orbit generation and parameter estimation computer programs, including gravity anomalies as parameters. The main contribution of this study, however, lies in the systematic investigation of the recovery of gravity anomalies in local and regional areas, and in establishing the optimum design of observations and the optimum mathematical model for the recovery.

2. MATHEMATICAL MODEL AND PROCEDURE OF RECOVERY

We will consider the observations during this study to be only the summed range rate, or the summed range. The unknowns to be recovered by the usual least squares procedure would be the residual gravity anomalies and the starting coordinates of the relay and close satellite at the epoch of starting the integration of the orbits of these satellites. We later find that the starting coordinates could not be recovered satisfactorily because of using observations over very short periods of satellite arcs from 4 to 20 minutes, and the starting coordinates were thus considered in this study to be well determined a-priori say, with other tracking data, and these values were then held 'fixed' in the estimation process by assigning them a very low variance. This is described in more detail later in Sec. 2.3.3. (Also see Sec. 6.1).

The initial or 'approximate' value of the residual gravity anomalies were considered to be zero. The computed value of the summed range rate or summed range was then obtained with respect to the position of the relay and close satellites obtained by integrating their orbits in the gravity field described only by the reference set of potential coefficients with the residual anomalies as zero. This misclosures between the 'observed' values (Sec. 2.3.2) and the computed values of the summed range rate or summed range, along with the matrix of partial derivatives of these observations with respect to the unknowns, were then used to recover the correction to the 'approximate' value of the residual anomalies, which was also the 'solution vector' as the approximate value of residual anomalies were zero. Following the notation of Uotila (1967), the solution vector X is obtained by:

$$X = -N^{-1}U = -(A'PA)^{-1}A'PL, \tag{2.1}$$

where A is the matrix of partial derivatives of the observations with respect to the unknowns, P is the weight matrix of observations, L is the vector of misclosures, N is the normals matrix and U is the 'constant' vector of the normal equations:

$$NX + U = 0 \tag{2.2}$$

Though the adjustment may essentially be described by equation (2.1), the actual scheme used allowed the possibility of treating the unknown parameters also as observations, and constraining their adjusted values to fulfill certain conditions. The actual scheme also allowed the elimination of arc parameters after processing observations in each arc, so that the unknowns actually solved for were the residual gravity anomalies. This scheme is described more fully in Sec. 2.2.1.

2.1 Computation of the Misclosure Vector and the Partial Derivatives Matrix

2.1.1 The Misclosure Vector

Following the treatment of Chin, Goad and Martin (1972), the geometry for obtaining the summed range or summed range rate is shown in Figure 2.1, where $\vec{R}_1$, $\vec{R}_2$ and $\vec{R}_s$ are the geocentric radius vectors to the relay and close satellites and the ground tracking station respectively at a specified time. Denoting the relay and close satellites by subscripts 1 and 2, and the upward and downward range by the subscripts u and d, we may represent the 4 ranges, i.e., from the ground tracking station to the relay satellite, from the relay satellite to the close satellite, and the 2 ranges on the return path to the ground tracking station, by R_{1u}, R_{2d}, R_{2u}, R_{1d} respectively. Then, representing the summed range from the ground tracking station to the relay satellite and then to the close satellite as R_s, we have:

$$R_s = \tfrac{1}{2}(R_{1u} + R_{2d} + R_{2u} + R_{1d}) \tag{2.3}$$

The ranges on the right hand side of equation (2.3) may be expressed in terms of the geocentric radius vectors $\vec{R}_1$, $\vec{R}_2$, $\vec{R}_s$, but we have to specify the times at which these radius vectors are to be so expressed. If we denote the time at which the signal is received back at the ground tracking station by t, and the transit time along the 4 ranges by Δt with appropriate subscripts, we have:

$$R_{1d} = \left|\vec{R}_1(t - \Delta t_{1d}) - \vec{R}_s(t)\right| \tag{2.4}$$

$$R_{2u} = \left|\vec{R}_2(t - \Delta t_{1d} - \Delta t_{2u}) - \vec{R}_1(t - \Delta t_{1d})\right| \tag{2.5}$$

$$R_{2d} = \left|\vec{R}_1(t - \Delta t_{1d} - \Delta t_{2u} - \Delta t_{2d}) - \vec{R}_2(t - \Delta t_{1d} - \Delta t_{2u})\right| \tag{2.6}$$

$$R_{1u} = \left|\vec{R}_s(t - \Delta t_{1d} - \Delta t_{2u} - \Delta t_{2d} - \Delta t_{1u}) - \vec{R}_1(t - \Delta t_{1d} - \Delta t_{2u} - \Delta t_{2d})\right| \tag{2.7}$$

We have assumed in equations (2.4) to (2.7) that there are no transponder delays at the 2 satellites. A comparatively large transponder delay of 4μsec. would affect the summed range of about 78,000 km by only 1 cm; but in practice the actual transponder delays of the satellites could also be taken into account.

The radius vectors at the required times in equations (2.4) to (2.7) can be computed knowing the inertial coordinates of the satellites and the ground tracking station at those times, and we may thus compute the summed range R_s at any particular time, say t, from equation (2.3). The summed range rate, $\dot{R}_s$, would be its time derivative, to be denoted by a dot on the top, and expressed in terms of the time derivatives of the 4 ranges, i.e.,

$$\dot{R}_s = \tfrac{1}{2}(\dot{R}_{1u} + \dot{R}_{2d} + \dot{R}_{2u} + \dot{R}_{1d}) \tag{2.8}$$

and, we can readily see from equation (2.4) that

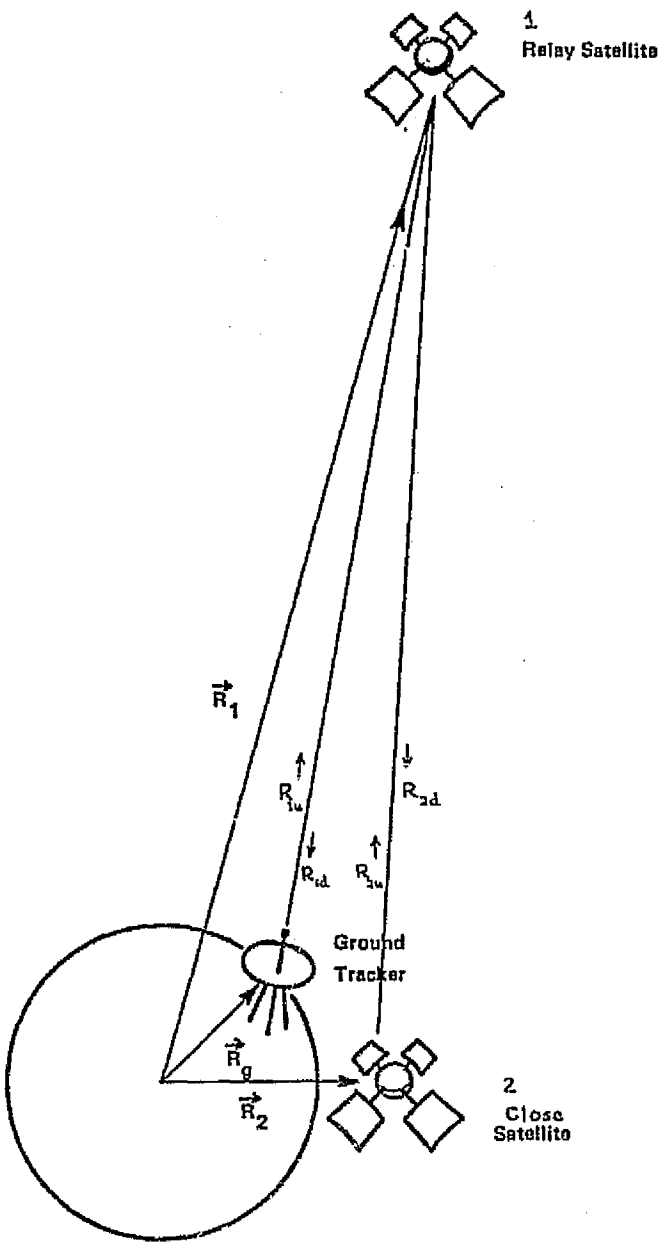

Figure 2.1 Geometry for Satellite-Satellite Tracking

$$\dot{R}_{1d} = \frac{d}{dt} \left| \vec{R}_1(t-\Delta t_{1d}) - \vec{R}_s(t) \right|$$

$$= \frac{[(\dot{\vec{R}}_1(t-\Delta t_{1d}) - \dot{\vec{R}}_s(t)) \cdot (\vec{R}_1(t-\Delta t_{1d}) - \vec{R}_s(t))]}{\{[(\vec{R}_1(t-\Delta t_{1d}) - \vec{R}_s(t)) \cdot (\vec{R}_1(t-\Delta t_{1d}) - \vec{R}_s(t))]\}^{\frac{1}{2}}} \qquad (2.9)$$

with similar expressions for $\dot{R}_{2u}$, $\dot{R}_{2d}$, $\dot{R}_{1u}$ from equations (2.5) to (2.7). The dot between expressions inside square brackets denotes the scalar dot product.

The summed range rate $\dot{R}_s$ at any particular time, say t, may then be computed knowing the inertial velocities of the satellites and the ground tracking station at the required times in equation (2.4) to (2.7), in addition to their inertial coordinates at those times. The summed range observations are thus a function of the inertial coordinates, while the summed range rate observations are a function of both the inertial coordinates and inertial velocities of the relay and close satellites and the ground tracking station at the required times.

The simulation of 'observations' will be described in Sec. 2.3.2. The integration of orbits of the relay and close satellites to obtain their inertial coordinates and velocities, will also be discussed in Sec. 2.3.2. The inertial coordinates of the ground tracking station are obtained by a rotational transformation of its cartesian coordinates about the earth's rotation axis by the Greenwich hour angle of the true equinox of date, and by applying precession and nutation for the period of time from 0.0 hr. of the reference day. This has been described in detail in Volume I Sections 3 to 5 of Geodyn System Description (1972) and has not been repeated here. The computed value of R_s or $\dot{R}_s$, at the time of observation may then be obtained from equations (2.3) and (2.8), and the vector of misclosures, L of equation (2.1), computed. We may now discuss the computation of the partial derivatives matrix A.

2.1.2 The Partial Derivatives Matrix

If we represent the unknown parameters, whose values are to be recovered from the adjustment process, by β, then we have to form the partial derivatives of the observations, R_s or $\dot{R}_s$, with respect to these parameters. From equation (2.3), we have:

$$\frac{\partial R_s}{\partial \beta} = \frac{1}{2}\left(\frac{\partial R_{1u}}{\partial X_{1i}} + \frac{\partial R_{2d}}{\partial X_{1i}} + \frac{\partial R_{2u}}{\partial X_{1i}} + \frac{\partial R_{1d}}{\partial X_{1i}} \right) \frac{\partial X_{1i}}{\partial \beta}$$

$$+ \frac{1}{2}\left(\frac{\partial R_{2d}}{\partial X_{2i}} + \frac{\partial R_{2u}}{\partial X_{2i}} \right) \frac{\partial X_{2i}}{\partial \beta} \qquad (2.10)$$

where X_{1i}, X_{2i} are the inertial coordinates of the relay and close satellites respectively, and summation over i from 1 to 3 is implied. This summation convention for a repeated subscript would also be understood to apply in subsequent expressions.

Though the ranges in equations (2.4) to (2.7) refer to coordinates of the satellites at slightly different times, we may ignore these differences while computing the partials in equation (2.10). It may then be further simplified by putting:

$$\frac{\partial R_{1u}}{\partial X_{1i}} \simeq \frac{\partial R_{1d}}{\partial X_{1i}} \; ; \; \frac{\partial R_{2d}}{\partial X_{1i}} \simeq \frac{\partial R_{2u}}{\partial X_{1i}} \tag{2.11}$$

We also note that:

$$\frac{\partial R_{2d}}{\partial X_{2i}} = -\frac{\partial R_{2d}}{\partial X_{1i}} \; ; \; \frac{\partial R_{2u}}{\partial X_{2i}} = -\frac{\partial R_{2u}}{\partial X_{1i}} \tag{2.12}$$

The expression for the partials $\frac{\partial R_s}{\partial \beta}$ may then be simplified by substituting equations (2.11) and (2.12) in equations (2.10) as:

$$\frac{\partial R_s}{\partial \beta} \simeq \frac{\partial R_{1d}}{\partial X_{1i}} \frac{\partial X_{1i}}{\partial \beta} + \frac{\partial R_{2u}}{\partial X_{1i}} \left(\frac{\partial X_{1i}}{\partial \beta} - \frac{\partial X_{2i}}{\partial \beta} \right) \tag{2.13}$$

We may similarly compute the partials of the summed range rate from equation (2.8), where we note from equation (2.9) that both the inertial coordinates and the inertial velocities of the satellites are involved. We may again use the analogous simplification to equation (2.11) that partials of upward range rate with respect to inertial coordinates and velocities are approximately equal to the corresponding partials of the downward range rate, when we get:

$$\begin{aligned} \frac{\partial \dot{R}_s}{\partial \beta} \simeq & \left(\frac{\partial \dot{R}_{1d}}{\partial X_{1i}} + \frac{\partial \dot{R}_{2u}}{\partial X_{1i}} \right) \frac{\partial X_{1i}}{\partial \beta} + \left(\frac{\partial \dot{R}_{1d}}{\partial \dot{X}_{1i}} + \frac{\partial \dot{R}_{2u}}{\partial \dot{X}_{1i}} \right) \frac{\partial \dot{X}_{1i}}{\partial \beta} \\ & + \frac{\partial \dot{R}_{2u}}{\partial X_{2i}} \frac{\partial X_{2i}}{\partial \beta} + \frac{\partial \dot{R}_{2u}}{\partial \dot{X}_{2i}} \frac{\partial \dot{X}_{2i}}{\partial \beta} \end{aligned} \tag{2.14}$$

It is easy to see from equation (2.9) that analogous relations to equation (2.12) also hold for the partials of the range rate with respect to inertial coordinates and velocities, which simplifies equation (2.14) as:

$$\begin{aligned} \frac{\partial \dot{R}_s}{\partial \beta} \simeq & \frac{\partial \dot{R}_{1d}}{\partial X_{1i}} \frac{\partial X_{1i}}{\partial \beta} + \frac{\partial \dot{R}_{2u}}{\partial X_{1i}} \left(\frac{\partial X_{1i}}{\partial \beta} - \frac{\partial X_{2i}}{\partial \beta} \right) \\ & + \frac{\partial \dot{R}_{1d}}{\partial \dot{X}_{1i}} \frac{\partial \dot{X}_{1i}}{\partial \beta} + \frac{\partial \dot{R}_{2u}}{\partial \dot{X}_{1i}} \left(\frac{\partial \dot{X}_{1i}}{\partial \beta} - \frac{\partial \dot{X}_{2i}}{\partial \beta} \right) \end{aligned} \tag{2.15}$$

Finally, it may be verified from equations (2.9) and (2.4), and similar expressions, that

$$\frac{\partial \dot{R}_{1d}}{\partial \dot{X}_{1i}} = \frac{\partial R_{1d}}{\partial X_{1i}} \; ; \quad \frac{\partial \dot{R}_{2u}}{\partial \dot{X}_{1i}} = \frac{\partial R_{2u}}{\partial X_{1i}} \tag{2.16}$$

so that equation (2.15) becomes:

$$\begin{aligned} \frac{\partial \dot{R}_s}{\partial \beta} = & \frac{\partial \dot{R}_{1d}}{\partial X_{1i}} \frac{\partial X_{1i}}{\partial \beta} + \frac{\partial \dot{R}_{2u}}{\partial X_{1i}} \left(\frac{\partial X_{1i}}{\partial \beta} - \frac{\partial X_{2i}}{\partial \beta} \right) \\ & + \frac{\partial R_{1d}}{\partial \dot{X}_{1i}} \frac{\partial \dot{X}_{1i}}{\partial \beta} + \frac{\partial R_{2u}}{\partial X_{1i}} \left(\frac{\partial \dot{X}_{1i}}{\partial \beta} - \frac{\partial \dot{X}_{2i}}{\partial \beta} \right), \end{aligned} \tag{2.17}$$

where, as before, the summation over i from 1 to 3 is implied.

In equation (2.17), the value of the partials of range rate and range, with respect to the inertial coordinates, i.e. expressions of the type

$$\frac{\partial \dot{R}_{1d}}{\partial \dot{X}_{1i}} \; , \quad \frac{\partial R_{1d}}{\partial X_{1i}}$$

are easily computed from geometrical expressions given in equations (2.9) and (2.4). We may thus confine our remarks to the evaluation of the variational partials

$$\frac{\partial X_{1i}}{\partial \beta} \; , \quad \frac{\partial X_{2i}}{\partial \beta} \tag{2.18}$$

which are obtained by the integration of the variational equations, as referred to either of the two satellites, by:

$$\frac{\partial \ddot{X}_i}{\partial \beta} = \frac{\partial}{\partial \beta} \left(\frac{\partial V}{\partial X_i} \right) = \frac{\partial}{\partial \beta} \left(\frac{\partial U}{\partial X_i} + \frac{\partial T}{\partial X_i} \right) \tag{2.19}$$

where V is the earth's gravitational potential comprising of the normal potential U defined by a set of fully normalized spherical harmonic coefficients, $\overline{C_{nm}}$, $\overline{S_{nm}}$ up to degree N_{max} and the disturbing potential T due to a set of residual gravity anomalies $\Delta g'$, i.e.,

$$U = \frac{kM}{r} \left[1 + \sum_{n=2}^{N_{max}} \left(\frac{a_e}{r} \right)^n \sum_{m=0}^{n} \left(\overline{C_{nm}} \cos m\lambda + \overline{S_{nm}} \sin m\lambda \right) \overline{P_{nm}}(\sin \phi') \right] \tag{2.20}$$

and

$$T = \frac{R}{4\pi} \iint_{\sigma} \Delta g' \, S(r,\psi) \, d\sigma \tag{2.21}$$

In equation (2.20), kM is the gravitational constant times the earth's mass; a_e is the equatorial radius of the reference ellipsoid; r is the geocentric radius vector of the satellite of geocentric latitude φ' and longitude λ, and $\overline{P_{nm}}(\sin\varphi')$ are the fully normalized associated Legendre functions. In equation (2.21), R is the radius of the mean earth sphere, $S(r, \psi)$ is the extended Stokes function (Heiskanen and Moritz, 1967, page 235), ψ is the spherical distance between the sub-satellite point and the surface area $d\sigma$, over which $\Delta g'$ is the residual gravity anomaly, and is given by:

$$\Delta g' = \Delta g_T - \Delta g_{PC} \tag{2.22}$$

where Δg_T is the free air gravity anomaly and Δg_{PC} is the gravity anomaly implied by the potential coefficients used in equation (2.20). Equation (2.22) will be discussed further in Sec. 3.1 to 3.3.

The first term on the right hand side of equation (2.19) may be put as:

$$\frac{\partial}{\partial\beta}\left(\frac{\partial U}{\partial X_i}\right) = \frac{\partial^2 U}{\partial X_i \partial X_j} \quad \frac{\partial X_j}{\partial \beta}; \quad i,j = 1,2,3 \tag{2.23}$$

and as we are taking the reference set of potential coefficients to be known constants, there are no direct partials of U with respect to β. The expressions for evaluating $\partial^2 U/\partial X_i \partial X_j$ are given in detail in Volume I Sec. 8.3.1 of the Geodyn System Description (1972).

While considering the second term on the right hand side of equation (2.19) we need only consider the evaluation of direct partials with respect to a particular gravity anomaly $\Delta g'_k$ given by:

$$\frac{\partial}{\partial \Delta g'_k}\left(\frac{\partial T}{\partial X_i}\right) = \frac{\partial}{\partial \Delta g'_k}\left(\frac{\partial T}{\partial r} \quad \frac{\partial r}{\partial X_i} + \frac{\partial T}{\partial \varphi'} \quad \frac{\partial \varphi'}{\partial X_i} + \frac{\partial T}{\partial \lambda} \quad \frac{\partial \lambda}{\partial X_i}\right)$$

$$= \frac{R}{4\pi} \quad \frac{\partial}{\partial \Delta g'_k}\left(\frac{\partial r}{\partial X_i} \sum_k \Delta g'_k \left.\frac{\partial S}{\partial r}\right|_k d\sigma_k + \frac{\partial \varphi'}{\partial X_i} \sum_k \Delta g'_k \left.\frac{\partial S}{\partial \varphi'}\right|_k d\sigma_k \right.$$

$$\left. + \frac{\partial \lambda}{\partial X_i} \sum_k \Delta g'_k \left.\frac{\partial S}{\partial \lambda}\right|_k d\sigma_k \right)$$

$$= \frac{R}{4\pi}\left(\frac{\partial r}{\partial X_i}\frac{\partial S}{\partial r}\bigg|_k + \frac{\partial \varphi'}{\partial X_i}\frac{\partial S}{\partial \varphi'}\bigg|_k + \frac{\partial \lambda}{\partial X_i}\frac{\partial S}{\partial \lambda}\bigg|_k\right) d\sigma_k \tag{2.24}$$

In equation (2.24), we have approximated the integral in equation (2.21) by a summation and have expressed the derivatives of the anomalous potential T in terms of the derivatives of the extended Stokes function $S(r, \psi)$. We then carry out the differentiation with respect to a particular mean gravity anomaly $\Delta g'_k$ given over a block of area $d\sigma_k$. The derivatives of r, φ', λ with respect to $X_i (X_1, X_2, X_3)$ can easily be shown to be given by:

$$\frac{\partial r}{\partial X_i} = \frac{X_i}{r} \tag{2.25}$$

$$\frac{\partial \varphi'}{\partial X_i} = \frac{1}{(X_1^2 + X_2^2)^{\frac{1}{2}}}\left(-\frac{X_2 X_1}{r^2} + \frac{\partial X_2}{\partial X_i}\right) \tag{2.26}$$

$$\frac{\partial \lambda}{\partial X_i} = \frac{X_1}{X_1^2 + X_2^2}\left(\frac{\partial X_2}{\partial X_i} - \frac{X_2}{X_1}\frac{\partial X_1}{\partial X_i}\right) \tag{2.27}$$

while the derivatives of the extended Stokes function with respect to r, ψ, are given in Heiskanen and Moritz (1967, pages 234, 235), as:

$$\frac{\partial S}{\partial r}\bigg|_k = -\frac{t^2}{R}\left(\frac{1-t^2}{D_k^3} + \frac{4}{D_k} + 1 - 6D_k - t\cos\psi_k\left(13 + 6\ell n\,\frac{1 - t\cos\psi_k + D_k}{2}\right)\right) \tag{2.28}$$

$$\frac{\partial S}{\partial \varphi'}\bigg|_k = \frac{\partial S(r,\psi)}{\partial \psi}\frac{\partial \psi}{\partial \varphi'} = -\frac{\partial S}{\partial \psi}\bigg|_k \cos\alpha_k \tag{2.29}$$

$$\frac{\partial S}{\partial \lambda}\bigg|_k = \frac{\partial S(r,\psi)}{\partial \psi}\frac{\partial \psi}{\partial \lambda} = -\frac{\partial S}{\partial \psi}\bigg|_k \cos\varphi' \sin\alpha_k \tag{2.30}$$

$$\frac{\partial S}{\partial \psi}\bigg|_k = -t^2 \sin\psi_k\left(\frac{2}{D_k^3} + \frac{6}{D_k} - 8 - 3\,\frac{1 - t\cos\psi_k - D_k}{D_k \sin^2\psi_k} - 3\ell n\,\frac{1 - t\cos\psi_k + D_k}{2}\right) \tag{2.31}$$

where

$$t = R/r \tag{2.32}$$

$$D_k = \ell_k / r = (r^2 + R^2 - 2Rr\cos\psi_k)^{\frac{1}{2}}/r = (1 - 2t\cos\psi_k + t^2)^{\frac{1}{2}} \tag{2.33}$$

and ℓ_k is the distance of the satellite from the gravity anomaly $\Delta g'_k$ of geocentric latitude φ'_k and longitude λ_k; ψ_k is the spherical distance of the gravity anomaly $\Delta g'_k$ from the subsatellite point (φ', λ); and α_k is the azimuth of the gravity anomaly $\Delta g'_k$ from the subsatellite point. ψ_k, and α_k are given by:

$$\cos\psi_k = \sin\varphi' \sin\varphi'_k + \cos\varphi' \cos\varphi_k \cos(\lambda_k - \lambda), \tag{2.34}$$

and

$$\tan\alpha_k = \frac{\cos\varphi'_k \sin(\lambda_k - \lambda)}{\cos\varphi' \sin\varphi'_k - \sin\varphi' \cos\varphi'_k \cos(\lambda_k - \lambda)} \tag{2.35}$$

For mean gravity anomalies at a sufficient distance from the subsatellite point, say $\psi_k > 35^\circ$, we may compute the value of $\frac{\partial}{\partial \Delta g'_k}(\partial T/\partial X_1)$ at the center of the anomaly block, but for gravity anomalies close to the subsatellite point, we need to subdivide the anomaly block into ℓ sub-blocks to minimize quadrature errors, and compute it as:

$$\frac{\partial}{\partial \Delta g'_k}\left(\frac{\partial T}{\partial X_1}\right) = \frac{R}{4\pi}\left(\frac{\partial r}{\partial X_1} \sum_{\ell} \frac{\partial S}{\partial r}\bigg|_{\ell} d\sigma_\ell + \frac{\partial \varphi'}{\partial X_1} \sum_{\ell} \frac{\partial S}{\partial \varphi'}\bigg|_{\ell} d\sigma_\ell \right. \tag{2.36}$$

$$\left. + \frac{\partial \lambda}{\partial X_1} \sum_{\ell} \frac{\partial S}{\partial \lambda}\bigg|_{\ell} d\sigma_\ell \right)$$

The anomaly blocks were subdivided into 4, 9, or 16 sub-blocks when $35^\circ > \psi_k > 20^\circ$, $20^\circ > \psi_k > 12^\circ.5$ and $12^\circ.5 > \psi_k > 0^\circ$ respectively, as per Hajela (1972).

Further discussion regarding the integration of the variational equations (2.19) may be seen in Rapp (1971a) and Geodyn System Description Volume I (1972).

2.2 The Adjustment Scheme

2.2.1 The Correction Vector

In elaboration of the remarks before Sec. 2.1, we may in general terms, describe the mathematical model, as:

$$F(L_{F_a}, L_{X_a}) = 0, \tag{2.37}$$

where L_{F_a} is the vector of observations of summed range rate, or summed range, related through the function F to the vector L_{X_a} of unknown parameters being estimated, i.e. the arc parameters and the residual gravity anomalies, and the subscript 'a' represents their adjusted values.

Further, if any constraints are to be imposed on the adjusted values of parameters to fulfill certain conditions, we may express these in the form:

$$G(L_{X_a}) = 0 \tag{2.38}$$

The linearized form of the equations (2.37) and (2.38) is:

$$B_F V_F + B_{FX} V_X + W_F = 0 \tag{2.39a}$$

$$B_{GX} V_X + W_G = 0 \tag{2.39b}$$

where B represents the partials matrix of the functions F and G with respect to the observed quantities (B_F) and the unknown parameters (B_{FX}, B_{GX}); V represents the correction vectors (V_F, V_X); and W represents the misclosure vectors (W_F, W_G) when the initial or 'approximate' values of the observed quantities and unknown parameters are substituted in equations (2.37) and (2.38).

If we represent the weight matrices of the observed quantities by P_F and of the unknown parameters by P_X, it may be shown (Mikhail, 1970), that for the usual least value of the sum of squares of the weighted residuals (or correction vectors) under the condition that the equations (2.39) are satisfied, i.e., for a minimum value of φ given by:

$$\varphi = V_F' P_F V_F + V_X' P_X V_X - 2K_F'(B_F V_F + B_{FX} V_X + W_F) - 2K_G'(B_{GX} V_X + W_G) \tag{2.40}$$

where K_F, K_G are the Lagrange multipliers, the solution is obtained by:

$$\begin{bmatrix} V_X \\ -K_G \end{bmatrix} = \begin{bmatrix} B_{FX}' P_F B_{FX} + P_X & B_{GX}' \\ B_{GX} & 0 \end{bmatrix}^{-1} \begin{bmatrix} -B_{FX}' P_F W_F + P_X W_X \\ -W_G \end{bmatrix}, \tag{2.41}$$

where W_X is the vector of difference between the observed value of parameters, and the approximate value used in computing the misclosures W_F and W_G. This enables the a-priori estimates of residual gravity anomalies from terrestrial data to be used in a combination solution with satellite to satellite tracking data.

If there were no conditions to be satisfied by the adjusted values of the unknown parameters, i.e. if we delete equations (2.38), (2.39b) and the last term in equation (2.40), the correction vector V_X for the unknown parameters would be given by:

$$V_X = (B_{FX}' \; P_F B_{FX} + P_X)^{-1} \; (-B_{FX}' P_F \; W_F + P_X W_X) \tag{2.42}$$

The matrices B_{FX} and P_X may be partitioned according to the correction vector V_X referring to arc parameters and the residual gravity anomalies, represented by the subscripts 'a' and 'k' respectively, i.e.,

$$V_X' = (V_a \; , \; V_k)$$

$$B_{FX} = (B_a \; , \; B_k)$$

$$P_X = \begin{bmatrix} \Sigma_a & 0 \\ 0 & \Sigma_k \end{bmatrix}^{-1} = \begin{bmatrix} P_a & 0 \\ 0 & P_k \end{bmatrix}$$

$$W_X' = (W_a \; , \; W_k) \tag{2.43}$$

where Σ_a , Σ_k are the a-priori variance-covariance matrices of the arc parameters and residual gravity anomalies respectively, and we have taken the scalar variance of unit weight, σ_0^2, as unity.

Equation (2.42) may then be represented by:

$$\begin{bmatrix} V_a \\ V_k \end{bmatrix} = \begin{bmatrix} B_a' \Sigma_F^{-1} B_a + \Sigma_a^{-1} & B_a' \Sigma_F^{-1} B_k \\ (B_a' \Sigma_F^{-1} B_k)' & B_k' \Sigma_F^{-1} B_k + \Sigma_k^{-1} \end{bmatrix}^{-1}$$

$$\begin{bmatrix} -B_a' \Sigma_F^{-1} W_F + \Sigma_a^{-1} & W_a \\ -B_k' \Sigma_F^{-1} W_F + \Sigma_k^{-1} & W_k \end{bmatrix}$$

$$= \begin{bmatrix} N_a & N_{ak} \\ N_{ak}' & N_k \end{bmatrix}^{-1} \begin{bmatrix} -U_a \\ -U_k \end{bmatrix} \tag{2.44}$$

Equation (2.44) may be solved for V_k (Uotila, 1967) as:

$$V_k = (N_k - N'_{ak}\ N_a^{-1}\ N_{ak})^{-1}\ (-U_k + N'_{ak}\ N_a^{-1}\ U_a) \tag{2.45}$$

We may now consider the expressions for the arc parameters in equation (2.44) to be partitioned according to individual arcs, i.e.

$$N_a = \begin{bmatrix} N_1 & & 0 \\ & N_2 & \\ 0 & & \ddots \end{bmatrix}$$

$$N'_{ak} = (N'_{a_1 k},\ N'_{a_2 k}, \ldots)$$

$$U'_a = (U_{a_1},\ U_{a_2}, \ldots)$$

$$\Sigma_a = \begin{bmatrix} \Sigma_{a_1} & & 0 \\ & \Sigma_{a_2} & \\ 0 & & \ddots \end{bmatrix}, \tag{2.46}$$

where we have assumed that firstly, there is no covariance between the arc parameters for different arcs; and secondly, that the observations in any given arc do not depend on the arc parameters of any other arcs. Then it may be shown (Geodyn Vol. I Sec. 10.2, 1972) that the terms referring to arc parameters in equation (2.45) are obtained as summations for individual arcs. Denoting the r^{th} arc with subscript r, equation (2.45) may be represented by:

$$V_k = (N_k - \sum_r N'_{rk}\ N_r^{-1} N_{rk})^{-1}\ (-U_k + \sum_r N'_{rk}\ N_r^{-1}\ U_r), \tag{2.47}$$

which is the form in which individual arc parameters are successively eliminated, as observations in each arc are processed to give, say for the r^{th} arc, N_r, N_{rk}, U_r; and the contribution to N_k, U_k from the observations in the r^{th} arc.

The expressions for the correction vector V_a for the arc parameters, and for its partition according to individual arc V_r, are given in Geodyn Vol. I Sec. 10.2 (1972), and have not been given here, as it was found that these could not be recovered from short arcs of 4 to 20 minutes duration. Accordingly the starting values of inertial coordinates and velocities for each arc were fixed by assigning them very low variances. This resulted in the summation terms for the arc parameters in equation (2.47) becoming much smaller than the terms for the residual anomalies, and the correction vector V_k could in effect be represented as:

$$V_k = -N_k^{-1} U_k \ ,$$

which is essentially the same as equation (2.1).

Further, as mentioned in Chapter 1, the correction vector V_k was recovered in all the investigations throughout this study from satellite data only, i.e. summed range rate, or summed range, observations. Accordingly, the weight matrix for the residual gravity anomalies, P_k in equation (2.43), was always (except Sec. 5.2, 5.3) kept as 0.

2.2.2 Weight Matrix

The standard deviation of all summed range rate observations was taken as 0.08 cm/sec. based on an integration interval of 10 seconds. All covariances were assumed to be zero resulting in the variance-covariance matrix of observations, and hence the weight matrix P_f, being diagonal (scalar variance of unit weight σ_0^2 was kept as 1). The assumption of zero covariance is reasonable if all observations, say at 10 seconds interval, are used without converting them to 'synthetic' observations, say at 1 minute interval. The observations at 1 minute interval were used in Sec. 4.1, but these could still be considered as independent observations, as all intervening observations at 10 seconds interval were ignored. However, the effect of using all independent observations, at 10 seconds interval, has been investigated in Sec. 4.1 and no observations were 'thrown away' in later sections.

The standard deviation of summed range observations was taken as 10 meters (NASA, 1974, p. 4-78), and all observations were considered to be independent. The summed range observations have been used in one test only in Sec. 4.1.5. As these gave very poor anomaly recovery, only summed range rate observations were used in all other investigations.

2.2.3 Constraints for Harmonic Coefficients

We may now specify if any constraints are to be imposed on the adjusted values of residual gravity anomalies to fulfill any conditions, as in equation (2.38). If the set of anomalies being recovered was a global one, then clearly the 6 coefficients of degree 0, 1 and some of degree 2; i.e. $a'_{0,0}$; $a'_{1,0}$; $a'_{1,1}$; $b'_{1,1}$; $a'_{2,1}$; $b'_{2,1}$ should be zero in the spherical harmonic expansion of the adjusted residual anomalies:

$$\Delta g'_k = \sum_{n=0}^{\infty} \sum_{m=0}^{n} (a'_{nm} \cos m\lambda + b'_{nm} \sin m\lambda)\, P_{nm}(\sin\varphi') \qquad (2.48)$$

This would correspond to the mean value of the residual gravity anomalies over the whole earth being zero, the origin of the coordinate system being at the center of gravity of the earth, and the Z axis of the coordinates system coinciding with the mean rotation axis of the earth. The formation of these 6 condition equations has been described by Rapp (1971a).

However, while these conditions may be held for anomalies over the whole earth, there is no clear justification for them to hold over regional areas, even as large as say 1/8th of the globe, investigated in Sec. 4.1. The contributions to the fully normalized harmonic coefficients $\overline{a_{nm}}'$, $\overline{b_{nm}}'$ given by:

$$\begin{Bmatrix} \overline{a_{nm}}' \\ \overline{b_{nm}}' \end{Bmatrix} = \frac{1}{4\pi} \iint_{\sigma} \Delta g' \, \overline{P_{nm}} (\sin\varphi') \begin{Bmatrix} \cos m\lambda \\ \sin m\lambda \end{Bmatrix} d\sigma \qquad (2.49)$$

from a regional area σ_1, may be balanced by other regions σ_2, σ_3, ...; so that if a harmonic coefficient is zero over the whole earth, it is not required to be zero separately over regional areas.

The effect of imposing the 6 conditions for low degree harmonic coefficients of degree 0, 1 and some degree 2 being zero, was tested in Sec. 4.1.4 over an area of latitudinal extent 70° and longitudinal extent of about 60°. The anomaly recovery was found to become worse when these conditions were imposed as compared to the adjustment without imposing any conditions.

Again, if the residual gravity anomalies were recovered over the whole earth, it could be argued that as the gravity anomaly, Δg_{PC}, equivalent to the effect of the potential coefficients up to degree N_{max} has been removed in equation (2.22), the values of $\overline{C_{nm}}'$, $\overline{S_{nm}}'$ (see equation (2.20)) up to degree N_{max} as obtained from the adjusted values of the residual gravity anomalies, $\Delta g_a'$, should be zero, i.e.,

$$\begin{Bmatrix} \overline{C_{nm}}' \\ \overline{S_{nm}}' \end{Bmatrix} = \frac{1}{4\pi\gamma(n-1)} \iint_{\sigma} \Delta g_a' \, \overline{P_{nm}} (\sin\varphi') \begin{Bmatrix} \cos m\lambda \\ \sin m\lambda \end{Bmatrix} d\sigma$$

$$= \frac{1}{\gamma(n-1)} \begin{Bmatrix} \overline{a_{nm}}' \\ \overline{b_{nm}}' \end{Bmatrix}$$

$$= 0 \quad \text{for } m \le n \le N_{max}, \qquad (2.50)$$

where γ is the average value of gravity over the earth, say 979.8 gals. Equation (2.50) corresponds to the coefficients up to degree N_{max} in the spherical harmonic expansion of the adjusted residual gravity anomalies being zero, i.e. only higher degree ($>N_{max}$) harmonics are present in the expansion of $\Delta g_a'$. Similar constraints in the case of residual surface densities are recommended in Geodyn Vol. 1, Sec. 8.3.2.4 (1972).

However, if we cannot justify constraints for low degree harmonic coefficients in regional areas, in contrast to a global coverage, there is still less justification for higher degree ($2 < n \leq N_{max}$) constraints. Hence, except for the test in Sec. 4.1.4, no constraints were imposed on the adjusted value of the residual gravity anomalies in regional or local areas in other investigations in this study.

2.3 Procedure of Computations

2.3.1 Orbital Parameters of the Close Satellite

The generation of residual mean gravity anomalies over 10°, 5° and 2°.5 equal area blocks will be described in Sec. 3.2 and 3.3. After obtaining the value of the earth's gravitational potential by equations (2.20) and (2.21), we would like to choose the orbital parameters of the close satellites at a height of about 900 km and 250 km respectively, so that the trace of the subsatellite points 'samples' the area of investigation in an optimum manner. The choice of the orbital parameters for the relay satellite has been described in Sec. 1.1. We will now describe the choice of the orbital parameters at the same initial epoch, and in the same coordinate system, for the close satellite at a height of about 900 km. The orbital parameters for the close satellite at a height of about 250 km were chosen similarly.

The initial values used were inclination $i = 115°$, eccentricity $e = .006$, and the nominal value of the semi-major axis $a = 7214$ km. The argument of preigee, ω, was obtained so that perigee occurred when the latitude of the subsatellite point was the same as the south bounding latitude, φ_s, of the area of investigation; i.e.,

$$\omega = \sin^{-1}(\sin\varphi_s / \sin i), \qquad -\pi/2 < \omega < \pi/2 \tag{2.51}$$

The right ascension of the ascending node, Ω, was obtained so that at the initial epoch (Greenwich siderial time = θ_0), the longitude of the subsatellite point was $\lambda_w + s/2$, where λ_w is the longitude of the western limit of the area of investigation and $s°$ is the size of the gravity anomaly blocks, say 10°.

$$\alpha' = \cos^{-1}(\cos\omega/\cos\varphi_s),\ -\pi/2 < \alpha' < \pi/2$$

$$\Omega = \lambda_w + s/2 + \theta_0 - \alpha' \qquad (2.52)$$

The value of the semi-major axis was optimized so that when the subsatellite trace starts again over the area of investigation, after completing its trajectory in longitude around the earth, it is offset from the initial trace computed in equations (2.51) and (2.52) by s°. This is obtained by first computing the ratio k' of the mean motion n of the satellite, to the siderial rotation rate $\dot{\theta}$ of the earth. The mean motion is corrected for the perturbation in mean motion, Δn, and the motion of perigee $\dot{\omega}$ due to the second zonal harmonic $C_{2,0}$ only. Lunisolar contributions are also included, but have not been shown in the equations given below. The ratio k' is rounded off to the nearest integer and $s^\circ/2\pi$ is reduced from it. If we now multiply it by $\dot{\theta}$ and remove Δn and $\dot{\omega}$ terms, we get the new value of mean motion $\bar{n}$, which will ensure the condition of the initial and next subsatellite traces starting over the area being offset by s°. The optimized value $\bar{a}$ of the semi-major axis is then obtained from $\bar{n}$ by Kepler's third law. The above algorithm may be represented by the following equations:

$$n = (kM)^{\frac{1}{2}}\, a^{-3/2}$$

$$\Delta n = \frac{3n\, C_{2,0}\, a_e^2}{4(1-e^2)^{3/2}\, a^2}\,(3\cos^2 i - 1)$$

$$\dot{\omega} = \frac{3n\, C_{2,0}\, a_e^2}{4(1-e^2)^2\, a^2}\,(1 - 5\cos^2 i)$$

$$k' = (\dot{n} + \Delta n + \dot{\omega})/\dot{\theta} \qquad (2.53)$$

$$k' = \text{integer part of } (k' + 1/2) - s^\circ/2\pi$$

$$\bar{n} = k'\dot{\theta} - \Delta n - \dot{\omega}$$

$$\bar{a} = (kM)^{1/3}\,(\bar{n})^{-2/3}$$

The algorithm represented by equations (2.51) to (2.53) has been described by Kaula (1972, pages 25, 26), and the initial orbital parameters for the close satellite in this study were computed using a shortened version of the subroutines kindly supplied by him. The optimized values of the Keplerian elements at the

initial epoch of 690921 (YYMMDD) 01 hr. 33 min. 36.3 sec. were:

$$\begin{aligned} a &= 7258.48...\text{km} & M &= 0.0 \\ e &= 0.006 & \omega &= 0.0 \\ i &= 115^\circ & \Omega &= 238^\circ.59... \end{aligned} \tag{2.54}$$

with the latitude and longitude of the subsatellite point being 0° and 215° E. respectively.

The corresponding inertial coordinates and velocities, in terms of the inertial coordinate system defined by the true of date coordinates of the reference date 690921.0, were:

$$\begin{aligned} X_{21} &= -3759.56...\text{km} & \dot{X}_{21} &= -2.689...\text{km/sec} \\ X_{22} &= -6157.99...\text{km} & \dot{X}_{22} &= 1.641...\text{km/sec} \\ X_{23} &= 0.0 ...\text{km} & \dot{X}_{23} &= 0.675...\text{km/sec} \end{aligned} \tag{2.55}$$

The period of orbit of this satellite was 102.4 minutes, the average altitude for ascending arcs was about 854 km and for the descending arcs, it was about 908 km. The observations pertaining to this close satellite have been used in Sec. 4.1 and Sec. 5.1.

The initial values for the close satellite at a height of about 250 km were $i = 115^\circ$, $e = .0005$, nominal value for $a = 6626$ km, and $s^\circ - 2^\circ.5$. The optimized values of the Keplerian elements at the initial epoch were:

$$\begin{aligned} a &= 6632.84...\text{km} & M &= 0.0 \\ e &= 0.0005 & \omega &= 0.0 \\ i &= 115^\circ & \Omega &= 248^\circ.88... \end{aligned} \tag{2.56}$$

with the latitude and longitude of the subsatellite point being 0° and $261^\circ.25$ E. respectively.

The corresponding inertial coordinates and velocities were:

$$\begin{aligned} X_{21} &= 1702.63...\text{km} & \dot{X}_{21} &= -3.167...\text{km/sec} \\ X_{22} &= -6407.16...\text{km} & \dot{X}_{22} &= -0.841...\text{km/sec} \\ X_{23} &= 0.0 ...\text{km} & \dot{X}_{23} &= 7.029...\text{km/sec} \end{aligned} \tag{2.57}$$

The period of orbit of this satellite was 89.5 min., and the average altitude was about 255 km. The observations pertaining to this arc have been used in Sec. 4.2 and Sec. 5.2.

2.3.2 Simulation of Observations

Having obtained the inertial position and velocity vectors at the initial epoch in equations (2.55) and (2.57), the inertial position and velocity vectors of the satellite at any later time could be obtained by integrating the equations of motion:

$$\ddot{X}_i = \frac{\partial V}{\partial X_i} = \frac{\partial U}{\partial X_i} + \frac{\partial T}{\partial X_i} \qquad (2.58)$$

where the symbols are the same as in equations (2.19) to (2.21). Initially, the purpose of this integration was to obtain the inertial position and velocity vectors over an extended period of time of 8 to 32 days, and to obtain the latitude and longitude of the subsatellite points at a specified interval, to determine the incidence of satellite trajectories over the area of investigation. After these trajectories were plotted, it was possible to choose the particular trajectories as in Chapters 4 and 5, and the approximate duration for which the observational data need to be simulated. As each ascending or descending satellite trajectory in the area would later be used as an individual arc, and the starting coordinates for these individual arcs would have no relation to each other, these starting coordinates need not be computed with full rigor. Accordingly, only the first term on the right hand side of equation (2.58) was used in this initial integration of the orbits of the close satellites, and also of the relay satellite, using the Cowell orbit generator program (Cigarski, Velez, 1967). As the gradient of the anomalous potential T, due to the residual gravity anomalies, was not used in these computations, it resulted in a very considerable saving of computer time (Sec. 6.2).

The Cowell orbit generator program is fully described in the above referenced publication and does not need any elaboration here. The integration model was kept as fixed order and fixed step. The order of integration for all the 3 satellites was kept as 11 (Velez, 1968, page 9), while the fixed step size was kept as 5, 1 and $\frac{1}{2}$ minutes respectively (Robinson, 1970) for the relay satellite, and the close satellites at heights of about 900 and 250 km.

For the simulation of 'observations' for 4 to 20 minutes along the arcs chosen for investigation in Chapters 4 and 5, the orbits of the satellites were integrated using the gradients of both the normal and anomalous potentials in equation (2.58), by the Geodyn program (Nov. 1972), which was modified to accept residual gravity anomalies. The expressions for $\partial U/\partial X_i$ are described in Geodyn Vol. I, Sec. 8.3.1 (1972). The expression for $\partial T/\partial X_i$ from equations (2.24), (2.29) and (2.30) is:

$$\frac{\partial T}{\partial X_i} = \frac{R}{4\pi} \frac{\partial r}{\partial X_i} \sum_k \Delta g'_k \left.\frac{\partial S}{\partial r}\right|_k d\sigma_k - \frac{\partial \varphi'}{\partial X_i} \sum_k \Delta g'_k \left.\frac{\partial S}{\partial \psi}\right|_k \cos\alpha_k \, d\sigma_k$$

$$- \frac{\partial \lambda}{\partial X_i} \cos\varphi' \sum_k \Delta g'_k \left.\frac{\partial S}{\partial \psi}\right|_k \sin\alpha_k \, d\sigma_k \qquad (2.59)$$

which may be evaluated using equations (2.25) to (2.28) and (2.31) to (2.35). Further, as in equation (2.36), the value of the derivatives of the Stokes' function in equation (2.59) were evaluated by quadrature by dividing the kth anomaly block into ℓ sub-blocks (4, 9, or 16 as per limiting values of ψ_k given below equation (2.36)):

$$\left.\frac{\partial S}{\partial r}\right|_k d\sigma_k = \sum_\ell \left.\frac{\partial S}{\partial r}\right|_\ell d\sigma_\ell$$

$$\left.\frac{\partial S}{\partial \psi}\right|_k \begin{Bmatrix} \cos\alpha_k \\ \sin\alpha_k \end{Bmatrix} d\sigma_k = \sum_\ell \left.\frac{\partial S}{\partial \psi}\right|_\ell \begin{Bmatrix} \cos\alpha_\ell \\ \sin\alpha_\ell \end{Bmatrix} d\sigma_\ell \qquad (2.60)$$

The gradient of the anomalous potential at a particular satellite position X_i in equation (2.59) should ideally be obtained by summation of the index k over the whole earth. However, the contribution of the distant gravity anomalies ($\psi_k > 30^\circ$) is small, and it is optimal (Hirvonen and Moritz, 1963) to include the anomalies up to spherical distance $\psi_k \leq 30^\circ$ from the subsatellite point. Further, in the present study, the normal potential U in equation (2.58) includes the coefficients up to degree and order 12, and thus models the global effects. The summation in equation (2.59) using residual gravity anomalies $\Delta g'_k$ (equation (2.22)) could then be restricted to a still smaller value for ψ_k. However, for all investigations in this study, the residual gravity anomalies were included up to a spherical distance 30° around the area of investigation. This will be further explained in Sec. 3.4.

The actual simulation of observations in the modified Geodyn program was done by first writing on a magnetic tape, in the Geos-2 data center format (Geodyn Systems Description Vol. III pages C-22 to C-26, 1972), zero value for observations of summed range rate, or summed range, for all times for which observations were required to be simulated. These zero observations were then used in the data reduction mode of the Geodyn program, with the earth's gravity field described by residual gravity anomalies up to 30° all around the area of investigation, besides the spherical harmonic potential coefficients up to degree and order 12 (hereafter referred to as (12, 12) potential coefficients. The

orbits of the relay and close satellite were then generated in this gravity field using equations (2.58) to (2.60), and the computed values of summed range rate $\dot{R}_s$, or summed range R_s, were obtained as in equation (2.8) and (2.3) corresponding to the times of the zero observations. The misclosures between the zero observations and the corresponding computed values were then written out on another tape, which was subsequently reformatted in the Geos-2 data center format to give the required simulated observations. A subset of the simulated observations could be prepared by deleting some observations near the beginning or ending of the 'satellite arc' for the subsatellite points to lie within specified bounding values.

2.3.3 Reduction and Adjustment of Data

The simulated observations for the desired number of satellite arcs could then be processed in another Geodyn program in the data reduction mode, with the earth's gravity field now described only by the (12, 12) potential coefficients. The computed value of $\dot{R}_s$, or R_s, now refers to the approximate value of the residual gravity anomalies as zero, and the misclosure vector from the simulated observations is obtained as outlined in Sec. 2.1.1. The variational equations (2.19) for the arc parameters, and the desired number of residual gravity anomalies, are integrated along with the integration of the equations of motion for the satellite orbits. The order of integration for the variational equations was kept as 11 as in the equations of motion, but the step size was increased to 75 and 35 seconds, from 60 and 30 seconds for the equations of motion, for the close satellites at heights of about 900 and 250 km respectively.

The normals matrix and the constant vector of equation (2.47), are formed by a summation process by the contributions of observations from each arc, and the accumulated values are written out on magnetic tape after the processing of observations of each arc, starting from the first arc. It is therefore possible to separate out the contributions to the normals matrix and the constant vector for each arc individually, and then, if so desired, to combine them in any order after deleting the contributions of the observations of any arc, if required.

After the normals and constant vector are finally formed for the desired number of arcs, we may invert the normals matrix and solve for the unknown parameters, the residual gravity anomalies in this study, as in equation (2.47). We may also like to solve for a smaller subset of anomalies. This is possible without having to form the normals and constant vector afresh. We may visualize it with refernce to equation (2.1), where if the k^{th} parameter is not required to be included in the solution, we may delete the k^{th} element in the solution and constant vectors X and U, and the k^{th} row and column of the normals matrix N. The process may be repeated till all the required number of elements in X and U, and all the rows and columns of N, are deleted for all the parameters not required to be included in the solution. In actual practice, advantage is taken of the symmetry of the normals matrix in reducing the computer core storage, by storing column-wise only the lower triangular portion of the normals matrix in a 'packed' vector form. Careful manipulation is then required to ensure that

only the required elements of the rows and columns pertaining to the parameters being deleted from the solution, are removed from their respective locations from the packed vector form of the normals matrix; and after their removal the normals matrix is 'repacked' correctly.

3. GRAVITY ANOMALIES FOR DATA SIMULATION

3.1 10°, 5° and $2^\circ.5$ Equal Area Blocks

The residual gravity anomalies $\Delta g'$ used in this study were a set of terrestrial free air gravity anomalies Δg_T, from which we have subtracted the value of gravity anomaly Δg_{PC} implied by a set of reference potential coefficients considered as known constant values, i.e.

$$\Delta g' = \Delta g_T - \Delta g_{PC} \tag{3.1}$$

The set of terrestrial gravity anomalies were mean anomalies defined over equal area blocks. We first consider a 10° equal area block in terms of a $10^\circ \times 10^\circ$ 'basic' block, as defined by Rapp (1971b). Its latitude limits were defined by the equator and $\pm 10^\circ$ parallel of latitude, and longitudinal extent as 10° starting from the Greenwich meridian and proceeding east. The latitudinal extent of all other blocks was everywhere 10° starting from equator, and proceeding north or south. The longitudinal extent $\Delta\lambda$ of a block was determined to meet 3 requirements, i.e. its area A_s will be nearly equal to the area of the basic block A_B; there will be integer number of blocks n in each latitude zone; and starting from the Greenwich meridian and proceeding east, its eastern longitude λ_E will be an integer number of degrees. Denoting the north and south limits of a block by φ_N and φ_S and its east and west limits by λ_E and λ_W, the above requirements may be expressed as:

$$A_s = \int_{\varphi_S}^{\varphi_N} \int_{\lambda_W}^{\lambda_E} \cos\varphi \, d\varphi \, d\lambda = \Delta\lambda (\sin\varphi_N - \sin\varphi_S)$$

$$= A_B = \frac{10^\circ}{\pi} \sin 10^\circ,$$

$$\Longrightarrow \quad \Delta\lambda = A_B/(\sin\varphi_N - \sin\varphi_S)$$

$$n = \text{integer part of } (360^\circ/\Delta\lambda^\circ + 0.5) \tag{3.2}$$

$$\Delta\lambda^\circ = 360^\circ/n$$

$$\lambda^\circ_{E_i} = \text{integer part of } (i\Delta\lambda^\circ + 0.5), \; i = 1, \; n-1,$$

$$\lambda^\circ_{E_n} = 360^\circ$$

We next consider a 5° equal area block. This was defined as in Hajela (1973), to be 4 component blocks of a 10° equal area block. The latitudinal extent of all 5° equal area blocks was then 5° starting from the equator and proceeding north or south. The longitudinal extent was however fixed to ensure

that the extreme limits of the 4 component 5° equal area blocks, on the west and the east, were the same as that of the 10° equal area block; and the limit in the center of the 10° equal area block was obtained to be half of its longitudinal extent rounded off to the nearest integer degrees. Figure 3.1 clarifies these divisions.

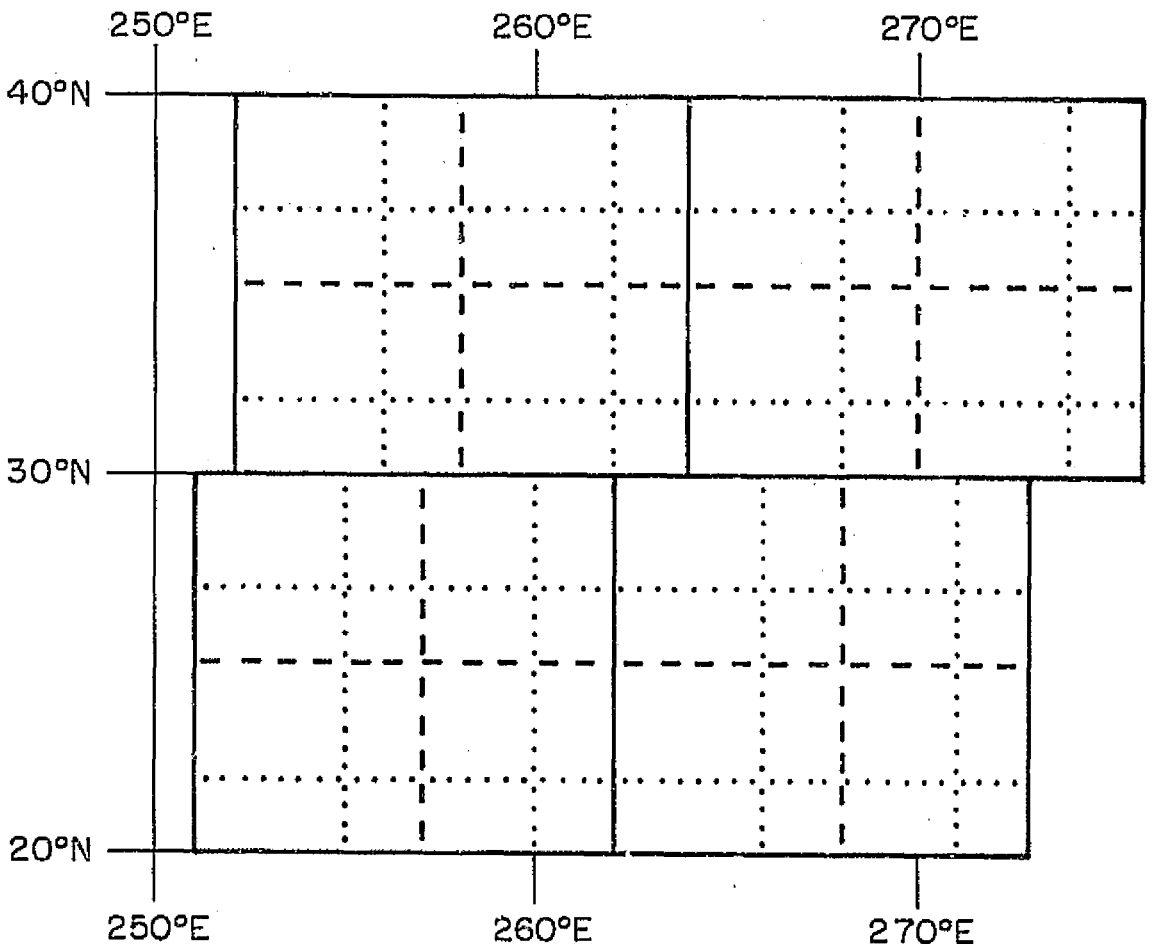

Figure 3.1 Scheme of Subdivision of 10° Equal Area Blocks Into 5° and 2°.5 Equal Area Blocks.

This scheme of obtaining 5° equal area blocks as 4 components of a 10° equal area block does result in the area of several 5° blocks not closely fulfilling the equal area condition, as shown in the last column of Table 2B, page 7 of Hajela (1973). This scheme however, enables the gravity anomaly of 4 5° blocks to be meaned to give the gravity anomaly of a 10° block, which is very useful.

The $2^\circ.5$ equal area blocks were similarly obtained as 4 component blocks of a 5° equal area block. The 5° equal area blocks had been subdivided into 25 1° equal area blocks for the purpose of prediction of anomalies, as described in Sec. 3, page 4 of Rapp (1972). These 25 1° equal area blocks were then grouped into 9 blocks to give the north-west component $2^\circ.5$ block, 6 blocks each to give the north-east and south-west component $2^\circ.5$ block, and 4 blocks to give the south-east component $2^\circ.5$ block. This scheme resulted in the $2^\circ.5$ equal area blocks being considerably unequal in area, but the basic characteristic of being able to mean the gravity anomalies, after weighting according to area, from smaller blocks to successively larger blocks was maintained. Thus the values in $1^\circ \times 1^\circ$ equiangular blocks could be meaned to give the value in a 1° equal area block, and latter values could be successively meaned to give the values for $2^\circ.5$, 5° and 10° equal area blocks. The scheme of subdivision into component blocks has been shown in Figure 3.1 illustrating 4 10° equal area blocks, 16 5° equal area blocks and 64 $2^\circ.5$ equal area blocks. The word 'equal area' blocks has been retained to differentiate from equiangular blocks. However, as we shall be using throughout this study only the equal area blocks as per the scheme shown in Figure 3.1, we may also refer to them simply as 10°, 5°, and $2^\circ.5$ blocks, unless the word 'equal area' adds clarity to the description.

3.2 Reference Potential Coefficients Set and 10° Equal Area Residual Anomalies

The set of potential coefficients used as a reference to describe the earth's gravitational field, were those obtained by least squares collocation by Rapp (1973a). The mean gravity anomaly Δg_{PC} of a block, bounded by geocentric latitudes φ'_N, φ'_S and longitudes λ_E, λ_W, as implied by the potential coefficients up to degree N_{max}, is given by (Desrochers, 1971, page 13):

$$\Delta g_{PC} = \Delta g_0 + \frac{\gamma}{\Delta\lambda(\sin\varphi'_N - \sin\varphi'_S)} \sum_{n=2}^{N_{max}} (n-1) \left[\Delta\lambda\, \overline{C}^{*}_{n,0} \int_{\varphi'_S}^{\varphi'_N} \overline{P}_{n,0}(\sin\varphi')\cos\varphi'\, d\varphi' \right.$$

$$+ \sum_{m=1}^{n} \frac{1}{m} \left\{ \overline{C}_{n,m} (\sin m\lambda_E - \sin m\lambda_W) - \overline{S}_{n,m} (\cos m\lambda_E - \cos m\lambda_W) \right\} \qquad (3.3)$$

$$\left. \cdot \int_{\varphi'_S}^{\varphi'_N} \overline{P}_{n,m}(\sin\varphi')\cos\varphi'\, d\varphi' \right]$$

where

$$\Delta\lambda = \lambda_E - \lambda_W,$$

other symbols have the same meaning as in equation (2.20); Δg_0 is the average value of the mean gravity anomaly for the block size over the whole earth, $\overline{C}^*_{n,0}$ are the fully normalized zonal harmonics from which $\overline{C}_{2,0}$ and $\overline{C}_{4,0}$ have been subtracted for the reference ellipsoid, whose flattening f, is the same as used in the gravity formula for the terrestrial gravity anomalies. These are given by (Mueller, 1964):

$$\overline{C}_{2,0} = -\frac{1}{\sqrt{5}}\left(\frac{2}{3}f - \frac{m}{3} + \frac{3}{7}fm - \frac{1}{3}f^2 + \ldots\right) \tag{3.4}$$

$$\overline{C}_{4,0} = -\frac{1}{\sqrt{9}}\left(\frac{4}{7}fm - \frac{4}{5}f^2 + \ldots\right) \tag{3.5}$$

where

$$m = \frac{\omega^2 a_e^3}{kM}, \tag{3.6}$$

and ω is the rotational velocity of the earth.

The constants used for the reference ellipsoid and the gravity formula were as used by Rapp (1972):

$$\begin{aligned} a_e &= 6,378,137.8\ \text{m} \\ f &= 1/298.258 \\ kM &= 3.986,013 \times 10^{14}\ \text{m}^3/\text{sec}^2 \\ \omega &= 7.292,115,146,7 \times 10^{-5}\ \text{rad/sec} \\ \gamma_e &= 978,033.51\ \text{mgals} \end{aligned} \tag{3.7}$$

$$\gamma = \gamma_e(1 + .005,302,43\sin^2\varphi - .000,005,87\sin^2 2\varphi) \tag{3.8}$$

We now consider the maximum degree N_{max} up to which the potential coefficients should be used. N_{max} should be large enough so that the R.M.S. value of $\Delta g'$ in equation (3.1) is as small as possible, so that when its approximate value is taken as zero in the adjustment scheme described in Sec. 2.2, the linearized form of equations (2.39) is adequate to give a solution vector without requiring iteration. On the other hand, N_{max} should not be larger than the degree of well determined potential coefficients from satellite data, nor larger than $146/s^\circ$ (Rapp, 1973b), where s° is the size of the mean gravity anomaly block. From the above considerations N_{max} should not exceed 14, as we would be using up to 10° blocks; and preferably not exceed 12, as from Rapp (1973a), we find that after degree 12, the number of potential coefficients having larger standard deviations than their magnitude increase rapidly.

The 10° terrestrial gravity anomalies, Δg_T, were those described by Hajela (1973, Table 8, pages 20 to 23). The mean value Δg_o for these anomalies was -1.4 mgals and R.M.S. value was 11.3 mgals (Table 7, ibid). If we subtract from these Δg_T, the values of Δg_{PC}, computed as in equation (3.3) with potential coefficients up to degree and order 12, we get the values of 10° residual anomalies $\Delta g'$ as in equation (3.1). The minimum, maximum, range and the R.M.S. values of $\Delta g'$ were reduced from the corresponding values of Δg_T as shown in Table 3.1, but the reduction was not large.

Table 3.1

Statistics for 10° Equal Area Mean Terrestrial and Residual Gravity Anomalies Using Potential Coefficients up to Degree and Order 12

	Terrestrial gravity anom. Δg_T (mgals)	Residual gravity anom. $\Delta g' = \Delta g_T - \Delta g_{PC}$ (mgals)
Maximum value	34	21
Minimum value	-41	-33
Range	75	54
Mean value	-1.4	0
R.M.S. value	11.3	8.3

It was then considered if in the formation of 10° terrestrial anomalies, we should have imposed conditions that the low degree potential coefficients, as generated from the terrestrial anomalies, should be the same as the well determined values from satellite data. This was done according to Snowden and Rapp (1968), which ensured:

$$\frac{1}{4\pi\gamma(n-1)} \iint_\sigma \Delta g_T \, \overline{P}_{nm}(\sin\varphi') \begin{Bmatrix} \cos m\lambda \\ \sin m\lambda \end{Bmatrix} d\sigma - \begin{Bmatrix} \overline{C}^*_{nm} \\ \overline{S}_{nm} \end{Bmatrix} = 0 \qquad (3.9)$$

for $m \le n$, $2 \le n \le N_{max}$, $\overline{C}^*_{2,0}$ and $\overline{C}^*_{4,0}$ reduced for $\overline{C}_{2,0}$ and $\overline{C}_{4,0}$ as in equations (3.4) and (3.5), and

$$\frac{1}{4\pi} \iint_\sigma \Delta g_T \, \overline{P}_{nm}(\sin\varphi') \begin{Bmatrix} \cos m\lambda \\ \sin m\lambda \end{Bmatrix} d\sigma = \begin{Bmatrix} \overline{a}_{nm} \\ \overline{b}_{nm} \end{Bmatrix} = 0 \qquad (3.10)$$

for $n = 1$, $m = 0, 1$,

and

$$\frac{1}{4\pi}\iint_{\sigma} \Delta g_T \, d\sigma - \Delta g_0 = 0 \qquad (3.11)$$

The adjustment of Δg_T was done for equations (3.9) to (3.11) for 3 values of N_{max}, i.e. 4, 8 and 12, which we may refer to as $\Delta g^{A}_{4,4}$, $\Delta g^{A}_{8,8}$, $\Delta g^{A}_{12,12}$ respectively. The value of residual gravity anomalies $\Delta g'_{n,n}$, n = 4, 8, 12 was then obtained from equation (3.1), where Δg_{PC} was computed from equation (3.3) using (12,12) potential coefficients for all the 3 cases, i.e.,

$$\Delta g'_{n,n} = \Delta g^{A}_{n,n} - \Delta g_{PC}(12,12), \quad n = 4, 8, 12$$

The statistics for $\Delta g^{A}_{n,n}$ and $\Delta g'_{n,n}$ have been given in Table 3.2.

Table 3.2

Statistics for 10° Equal Area Mean Residual Gravity Anomalies and Terrestrial Gravity Anomalies Adjusted for (4,4), (8,8) and (12,12) Potential Coefficients

	$\Delta g^{A}_{4,4}$	$\Delta g'_{4,4}$	$\Delta g^{A}_{8,8}$	$\Delta g'_{8,8}$	$\Delta g^{A}_{12,12}$	$\Delta g'_{12,12}$
Maximum value	35	22	40	19	38	26
Minimum value	-42	-32	-45	-27	-60	-25
Range	77	54	85	46	98	51
Mean value	-1.4	0	-1.4	0	-1.4	0
R.M.S. value	12.4	7.8	14.0	7.17	15.4	7.11

Units are mgals.

We note from Table 3.2 that the lowest R.M.S. value of 7.1 mgals occurs for $\Delta g'_{12,12}$, i.e. when the terrestrial anomalies have been adjusted to (12,12) potential coefficients according to equations (3.9) to (3.11), though this is not very much lower than 8.3 mgals in Table 3.1, when the terrestrial anomalies were computed as in Hajela (1973) without imposing the conditions in equations (3.9) to (3.11). The residual anomalies used in Sec. 4.1 were however computed after imposing these conditions, as described later.

The value of $\int \overline{P}_{nm}(\sin\varphi') \cos\varphi' \, d\varphi'$ in equation (3.3) was computed using Gaussian quadrature formulas for 24 points, according to constants given in subroutine DQG24 in I.B.M. Scientific Subroutine Package (Version III, p. 302, 1970). To get the mean residual gravity anomaly in 10° blocks, say $\Delta g'_{10°}(I)$, we may use $\Delta g_{T_{10°}}$ and subtract $\Delta g_{PC_{10°}}$ computed for the 10° blocks using equation (3.3). This was done in Table 3.1. Alternatively, we may use terrestrial anomalies in the 4 component 5° blocks of a 10° block, say $\Delta g_{T_{5°}}$; and subtract from these the

values of $\Delta g_{PC_{5^\circ}}$, computed for 5° blocks using equation (3.3), to obtain the residual gravity anomalies in 5° blocks, $\Delta g'_{5^\circ}$. We may then form $\Delta g'_{10^\circ}$ (II) using the residual anomalies $\Delta g'_{5^\circ}$ in the 4 component 5° blocks of area $d\sigma_{5^\circ}$ by:

$$\Delta g'_{10^\circ}(\mathrm{II}) = \sum_{i=1}^{4} (\Delta g'_{5^\circ_i}\, d\sigma_{5^\circ_i}) \Big/ \sum_{i=1}^{4} d\sigma_{5^\circ_i} \qquad (3.12)$$

The difference $\Delta g'_{10^\circ}$ (I) - $\Delta g'_{10^\circ}$ (II) has been given in Table 3.3.

Table 3.3

10° Equal Area Mean Residual Gravity Anomalies.
Difference for Direct Computation Over 10° Block Δg_{10° (I)
Minus Meaned Value Over Component 5° Blocks, $\Delta g'_{10^\circ}$ (II)

Maximum value	3.1	mgals
Minimum value	-4.2	"
Range	7.3	"
Mean Value	0.0	"
R.M.S. value	0.6	"
No. of + elements	106	
No. of 0 elements	183	
No. of − elements	127	

The differences in Table 3.3 indicate the advisability of computing Δg_{PC} in equation (3.3) in 5° blocks, in contrast to 10° blocks. Accordingly, the global set of 1664 5° terrestrial anomalies was first computed as in Hajela (1973, Sec. 4). These 5° anomalies were then adjusted to satisfy equations (3.9) to (3.11) for the reference set of (12,12) potential coefficients. The residual anomalies in 5° blocks, $\Delta g'_{5^\circ}$, were obtained from these adjusted 5° terrestrial anomalies by subtracting $\Delta g_{PC_{5^\circ}}$, computed from equation (3.3). The global set of 416 10° residual anomalies were finally obtained from $\Delta g'_{5^\circ}$, using equation (3.12). 130 10° residual anomalies from this set will be used in Section 4.1.

3.3 2°.5, 5° and 10° Equal Area Residual Anomalies

The adjustment of terrestrial anomalies by equations (3.9) to (3.11) over the whole earth requires much computer time for small size blocks like 2°.5, when 4 x 1664 = 6656 anomalies have to be adjusted. We should then consider the formation and recovery of residual anomalies over regional areas. Also, as it is advisable to compute equation (3.3) over smaller blocks, it would be preferable to compute residual anomalies $\Delta g'$ directly over 1° equal area blocks, by considering Δg_T over these blocks as in Hajela (1973), and then using equations (3.3) and (3.1). As later (Tscherning and Rapp, 1974, p. 5) terrestrial gravity

data was now available than used in Hajela (1973), fresh estimates of 1° equal area terrestrial gravity anomalies were formed using this later data. If we did not have terrestrial gravity observations over any 1° equal area block, say $_p$, we could then predict the residual anomaly Δg_p^* directly from other computed residual anomalies in a 5° equal area block, according to Moritz (1969), Rapp (1972), by:

$$\Delta g_p^* = C_p (C+D)^{-1} \Delta g', \tag{3.13}$$

where $\Delta g'$ is the vector of already computed residual anomalies inside the 5° block. C_p is the vector of covariances of 1° equal area residual anomalies for the spherical distances between the $_p{}^{th}$ block, and the location of already computed residual anomalies inside the 5° block, C is the matrix of covariances of 1° equal area residual anomalies for spherical distances corresponding to the location of already computed residual anomalies. D is a diagonal matrix with the square of estimated standard deviation of already computed residual anomalies on the diagonal. As Δg_{pc} in equation (3.1) is computed from known constant values of the potential coefficients, the estimated standard deviation of 1° equal area residual anomalies was kept the same as that of the corresponding terrestrial anomalies.

The computation of the residual anomalies of 5° and 10° equal area blocks from the computed/predicted residual anomalies of 1° equal area blocks, was then done according to equations (9) and (12) of Hajela (1973). The computation of $2^\circ.5$ equal area residual anomalies, $\Delta g'_{2.5^\circ}$, was done from the 1° equal area residual anomalies $\Delta g'_{1^\circ}$ by:

$$\Delta g'^{\circ}_{2.5} = \frac{\sum_j \cos\varphi_{mj} \sum_i \Delta g'^{\circ}_{1_t}}{\sum_j \cos\varphi_{mj}} \tag{3.14}$$

where φ_{mj} was the mean latitude of the j^{th} 1° belt; $j=2$ or 3, was the number of 1° latitude belts in a $2^\circ.5$ equal area block; and $i=2$ or 3 was the number of 1° equal area residual anomalies in the j^{th} 1° belt of the $2^\circ.5$ equal area block.

The computation of the covariance function for 1° equal area residual anomalies, which was needed in equation (3.13), may now be described. The covariance function for the 1° equal area terrestrial anomalies was provided by Tscherning and Rapp (1974, Table 15, p.73). If we represent it by $C(\psi)$, where ψ is the spherical distance, we have (Heiskanen and Moritz, 1967, p.256):

$$C(\psi) = \sum_{n=2}^{\infty} c_n P_n(\cos\psi), \tag{3.15}$$

where c_n are the anomaly degree variances given (ibid, p. 259) by:

$$c_n = \sum_{m=0}^{n} (\bar{a}^2_{nm} + \bar{b}^2_{nm})$$

$$= \gamma^2 (n-1)^2 \sum_{m=0}^{n} (\bar{C}^{*2}_{nm} + \bar{S}^2_{nm}), \tag{3.16}$$

where the symbols have been defined earlier in equation (2.20), (3.3) and (3.9). Finally, $P_n(\cos\psi)$ are the Legendre's polynomials, which may be computed from the recursion formula (ibid, p.23):

$$P_n(\cos\psi) = -\frac{n-1}{n} P_{n-2}(\cos\psi) + \frac{2n-1}{n} \cos\psi \, P_{n-1}(\cos\psi), \tag{3.17}$$

with starting values from

$$P_0(\cos\psi) = 1, \quad P_1(\cos\psi) = \cos\psi \tag{3.18}$$

As the residual anomalies have been obtained from the terrestrial anomalies by subtracting the anomaly implied by (12,12) potential coefficients, the covariance function for the residual anomalies $C'(\psi)$ is simply obtained by:

$$C'(\psi) = \sum_{n=13}^{\infty} c_n P_n(\cos\psi) = C(\psi) - \sum_{n=2}^{12} c_n P_n(\cos\psi)$$

$$= C(\psi) - \gamma^2 \sum_{n=2}^{12} P_n(\cos\psi) \cdot (n-1)^2 \sum_{m=0}^{n} (\bar{C}^{*2}_{nm} + \bar{S}^2_{nm}) \tag{3.19}$$

The values of c_n, $n = 2, 12$ computed from the potential coefficients were taken directly from Rapp (1973a). The values of the covariance function for the 1° equal area terrestrial and residual anomalies for spherical distance up to 8° have been given in Table 3.4.

Table 3.4

Covariance Function for 1° Equal Area Terrestrial and Residual Anomalies Using Potential Coefficients up to Degree and Order 12

Spherical Distance ψ°	Covariance for Terrestrial Anomalies $C(\psi)$ mgals^2	Covariance for Residual Anomalies $C'(\psi)$ mgals^2
0.0	919.7	754.1
0.5	671.6	506.2
1.0	493.4	328.4
1.5	368.2	204.0
2.0	285.4	122.2
2.5	236.1	74.3
3.0	211.4	51.3
3.5	200.7	42.6
4.0	193.4	37.5
4.5	176.9	23.5
5.0	155.9	5.2
5.5	146.4	-1.3
6.0	141.4	-3.0
6.5	133.4	-7.6
7.0	124.9	-12.4
7.5	119.9	-13.6
8.0	117.4	-12.1

The value of $\int \overline{P}_{nn}(\sin\varphi')\cos\varphi' d\varphi'$ in equation (3.3) for latitudinal extent of 1° was now computed using Gaussian quadrature formulas with 4 points, according to constants given in subroutine DQG4 in I.B.M. Scientific Subroutine Package (Version III, p.300, 1970). The values of residual anomalies for 2°.5, 5° and 10° equal area blocks computed in this Section will be used in Sec. 4.2 and Chapter 5.

3.4 Extent of Anomalies for Simulation of Observations

As mentioned in Sec. 2.3.2, all observations used in Chapters 4 and 5 were simulated using (12,12) potential coefficients, and residual gravity anomalies up to 30° spherical distance beyond the area of investigation. We may now examine the utility of subdividing a large size anomaly block into component blocks of smaller size. Summed range rate observations, with close satellite at height of about 900km, were simulated for 2 satellite arcs, using (12,12) potential coefficients with 108 5° residual anomalies. In this case (Case 1), 40 5° residual anomalies covered the area of interest, traversed by subsatellite points of the

close satellite, and up to 10° spherical distance all around the area of interest. The balance 68 5° residual anomalies covered an area from 10° to 20° spherical distance all around the area of interest. In the second case (Case 2), the summed range rate observations were simulated for the same configuration, with (12,12) potential coefficients and 40 5° residual anomalies covering the area of interest and up to 10° spherical distance all around it. However, the 68 5° residual anomalies, 10° to 20° around the area of interest were replaced in Case 2 by 17 10° residual anomalies, meaned from the 68 5° blocks. The residual anomalies in Cases 1 and 2 are shown in Figure 3.2. The difference in summed range rate observations (Case 1 - Case 2) is shown in Table 3.5.

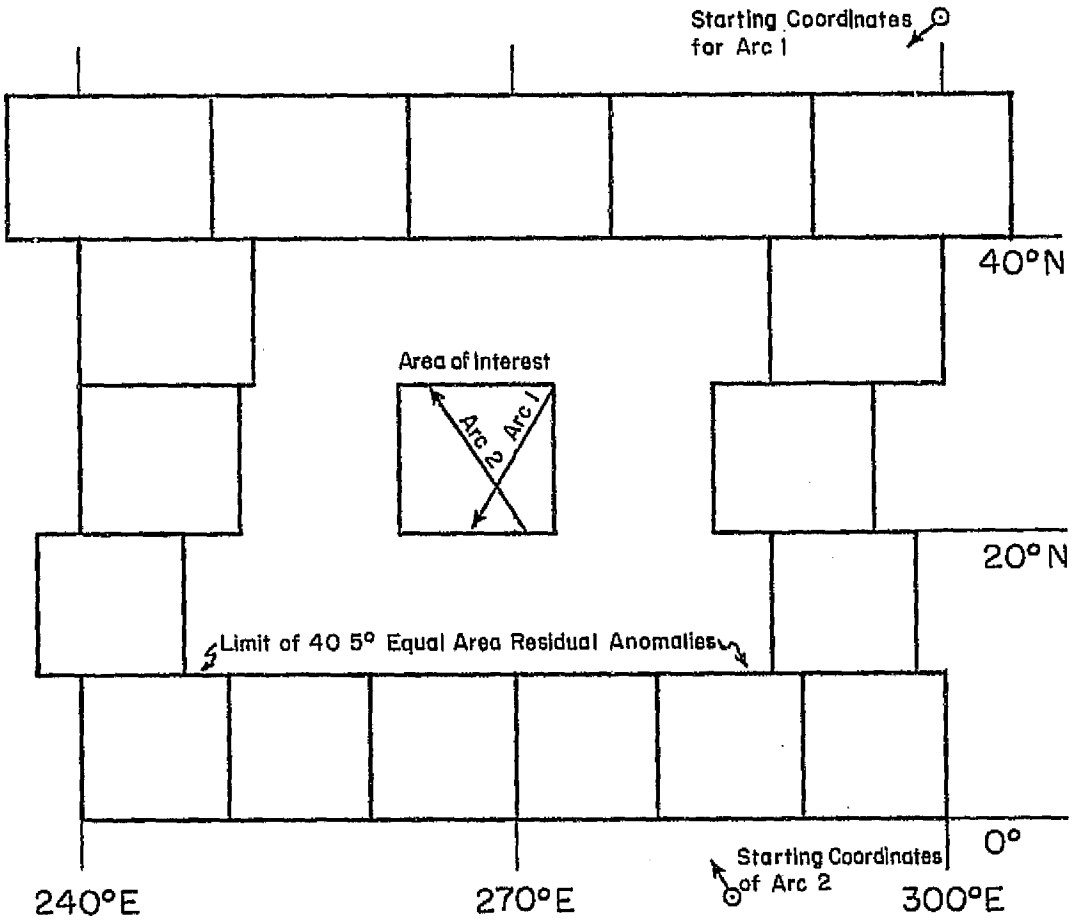

Figure 3.2 40 5° Equal Area Residual Anomalies Surrounded by 68 5° Equal Area Residual Anomalies (Case 1), or by 17 10° Equal Area Residual Anomalies (Case 2). Case 2 has been shown in the figure.

Table 3.5

Effect of Replacing 5° Component Residual Anomalies by 10° Residual Anomalies in Border Around Area of Interest. Summed Range Rate Differences, $\Delta\dot{R}_s$, in cm/sec. for 2 Arcs. Height of Close Satellite $\approx$ 900 km

ARC 1			ARC 2		
Time in Orbit (min.)	$\dot{R}_s$ (cm/sec.)	$\Delta\dot{R}_s$ (cm/sec.)	Time in Orbit (min.)	$\dot{R}_s$ (cm/sec.)	$\Delta\dot{R}_s$ (cm/sec.)
0.0	-429,601.11	0.008	0.0	242,740.97	-0.067
0.5	-406,451.67	0.005	0.5	267,327.63	-0.069
1.0	-382,674.46	0.002	1.0	293,476.90	-0.072
1.5	-358,300.73	-0.001	1.5	319,147.67	-0.075
2.0	-333,363.75	-0.002	2.0	344,300.73	-0.079
2.5	-307,898.79	-0.003	2.5	368,898.84	-0.085
3.0	-281,943.08	-0.004	3.0	392,906.82	-0.090

As the differences in summed range rate in Table 3.5 are less or about the same as standard deviation ($\leq 1\sigma$ level), we may replace the outer-most component 5° residual anomalies by the 10° residual anomalies. This reduced computer time from 1 min. 30.0 sec. to 0 min. 52.8 sec., i.e., by about 41%, in the test reported in Table 3.5. For simulating the summed range rate observations used in Sec. 4.2 and Sec. 5.1, in addition to the (12, 12) potential coefficients, 12 5° residual anomalies covered the area of interest, surrounded by 40 5° residual anomalies up to 10° spherical distance around the area of interest; and these were in turn surrounded by 37 10° residual anomalies from 10° to 30° spherical distance around the area of interest. These limits have been shown later in Figures 4.12 and 4.14 in Sec. 4.2.

The summed range rate observations used in Sec. 5.2 were similarly simulated using (12, 12) potential coefficients, and 104 $2^\circ.5$ residual anomalies covering the area of interest, and an area of 5° spherical distance all around the area of interest. These were surrounded by 26 5° residual anomalies covering the area from spherical distance 5° to 10° all around the area of interest; and finally, 37 10° residual anomalies covered the area from spherical distance 10° to 30° all around the area of interest. The limits of these $2^\circ.5$, 5° and 10° residual anomalies are shown in Figure 3.3.

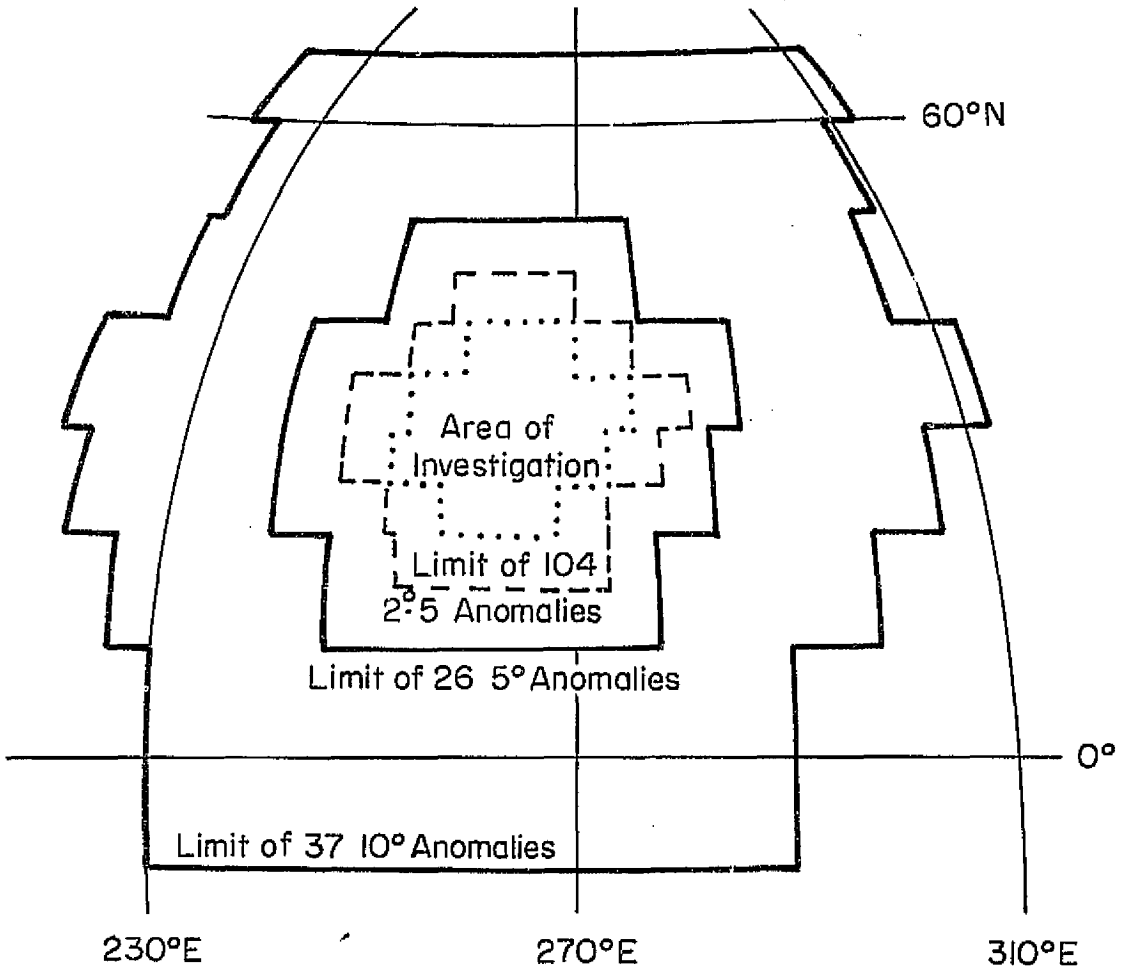

Figure 3.3 Extent of 2°.5, 5° and 10° Equal Area Residual Anomalies for Simulating Observations in Sec. 5.2 Up To 30° Spherical Radius All Around the Area of Investigation for the Recovery of 2°.5 Equal Area Anomalies.

4. RECOVERY OF GRAVITY ANOMALIES FROM STRONG SIGNAL

We discuss in this chapter the recovery of 10° and 5° equal area mean anomalies using the close satellite at heights of about 900 km and 250 km respectively. The recovery of 5° and 2°.5 equal area mean anomalies from the close satellite at heights of about 900 km and 250 km will be discussed in Chapter 5. The effect of 5° equal area mean anomalies on summed range rate, and summed range, observations will be stronger when the close satellite is at a height of 250 km, as compared to the case when the close satellite is at a height of about 900 km. We may therefore investigate various considerations and test procedures for anomaly recovery when the signal is strong, and apply these later to the case when the signal is comparatively weaker, making further modifications, as necessary.

We start in Sec. 4.1 with the discussion of recovery of 10° equal area mean anomalies with the close satellite at a height of about 900 km. We will first investigate the effect on anomaly recovery in regional areas, if we constrain the recovered anomalies to give zero value for some low degree harmonic coefficients, as discussed in Sec. 2.2.3. We will then investigate how effective summed range observations are in comparison to the summed range rate observations for recovering anomalies. The conclusions with respect to these two points will be given in the end of Sec. 4.1.5.

We will next consider the design of 'arcs', or the spacing of observations in an arc, as the close satellite orbits over the area of investigation, and also consider the spacing between arcs; and how these affect the anomaly recovery. We will then test various cases of anomaly recovery as affected by the relative location of observations and the anomalies being estimated; and arrive at the optimum model for recovery of 10° equal area mean anomalies. The conclusions reached in Sec. 4.1 would then be applied in Sec. 4.2 to the recovery of 5° equal area mean anomalies with the close satellite at a height of 250 km.

The summed range rate observations were used at 1 minute interval in Sec. 4.1 for the recovery of 10° anomalies. The standard deviation of these observations may then have been considered as .03 cm/sec., based on an integration interval of 1 min., instead of .08 cm/sec. based on an integration interval of 10 sec. This has been later discussed at the end of Sec. 4.1.9, and would simply result in the standard deviation of all recovered 10° anomalies being reduced by a factor of 3/8.

4.1 Recovery of 10° Equal Area Mean Anomalies From Close Satellite at Height of 900 km

4.1.1 Area of Investigation

The area chosen for investigation was centered on latitude 30°N. and longitude 270°E. (90°W.). Its latitudinal extent was 70° from 10°S. to 60°N., and longitudinal extent about 60° from 240° to 300°E. The longitudinal limits

varied slightly in each 10° latitude zone, according to the actual limits of the 10° equal area anomaly blocks in accordance with the scheme described in Sec. 3.1. The total number of 10° anomalies in this area was 37, and these were numbered from west to east in each latitude zone starting from the north-west of the area, and proceeding south. The limits of these anomalies, the center of the blocks and the numbering system have been shown in Figure 4.1. The figure also shows 'satellite arcs' described below.

4.1.2 Satellite Arcs

A total of 14 arcs were selected so that these were positioned symmetrically in the area. There were 7 ascending arcs, with the subsatellite point moving from south-east to north-west; and 7 descending arcs with the subsatellite point moving from north-east to south-west. The number of arcs selected gave a longitudinal spacing of about 6° between two adjacent ascending (or 2 adjacent descending) arcs in the center of the area, which was close to half the longitudinal extent of the 10° equal area anomaly blocks. If we consider all 14 arcs, i.e. summed range rate, or summed range, observations at specified time intervals over all 14 arcs, there would in general be portions of 2 ascending and 2 descending arcs over each anomaly block in the central area, and portions of 2 ascending (or 2 descending) arcs over each anomaly block in the 4 corners. If we remove alternate ascending and descending arcs, and consider the remaining 8 arcs, the portions of arcs over any specific anomaly block would be halved when compared to the density obtained with 14 arcs. To enable convenient numbering of arcs for investigation of anomaly recovery with different arc spacing, the latter 8 arcs were numbered from 1 to 8, and the balance 6 arcs out of the total of 14 arcs were numbered from 9 to 14.

The 14 arcs with their numbers, and the direction of arrow to distinguish an ascending or descending arc, are shown in Figure 4.1. The inter-se numbering in Arcs 1 to 8 and in Arcs 9 to 14 was according to the starting time of the arc. The arcs were chosen to be of 19 minutes duration or more, so that if the summed range rate, or summed range, observations (hereafter 'observations') were considered at 1 minute interval, there would be at least 20 observations in an arc. No arcs were thus selected west of Arc No. 2 and Arc No. 4, or east of Arc No. 5 and Arc No. 7. The reason for choosing 1 minute interval of observations will be clarified in Sec. 4.1.3. The starting time and duration of each arc, and the latitude and longitude of first and last subsatellite point in each arc, are given in Table 4.1.

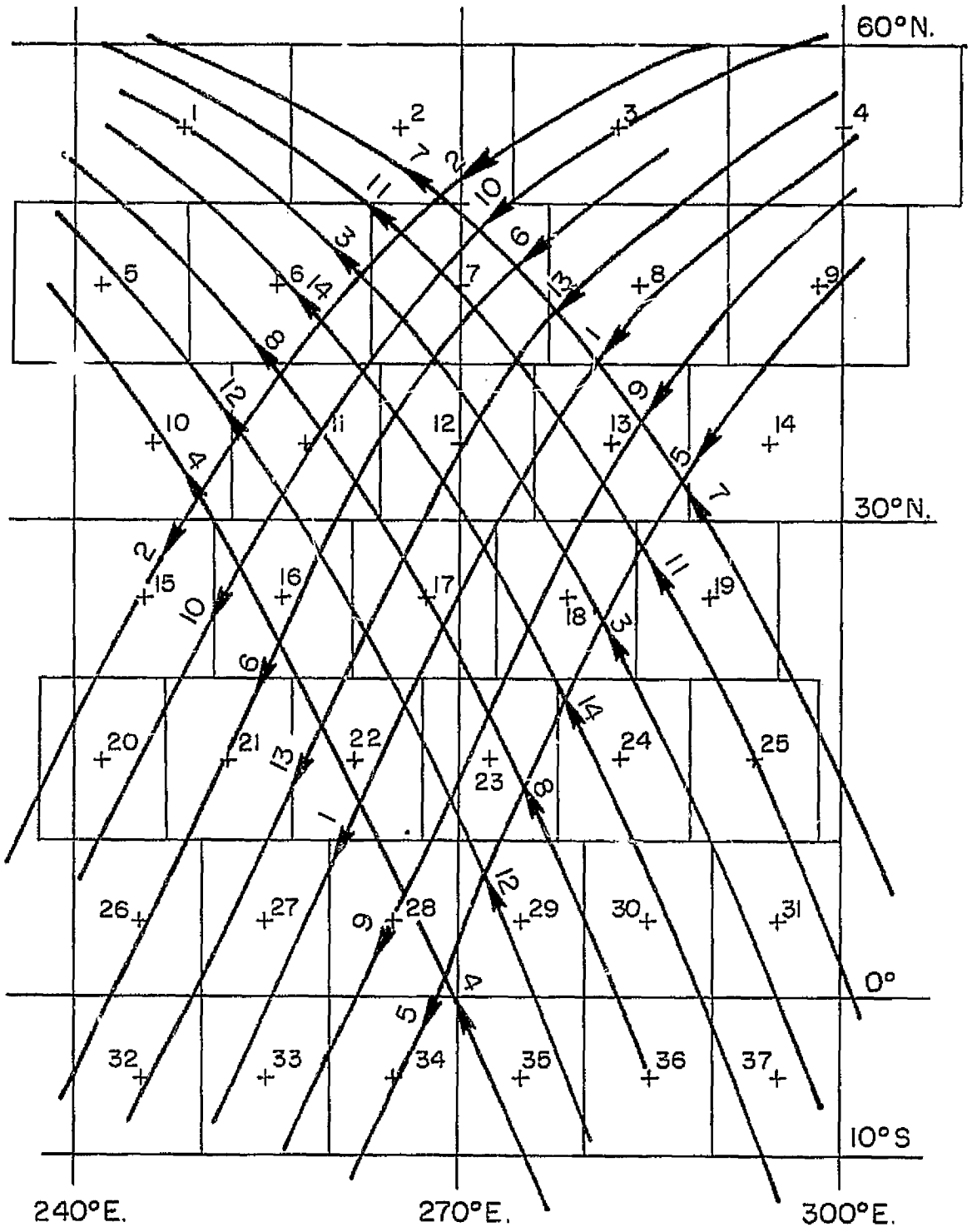

Figure 4.1 Satellite Arcs for Recovery of 10° Equal Area Mean Anomalies. Height of Close Satellite ≈ 900 km.

Table 4.1

Satellite Arcs Used for Recovery of
10° Equal Area Mean Anomalies

Arc No.	Ascending/ Descending Arc	Starting Time* Day	Hour	Min.	Sec.	Duration of Arc in Min.	First & Last Subsatellite Pts. for Close Sat. φ°	λ°	φ°	λ°
1	↙	0	09	05	0	21	55	301	-8	251
2	↙	0	10	45	0	19	60	289	6	233
3	↖	0	18	45	0	21	-6	298	57	244
4	↖	0	20	25	0	19	-14	277	46	238
5	↙	4	08	45	0	19	47	302	-11	262
6	↙	4	10	25	0	20	54	286	-6	239
7	↖	4	18	26	0	19	7	304	61	246
8	↖	4	20	05	0	19	-5	284	54	239
9	↙	2	08	55	0	20	51	301	-10	256
10	↙	2	10	33	0	19	61	298	8	240
11	↖	2	18	35	0	21	-1	302	60	242
12	↖	2	20	15	0	19	-9	281	50	239
13	↙	6	10	12	0	22	57	300	-8	244
14	↖	6	19	51	0	22	-13	295	55	243

* in elapsed time from 21 Sep. 69 01 hr. 33 min. 36.3 sec. (see Sec. 1.1)

4.1.3 Time Interval of Observations along an Arc

We may also consider along with the question of spacing of arcs roughly equal or half of the block size of anomaly being recovered, the question of spacing of observations or the time interval of observations along an arc in relation to the block size of anomaly being recovered. In Figure 4.2 (a) to (d), the location of subsatellite points at intervals of 1 minute are shown over 4 anomaly blocks for the arcs selected in Figure 4.1. The longitudinal scale has been reduced in Figure 4.2 (a), (b) to achieve equal area representation. We notice that, in general, the spacing of observations at 1 minute interval is symmetrical over all the blocks considering both along the arc as well as across the arc observations, and this was the reason for choosing 1 minute interval of observations along the arc. The spacing of observations across the arc is slightly less than the spacing of observations along the arc in the north, but the former increases progressively as we go to the southern portion of area. If we were to consider the observations at 30 sec. interval for this case of 10° equal area anomaly recovery with arc spacing about half the anomaly block size, the observations would be closely spaced along the arcs as compared to across the arcs. The reverse

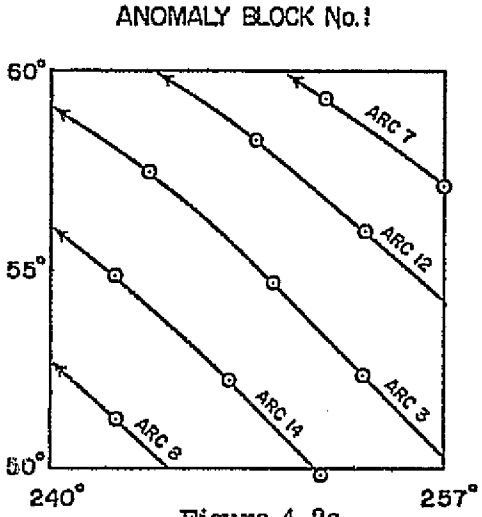

Figure 4.2a

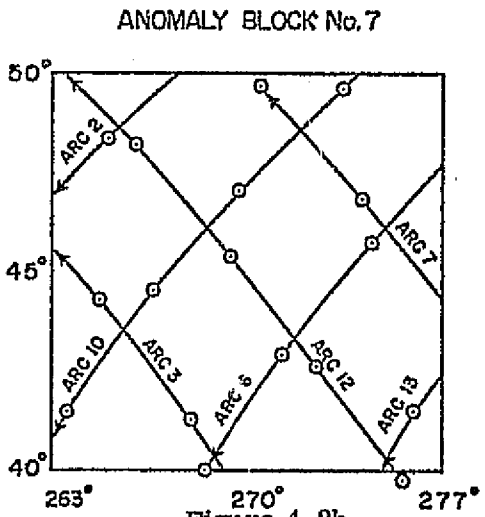

Figure 4.2b

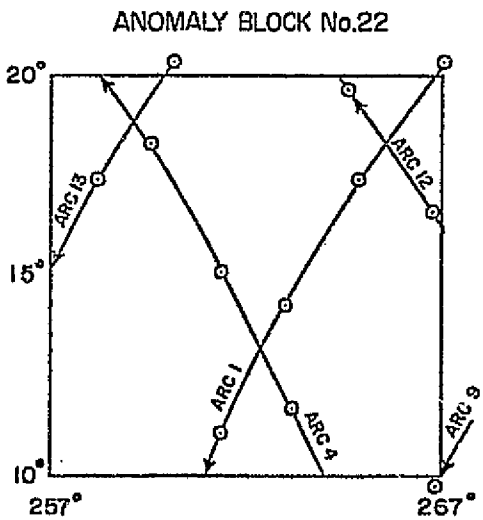

Figure 4.2c

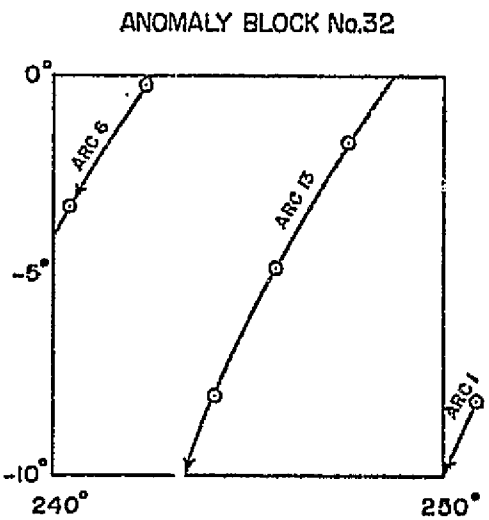

Figure 4.2d

Figure 4.2 Typical Spacing of Observations over 10° Equal Area Mean Anomaly Blocks. Height of Close Satellite ≈ 900 km. Arc Spacing≈ 6°, Time Interval Along Arc = 1 Min.

would be true if the observations were spaced at, say, 2 minutes interval.

To examine the effect of spacing of observations along the arc on anomaly recovery, summed range rate observations along 2 arcs, viz. Arc 13 and Arc 14, at time intervals of 30 sec., 60 sec., and 120 sec., were used for recovery of 9 anomalies in the central area. The anomalies and subsatellite points for the close satellite at 2 minute intervals are shown in Figure 4.3.

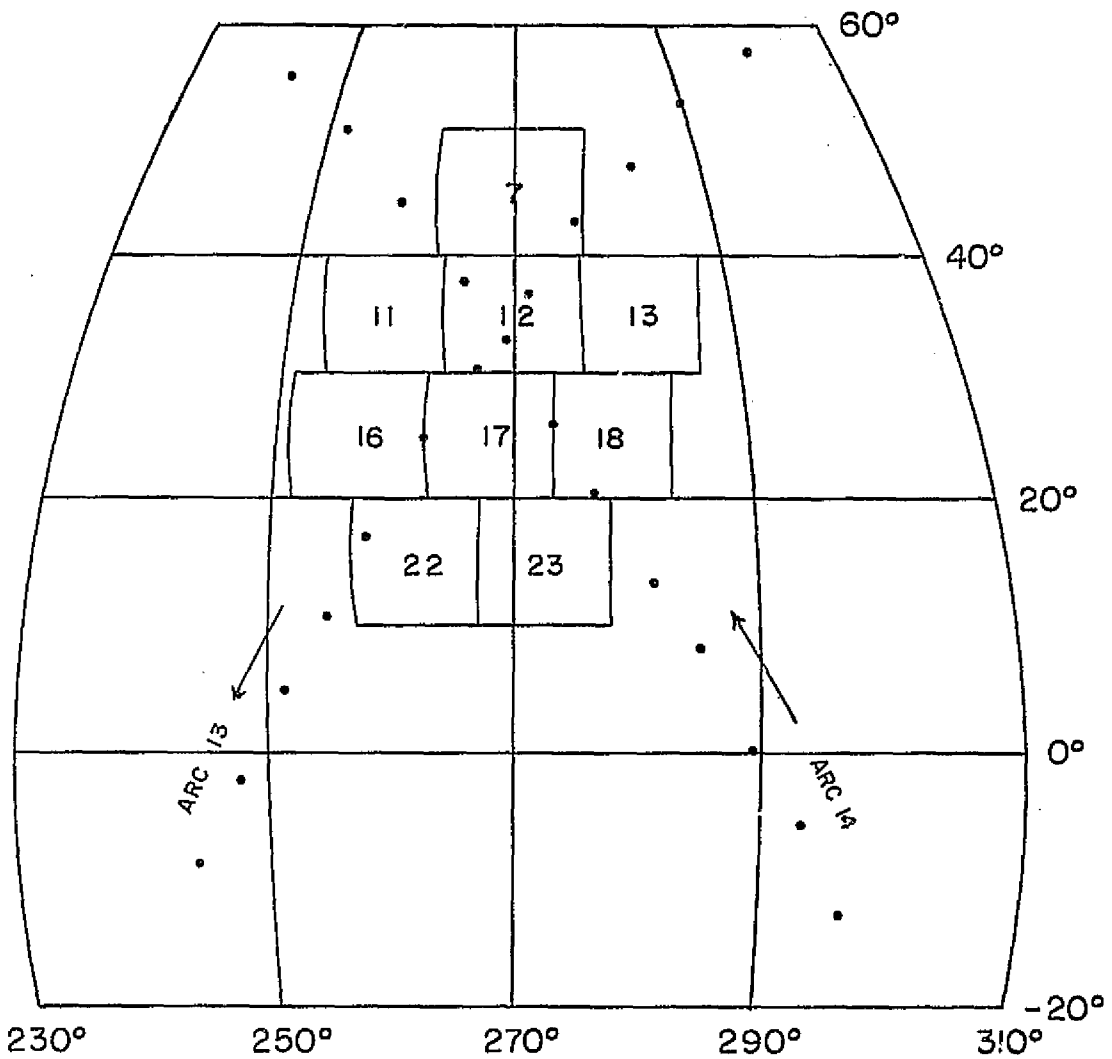

Figure 4.3 Along-Arc Spacing of Observations (Time Interval - 2 Min.)

From the figure, it is clear that the longitudinal spacing of arcs is much larger as compared to the spacing of observations along the arcs. Even at 2 minutes interval of observations along the arc, 2 more descending and 2 more ascending arcs would be needed (e.g. Arcs 9, 10, 11, 12 with reference to Figure 4.1) to achieve symmetry of observations. Because of this very sparse spacing of arcs, i.e. when about, say, 6 arcs (Arcs 9-14) should have been considered, only 2 arcs (Arcs 13, 14) have been considered, no satisfactory anomaly recovery could be expected. Further, if on a-priori considerations the spacing of arcs is inadequate for satisfactory anomaly recovery, this inadequate spacing of arcs cannot be expected to be compensated by increasing along-arc observations.

The above considerations are confirmed by the results shown in Table 4.2, where the discrepancies in recovered anomalies remain about the same when observations along the arc for Arcs 13, 14 are increased from 2 min. to 1 min. and then to 30 sec. The standard deviations however, decrease with increase in along-arc observations. Here, and in all subsequent discussions, the standard deviations (std. devn.) quoted are the square root of respective diagonal elements of the inverse normal matrix, without any modification for the size of residuals or degrees of freedom, i.e. the scalar variance of unit weight has been considered to be unity. The decrease in std. devn. may be explained by the partials for neighboring observations (with respect to anomalies being recovered) not being significantly different, when along-arc observations are arbitrarily increased without regard to adequate spacing of arcs. The ratio of std. devns., as along-arc observations are increased, are also shown in Table 4.2, and are nearly $1/\sqrt{2} = 0.71$.

Table 4.2

Anomaly Discrepancies and Ratio of Standard Deviation with Increased Along-Arc Observations

Anom	Center of Anomaly Block		Anomaly Discrepancy (mgals) Time Interval of Obsns.			Ratio of Std. Devn.	
No.	φ°	λ°	2 min.	1 min.	30 sec.	1 min. obsn./ 2 min. obsn.	30 sec. obsn/ 1 min. obsn.
7	45	270	4	4	4	.71	.72
11	35	258	-54	-54	-54	.70	.72
12	35	270	44	43	42	.70	.72
13	35	282	-36	-35	-35	.71	.72
16	25	256.6	-10	-14	-16	.75	.72
17	25	267.5	29	35	37	.75	.73
18	25	278.5	-35	-39	-40	.75	.72
22	15	262	-16	-15	-14	.71	.72
23	15	272.5	41	43	43	.71	.72

It is thus advisable to keep the time interval of observations along the arc, or along-arc spacing, roughly same as spacing between arcs considering the whole area, as was done in Figure 4.2. However, as we do not know a-priori what spacing between arcs would be adequate for anomaly recovery, we may keep a relatively close along-arc spacing, and after we have investigated the optimum spacing between arcs, the std. devns. of recovered anomalies may be multiplied by a factor of $\sqrt{n}$, if n is the average ratio of along-arc spacing to across-arc spacing of observations. This conclusion about std. devns. may be questioned as it is based on a test where the across-arc spacing was prima facie grossly inadequate. It was, however borne out again when 8 arcs were used, across-arc spacing roughly equal to anomaly block size, and along-arc spacing was varied from 1 minute to 30 sec. This test will be reported later at the end of Sec. 4.1.9.

4.1.4 Constraints for Low Degree Harmonic Coefficients

We now report the results of the effect of impoing six conditions to be satisfied by the recovered anomalies, as discussed in Sec. 2.2.3. All the 14 arcs in Figure 4.1 were used with summed range-rate observations and all 37 anomalies in Figure 4.1 were solved for. The expected value of anomalies, the recovered value of anomalies and their std. devns., with and without the conditions being imposed, are given in Table 4.3. The interval of observations for the case with conditions happened to be 30 sec., while that for the case without conditions was 1 minute, hence the std. devn. for the case with conditions have been quoted after multiplying by $\sqrt{2}$. The std. devn. for the range rate observations in both cases was kept as .08 cm/sec.

We find that though the std. devn. are about the same in both cases, the anomaly discrepancy is much larger when the constraints are imposed than when these are not imposed, the Root Mean Square (R.M.S.) value of the discrepancies being 13.1 and 4.9 mgals respectively. The R.M.S. value of the recovered anomalies in both cases may also be compared with the R.M.S. value of the expected anomalies. We may also calculate the correlation coefficient (ρ) of the recovered values ($\Delta g_s'$) with the expected values ($\Delta g_T'$) from the relation:

$$\rho = \frac{\sum_{n} \Delta g_s' \, \Delta g_T' / n}{\left(\sum_{n} \Delta g_s'^2 / n \right)^{\frac{1}{2}} \left(\sum_{n} \Delta g_T'^2 / n \right)^{\frac{1}{2}}} \qquad (4.1)$$

n being the number of anomalies recovered. These statistics are shown in Table 4.4, from which it is clear that imposition of constraints for low degree harmonic coefficients for anomaly recovery in regional areas, as opposed to global coverage, worsens the solution and is therefore not justified. We will comment on the 'goodness' of solution without constraints later in Sec. 4.1.9.

Table 4.3

Effect of Low Degree Harmonic Coefficient Constraints on Anomaly Recovery

Anom. No. (1)	Expected Anom. (2)	Soln. with Constraints Anom. (3)	s.d. (4)	Soln. without Constraints Anom. (5)	s.d. (6)	Anom. Discrepancy (3)-(2) (7)	(5)-(2) (8)
1	-2.2	-21.2	2.7	-1.6	3.2	-19.0	0.6
2	0.0	19.3	3.0	-2.1	3.2	19.3	-2.1
3	-5.9	-27.3	2.5	-6.9	2.7	-21.4	-1.0
4	-6.4	18.4	1.3	8.1	1.3	24.8	14.5
5	-0.6	19.8	3.1	0.4	3.6	20.4	1.0
6	5.7	-3.7	2.1	4.4	2.6	-9.4	-1.3
7	1.3	17.4	2.1	6.2	2.3	16.1	4.9
8	6.0	-14.9	2.1	-4.1	2.3	-20.9	-10.1
9	-3.8	-2.9	1.6	-4.9	1.6	0.9	-1.1
10	0.1	-11.1	3.5	-4.8	3.6	-11.2	-4.9
11	-5.3	-4.6	2.4	-2.4	2.5	0.7	2.9
12	-6.0	-6.9	2.3	-10.5	2.3	-0.9	-4.5
13	3.1	4.7	2.4	11.5	2.4	1.6	8.4
14	-1.7	13.1	2.0	-2.8	2.2	14.8	-1.1
15	3.1	7.6	4.2	3.5	4.4	4.5	0.4
16	13.0	9.7	3.1	12.4	3.3	-3.3	-0.6
17	-6.0	1.9	2.8	-4.6	2.9	7.9	1.4
18	5.2	3.2	3.0	-0.4	2.9	-2.0	-5.6
19	-9.8	-28.6	3.1	-8.8	3.4	-18.8	1.0
20	-11.4	-7.4	4.1	-12.3	4.4	4.0	-0.9
21	-8.2	-11.4	4.1	-6.4	4.2	-3.2	1.8
22	2.2	1.5	3.0	0.2	3.0	-0.7	-2.0
23	4.0	-5.0	2.5	4.2	2.6	-9.0	0.2
24	-4.7	1.9	3.3	4.8	3.4	6.6	9.5
25	-4.8	19.3	3.0	-8.8	3.4	24.1	-4.0
26	4.9	15.1	4.0	2.7	5.1	10.2	-2.2
27	2.4	1.3	4.2	3.7	4.5	-1.1	1.3
28	-2.3	7.0	3.1	-0.2	3.3	9.3	2.1
29	-2.0	-5.0	2.4	-7.3	2.3	-3.0	-5.3
30	8.6	19.8	2.7	3.1	3.4	11.2	-5.5
31	5.0	-20.0	2.4	-0.5	2.6	-25.0	-5.5
32	5.3	-11.6	2.4	6.8	5.0	-16.9	1.5
33	3.4	12.2	4.0	-4.8	4.6	8.8	-8.2
34	-6.1	-19.9	3.1	-2.7	3.5	-13.8	3.4
35	5.0	13.1	2.3	4.4	2.5	8.1	-0.6
36	-3.6	-15.9	3.3	4.5	4.0	-12.3	8.1
37	-0.8	10.3	1.8	4.2	1.9	11.1	5.0

Units of anomalies and standard deviations are mgals.

For convenience of reference, we will call this latter solution in columns 5 and 6 of Table 4.3 as Solution 10-1, 10° being the block size of anomaly recovery and 1 being the first solution to be considered.

Table 4.4

Statistics for Solutions With and Without Constraints for Low Degree Harmonic Coefficients

	Soln. with Constraints	
	Yes	No
R.M.S. value of anomaly discrepancy (mgals)	13.1	4.9
R.M.S. value of recovered anomalies (mgals)	13.9	5.9
R.M.S. value of expected anomalies (mgals)	5.4	5.4
Correln. coeff. (ρ) of recovered anom. with expected anomalies	0.33	0.63

4.1.5 Summed Range Observations vs. Summed Range Rate Observations

We may also briefly examine if anomaly recovery could be done using summed range observations. For this test, 37 anomalies were solved for using summed range observations along 14 arcs as in Figure 4.1. The std. devn. of observations was assumed as 10 meters (NASA, 1974, p. 4-78). The anomaly discrepancies ranged from -150 mgals to 180 mgals, with the R.M.S. value of 95 mgals. This test was conducted before the conclusions about not imposing constraints were reached, as described in the previous section, hence these discrepancies could be compared with column 7 in Table 4.3 for the constrained solution, and with the R.M.S. value of 13.1 mgals as per Table 4.4. As the anomaly discrepancies with summed range observations are so large as compared to summed range rate observations, it was not considered worthwhile to repeat the solution for the former without constraints.

The std. devn. of the recovered anomalies using summed range observations vary from 43 mgals to 475 mgals, with the RMS value of 225 mgals. The std. devn. of recovered anomalies would be reduced proportionately if the std. devn. of observations was reduced from 10 meters. However, as the observations were assumed to be independent with the same std. devn. for each observation, the weight matrix would be a diagonal matrix with all elements on the diagonal being the same number = $1/(\text{std. devn.})^2$, and hence the solution vector would be unaltered. With the usual notation of A as the partials matrix, P the weight matrix and I the unit matrix of corresponding size, L as the misclosure vector, the solution vector X would be unaffected in the relation:

$$X = -N^{-1}U = -(A'PA)^{-1}A'PL = -(A' \frac{1}{(s.d.)^2} IA)^{-1} A' \frac{1}{(s.d.)^2} IL$$

$$= -(s.d.)^2 (A'A)^{-1} \frac{1}{(s.d.)^2} A'L = -(A'A)^{-1} A'L \qquad (4.2)$$

We may therefore conclude that the design of arcs in Figure 4.1 is unable to recover anomalies with summed range observations in contrast to summed range rate observations. Further, as per remarks in the end of Sec. 4.1.4, we should not impose any constraints for low degree harmonic coefficients on the recovered anomalies in regional or localized areas. Accordingly, in all further tests we will use only summed range rate observations and not impose any constraints.

4.1.6 Spacing of Arcs

It is clear that the distribution of observations directly over an anomaly block will become more dense as the number of arcs is increased over the area, or in other words, the spacing between arcs is decreased. We may start with some suitable spacing of arcs in relation to the anomaly block size, e.g. same spacing as the block size, which will result in one ascending (and/or one descending) arc over each anomaly block. We may then examine the resulting anomaly recovery as we increase or decrease the spacing of arcs. We have already reported the results for arc spacing roughly half the anomaly size, i.e. 14 arcs, in columns 5, 6, and 8 of Table 4.3, without specifying the rationale for this choice. We may now consider this Solution 10-1 in relation to anomaly recovery with arc spacing roughly equal to the anomaly size, i.e. Arcs 1 to 8; and we may contrast it further with a rather unrealistic arc spacing of double the anomaly size, i.e. Arcs 2, 4, 5, and 7. These 4 arcs and the 37 anomalies being recovered are shown in Figure 4.4.

The statistics described in Sec. 4.1.4 are given in Table 4.5 for these 3 cases. We may mention again that the observations were summed range rate at 1 min. interval with std. devn. of .98 cm/sec., and 37 anomalies were solved for without imposing any constraints.

Table 4.5

Statistics for Anomaly Recovery with Arc Spacing of 2, 1 and 1/2 Times Anomaly Block Size

Arc Spacing/Anomaly Block Size	2	1	1/2
No. of Arcs	2, 4, 5, 7	1 to 8	1 to 14
R.M.S. value of anomaly discrepancy (mgals)	26.0	7.4	4.9
R.M.S. value of recovered anomalies (mgals)	26.9	8.4	5.9
R.M.S. value of expected anomalies (mgals)	5.4	5.4	5.4
Correln. coeff. (ρ) of recovered anom. with expected anom.	0.26	0.50	0.63

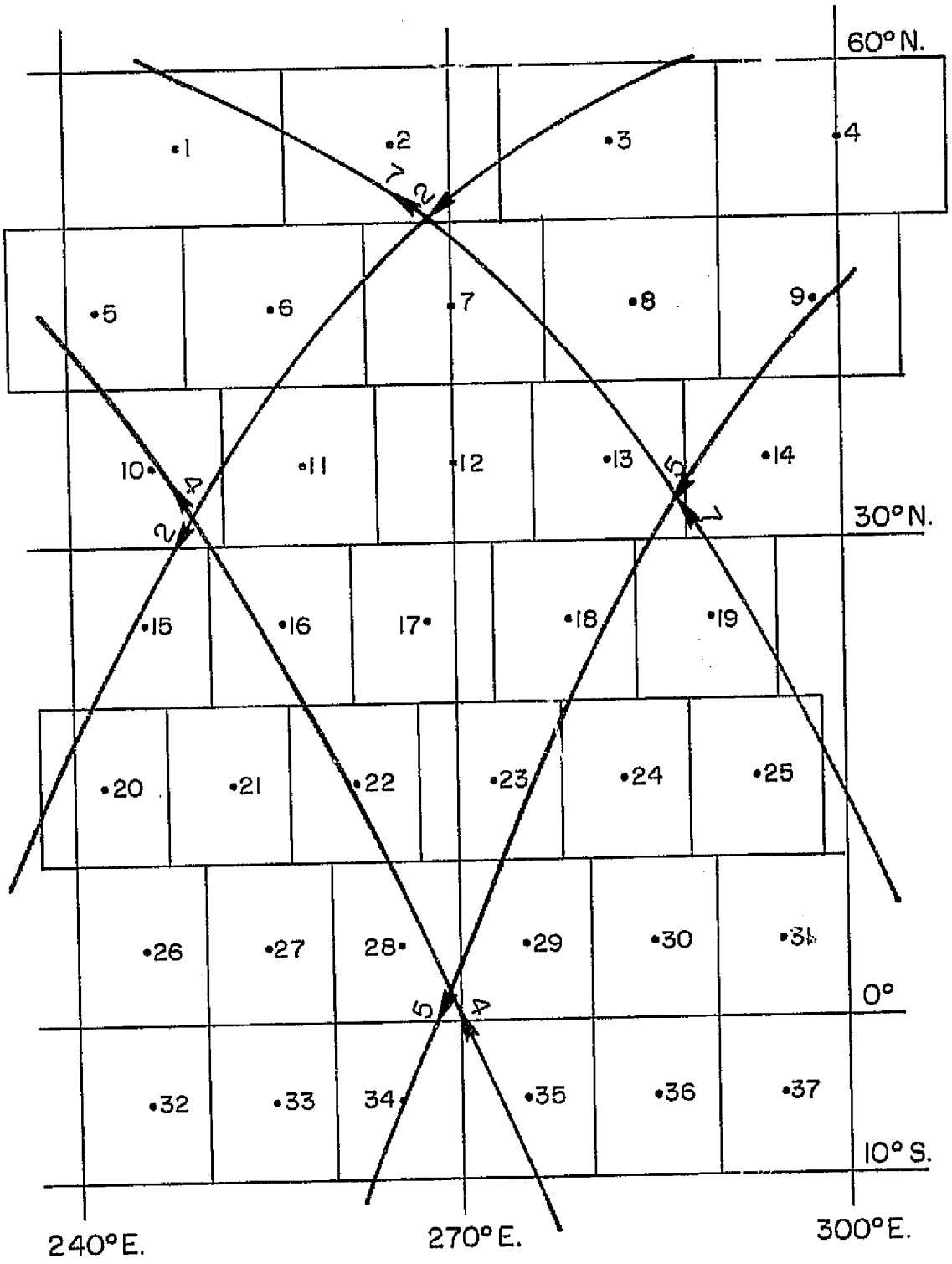

Figure 4.4 Spacing of Arcs at 2 times Anomaly Block Size.

It is obvious from Table 4.5 that arc spacing of twice the anomaly size, i.e. 4 Arcs is totally inadequate. Further, the std. devns. of recovered anomalies are tabulated in Table 4.6 for this case. With reference to the location of the 4 arcs in Figure 4.4, we find that the std. devns. of anomalies which are not covered by any of these arcs is much greater than for those anomalies which are covered by the arcs. It therefore appears necessary that each anomaly block being recovered must be covered by satellite observations directly over it.

Table 4.6

Standard Deviation of Anomalies for Inadequate Arc Spacing
Of 2 Times Anomaly Block Size

Anom No.	Std. devn	Anom No.	Std. devn	Anom No.	Std. devn	Anom No.	Std. devn	Anom No.	Std. devn	Anom No.	Std. devn	Anom No.	Std. devn
1	44	5	13	10	17	15	28	20	67	26	366	32	722
2	26	6	41	11	50	16	32	21	336	27	294	33	226
3	28	7	33	12	309	17	431	22	97	28	85	34	60
4	33	8	39	13	56	18	34	23	63	29	74	35	40
		9	20	14	24	19	22	24	155	30	292	36	111
								25	37	31	115	37	350

Unit of standard deviation is mgals.

4.1.7 Effect of Aliasing in Anomaly Recovery

From the discussion in the previous section, we now find that arc-spacing of roughly half the anomaly block size, i.e. Arcs 1 to 14 (or Solution 10-1) is to be preferred over arc-spacing roughly same as anomaly block size, i.e. Arcs 1 to 8. However, we also find from columns 6 and 8 of Table 4.3 that there are several large anomaly discrepancies which are about 3 times or more, of the std. devn. of the recovered anomalies, e.g. Anomaly No. 4, 8, 13, 24, 36 and there are several others which are about 2 times the std. devn. As there are no 'observational' errors in the simulated observations, the anomaly discrepancies should have, in general, been smaller.

Though we cannot rule out the possibility at this stage that we have not yet reached the optimum spacing of arcs in Solution 10-1, and should consider closer arc spacing instead of 1/2 the block size, the slow improvement in going from arc spacing roughly same as block size (Arcs 1 to 8) to half of block size (Arcs 1 to 14) as shown in Table 4.5 indicates that we ought to first investigate other reasons for the still unsatisfactory anomaly recovery. One such reason could be the inability of the anomalies on the periphery of the area to be recovered satisfactorily due to their adjacent anomalies, which are out of the area,

being ignored in the estimation process; or in other words, the effect of 'aliasing.'

We may then consider this 'aliasing' to have affected the recovery of peripheral anomalies, which may be the outermost anomalies in the area (see Figure 4.1), i.e. the anomalies in the north and south latitude zones (Anomaly No. 1 to 4, 32 to 37) and the anomalies on the west and east edge of other latitude zones (Anomaly No. 5,9; 10,14; 15,19; 20,25; 26,31). Though the observations used were over the whole area covered by 37 anomalies, which were then solved for, it may be argued that the values obtained for the 20 anomalies on the periphery may have been vitiated by aliasing, and only the remaining 17 anomalies may be recovered satisfactorily. The anomaly discrepancies of these 17 anomalies have been extracted from columns 8 and 6 of Table 4.3 from Solution 10-1 and given in Table 4.7.

Table 4.7

Discrepancies in Recovered Anomalies Unaffected by Aliasing

Anomaly No.	Discr.	s.d.	Anomaly No.	Discr.	s.d.	Anomaly No.	Discr.	s.d.	Anomaly No.	Discr.	s.d.	Anomaly No.	Discr.	s.d.
6	-1.3	2.6	11	2.9	2.5	16	-0.6	3.3	21	1.8	4.2	27	1.3	4.5
7	4.9	2.3	12	-4.5	2.3	17	1.4	2.9	22	-2.0	3.0	28	2.1	3.3
8	-10.1	2.3	13	8.4	2.4	18	-5.6	2.9	23	0.2	2.6	29	-5.3	2.3
									24	9.5	3.4	30	-5.5	3.4

Units of anomaly discrepancy and standard deviation are mgals.

In Table 4.7, we still find several large anomaly discrepancies, e.g. Anomaly No. 8, 13, 24, which are about 3 or more times the std. devn. If it is argued that not only the outermost but the next set of adjacent anomalies should also be rejected because of aliasing effect, we are left with Anomaly No. 12, 17, 22 and 23; but the anomaly discrepancy is still large for Anomaly No. 12. Further, when we consider that the anomaly discrepancies for many peripheral anomalies which may be supposed to have been affected by aliasing, is quite small (about 1/2 the s.d.) e.g. Anomaly No. 1,3,5,14,15,19,20,27,32,35 in Table 4.3, we have to conclude that aliasing, as defined above, does not appear to be the cause of the unsatisfactory anomaly recovery in Solution 10-1.

4.1.8 Relative Location of Anomalies and Arcs

Another reason, which may be considered for the unsatisfactory anomaly recovery in Solution 10-1, could be some weakness in anomaly recovery caused

by sparser distribution of observations in the corners of the area as compared to the central area. The anomaly blocks most densely covered by observations are No. 7, 11, 12, 13 and 17. We may, therefore recover only these 5 anomalies from the observations used in Solution 10-1, and compare the anomaly discrepancies of this solution with the discrepancies for the same 5 anomalies in Solution 10-1, where all 37 anomalies were estimated together. This has been done in Table 4.8.

Table 4.8

Effect of Reduction in Number of Recovered Anomalies.
Summed Range Rate Observations at 1 minute Interval for 14 Arcs

Anom. No.	No. of Anomalies Solved = 5		No. of Anomalies Solved = 37	
	Anom. Discr.	Std. Devn.	Anom. Discr.	Std. Devn.
7	-5.4	0.7	4.9	2.3
11	1.5	0.7	2.9	2.5
12	14.2	0.8	-4.5	2.3
13	-15.0	0.4	8.4	2.4
17	12.5	0.7	1.4	2.9

Units of anomaly discrepancy and standard deviation are mgals.

We first note that by including a large number of observations, which are not over the anomalies being recovered, the std. devns. of anomalies being recovered drop to unrealistically low values. The reason for the decrease in std. devn. in column 3 of Table 4.8, though the anomaly discrepancies are large in column 2, when we reduce the number of recovered anomalies, is not clear. This may be contrasted with increase in std. devns. though the anomaly discrepancies become lower, when a larger number of anomalies are solved for than what are covered by observations, and is discussed in remarks following Table 4.9. In any case, it is clear from Table 4.8 that the anomaly recovery has been worsened when we solve for a smaller number of anomalies than what are covered by observations, even if these were sparse observations. We may then run another test for the effect of relative location of anomalies and arcs by using all observations along 7 ascending arcs (and a separate test later by using 7 descending arcs), and solving for all 37 anomalies. The anomalies covered by the arcs should be recovered better than those not covered by them, as noted earlier in Table 4.6. The former anomalies may then be recovered by themselves alone using the same 7 arcs, and compared with their values with the case when all 37 anomalies were solved for. We would thus be interested only in the subset of anomalies covered by 7 ascending (or descending) arcs, Figures 4.5 and 4.6 respectively; and examining the effect of solving for a larger set of anomalies. We would have however ensured in this test that not only the density

of observations was uniform (1/2 anomaly block size both across and along-arc) over all anomalies of interest, but that there were no extra observations not over the anomalies of interest.

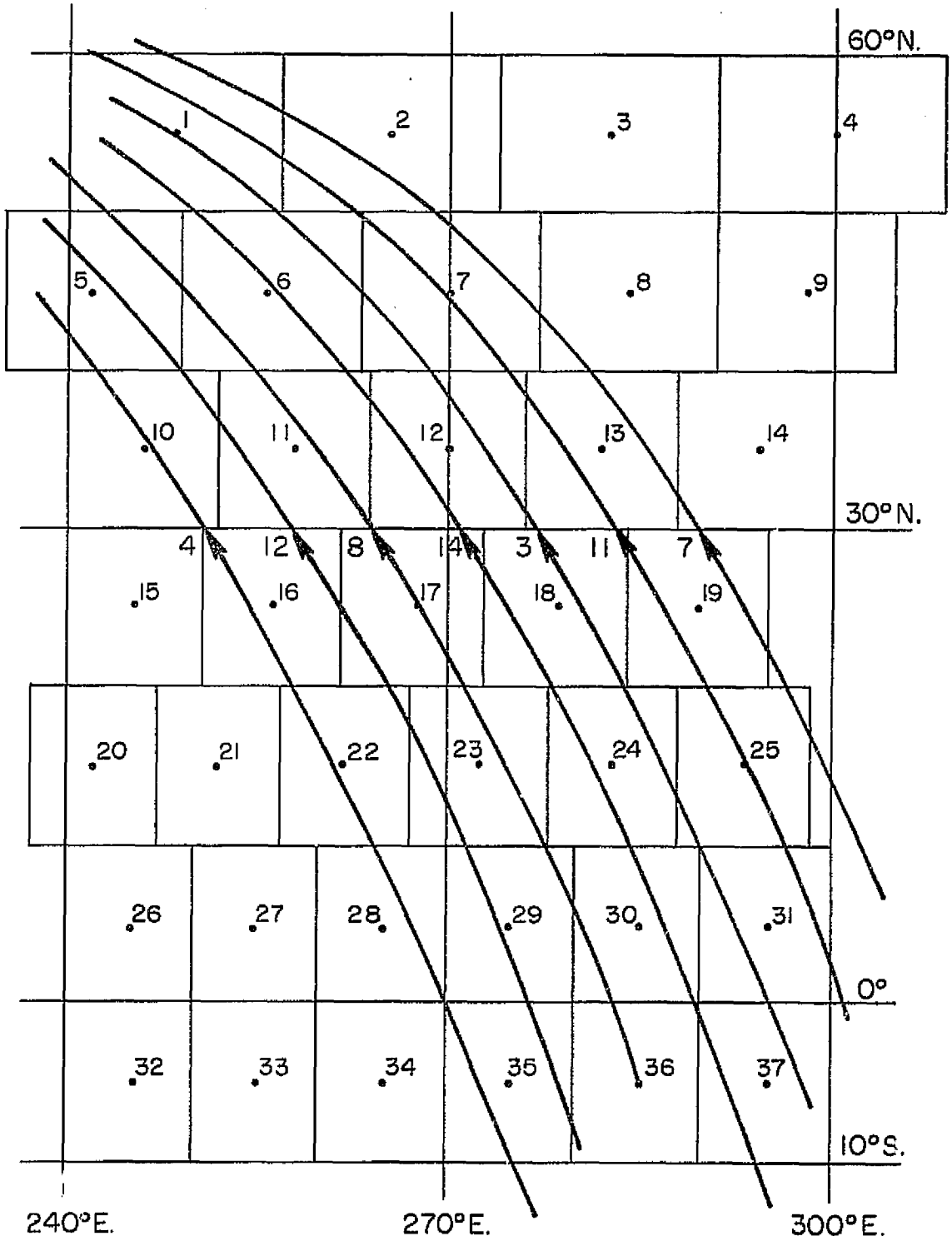

Figure 4.5 Relative Location of Anomaly Blocks and 7 Ascending Arcs.

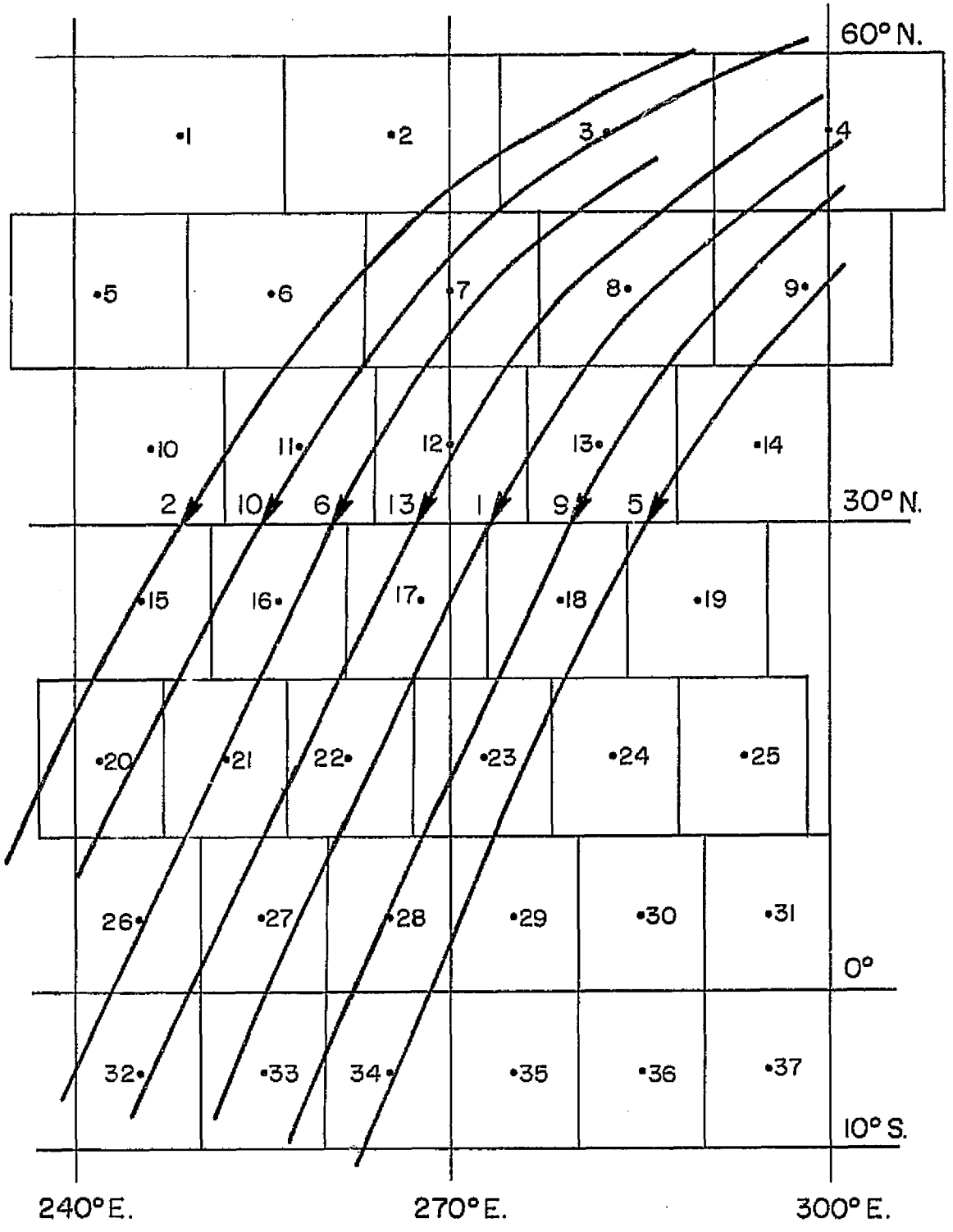

Figure 4.6 Relative Location of Anomaly Blocks and 7 Descending Arcs.

We first report in Table 4.9 results for all 37 anomalies, using either all ascending arcs or all descending arcs. The std. devn. has been given for all anomalies, whether they are covered by observations or not, to highlight the fact that the anomalies not covered by observations cannot be recovered. The anomaly discrepancy has however been shown only when it is not absurdly large, say when its absolute value is not greater than 10 mgals.

Table 4.9

Comparison of Anomaly Discrepancy and Standard Deviations for Anomalies Covered or Not Covered by Observations. Summed Range Rate Observations at 1 Min. Interval for 7 Arcs

Anom No.	Ctr. of Anom Block φ°	λ°	7 Ascending Arcs (Fig. 4.5) Anom. Covered by Obsns.	Anom. Discrep	Std. Devn	7 Descending Arcs (Fig. 4.6) Anom. Covered by Obsns.	Anom. Discrep	Std. Devn
1	55.0	248.5	Yes	5.9	6.8	No	1.3*	44.1
2	"	265.5	Partly	2.5	10.2	Partly	-2.2	19.7
3	"	282.5	No		51.8	Yes	-5.1	6.1
4	"	300.0	"		160.7	"	-8.1	4.4
5	45.0	242.0	Yes	-2.3	5.7	No		47.6
6	"	256.0	"	3.2	6.1	"		18.2
7	"	270.0	"	-4.7	5.6	Yes	3.2	6.6
8	"	284.0	No		21.6	"	-3.5	5.4
9	"	298.0	"		77.3	"	-3.4	4.0
10	35.0	246.0	Partly	-1.7	8.6	No		20.3
11	"	258.0	Yes	-1.5	6.3	Yes	1.2	7.4
12	"	270.0	"	4.5	5.5	"	-4.0	6.8
13	"	282.0	"	-8.5	6.9	"	-1.1	6.6
14	"	294.0	No		18.9	Partly	1.7	10.0
15	25.0	245.5	No		64.1	Yes	-2.2	7.5
16	"	256.5	Yes	-0.5	12.1	"	-0.7	7.0
17	"	267.5	"	-1.7	5.9	"	-1.8	7.0
18	"	278.5	"	0.7	5.5	"	-1.3	10.2
19	"	289.5	"	-1.5	6.0	No		44.9
20	15.0	242.0	No		506.0	Yes	-3.7	7.2
21	"	252.0	"		71.9	"	0.6	6.0
22	"	262.0	Yes	-0.7	14.4	"	-6.4	6.6
23	"	272.5	"	-1.0	6.1	"	2.1	10.2
24	"	283.0	"	-2.1	5.9	No		77.0
25	"	293.0	"	4.1	5.5	"		351.2
26	5.0	245.0	No		912.9	Yes	-2.2	6.1
27	"	255.0	"		164.3	"	0.3	6.5
28	"	265.0	Partly	6.0	20.4	"	0.5	8.7
29	"	275.0	Yes	-1.8	6.9	No		50.1
30	"	285.0	"	0.2	6.6	"	5.2*	275.0
31	"	295.0	"	-8.3	3.4	"		285.5
32	-5.0	245.0	No		838.9	Yes	-8.1	7.6
33	"	255.0	"		469.6	"	-5.2	8.0
34	"	265.0	"		60.8	Partly	-9.5	15.9
35	"	275.0	Yes	-3.3	7.2	No		115.9
36	"	285.0	"	-0.9	6.8	"		675.4
37	"	295.0	"	6.8	3.2	"		791.6

Units of anomaly discrepancy and standard deviation are mgals. Anomaly discrepancy not tabulated if absurdly large, i.e. if absolute value greater than 10 mgals

*Unrepresentative Value. Close agreement by chance.

We first consider the case when all 37 anomalies have been estimated though observations covered only a subset of these anomalies. Firstly, we find that the farther the location of anomaly from the observations (along the arcs), the larger is the std. devn., and the anomaly cannot be recovered when there are no observations directly over the anomaly block. Secondly, considering the std. devns. of anomalies covered by observations, these are all larger than the corresponding std. devns. in Solution 10-1 given in column 6 of Table 4.3. This appears to be due to solving for larger number of anomalies than covered by observations, and may be explained by the Normals matrix becoming ill-conditioned by their incorporation.

Next, we compare the anomaly recovery with the case when only the anomalies covered by observations are estimated, or what we may term as the anomalies of interest. There are 24 anomalies of interest in either case of 7 ascending and 7 descending arcs. The statistics for these 24 anomalies are given in Table 4.10.

Table 4.10

Effect of Solving for More Anomalies than Covered by Observations. Summed Range Rate Observations at 1 min. Interval for 7 Arcs

No. of Anomalies Solved for	7 Ascending Arcs 24	37	7 Descending Arcs 24	37
R.M.S. value of anom. discrepancy for 24 anomalies (mgals)	5.1	3.9	7.2	4.1
R.M.S. value of 24 recovered anomalies (mgals)	6.2	5.8	7.7	7.0
R.M.S. value of 24 expected anomalies (mgals)	5.2	5.2	5.7	5.7
Correln. coeff. (ρ) of recovered anom. with expected anom.	0.62	0.75	0.46	0.81

The results clearly point out that the anomaly recovery improves for anomalies covered by observations, if additional anomalies around the former anomalies of interest, are treated as unknowns and included in the estimation process. The latter additional anomalies are not covered by observations and cannot be recovered themselves, as evidenced by the very large std. devns. in Table 4.9, but their inclusion improves the model for recovery of anomalies of interest.

From Figures 4.5 and 4.6, we see that the additional anomalies were one or two anomaly blocks beyond the anomalies covered by observations, but they were not in a systematic pattern around the anomalies of interest. Another 2 solutions were therefore tried, which we shall term as Solutions 10-2 and 10-3.

These had respectively one and two additional anomalies on the periphery all around the 37 anomalies leading to a total number of 64 and 92 anomalies respectively, which were then solved for. The details, as reported below, for 37 anomalies were extracted from these Solutions 10-2 and 10-3 for comparison with Solution 10-1. The layout of 37, 64 and 92 anomalies for these 3 solutions is shown in Figure 4.7. Some statistics for these solutions are given in Table 4.11.

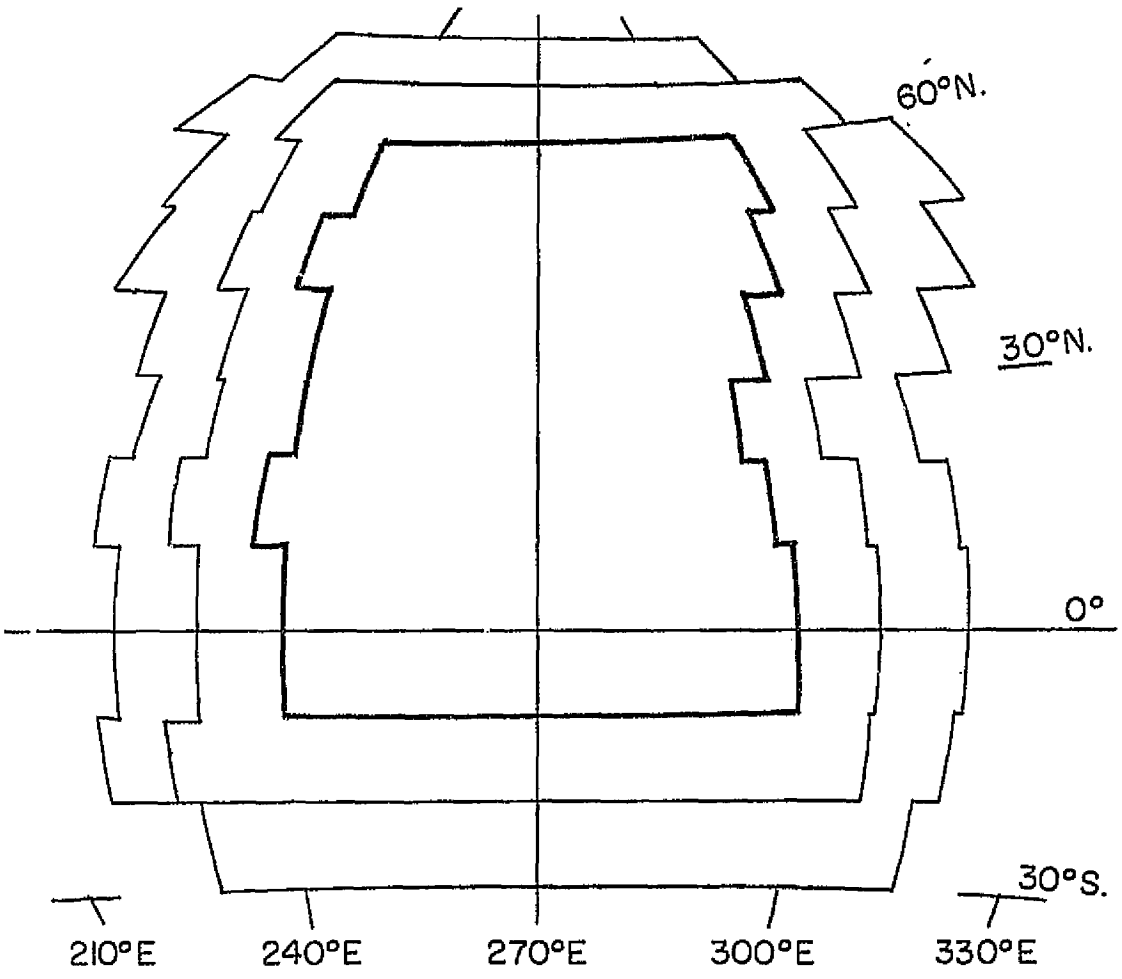

Figure 4.7 Layout of Anomalies for Solutions 10-1, 10-2, 10-3.
No. of Anomalies Solved for were 37, 64, 92 respectively.

Table 4.11

Statistics for Anomaly Recovery for 37 10° Equal Area Mean Anomalies Summed Range Rate Observations at 1 Min. Interval for 14 Arcs

No. of anomalies solved for	Soln. 10-1 37	Soln. 10-2 64	Soln. 10-3 92
R.M.S. value of anom. discrepancy for 37 anomalies (mgals)	4.9	0.3	0.3
Mean value of anom. discrepancy for 37 anomalies (mgals)	0.0	-0.1	0.3
Minimum value of anom. discrepancy for 37 anomalies (mgals)	-10.1	-0.7	0.1
Maximum value of anom. discrepancy for 37 anomalies (mgals)	14.5	0.8	0.4
Sum of squares of anom. discrepancy for 37 anomalies ($mgals^2$)	891.1	4.3	2.7
R.M.S. value of 37 recovered anomalies (mgals)	5.9	5.5	5.4
R.M.S. value of 37 expected anomalies (mgals)	5.4	5.4	5.4
Correln. coeff. (ρ) of recovered anom. with expected anomalies	0.63	0.9981	0.9988

The improvement in anomaly recovery by including one additional anomaly block all around the periphery, is strikingly illustrated in the results of going from Solution 10-1 to 10-2. The further improvement in going to Solution 10-3 is very little. In fact, the latter appears to be an almost perfect anomaly recovery but for a constant anomaly discrepancy of about 0.3 mgals. The 10° equal area anomalies are however not recovered at all in Solution 10-3, as described later, and the close agreement is illusory, for it merely shows the repeatability of the results. The summed range rate 'observations' were simulated using 130 anomalies, i.e. 3 10° blocks all around the periphery of 37 anomalies of interest; and now when we use these observations to recover 92 anomalies, i.e. up to 2 10° blocks all around the anomalies of interest, the process is virtually repeated in reverse order. The small anomaly discrepancy is due to a smaller subset of anomalies being recovered that what were used to generate the simulated observations. The almost constant value with a small magnitude of 0.3 mgals does however show that firstly, partials of observations with respect to the unknown parameters (10° anomalies) have been computed accurately enough for the anomalies to be well recovered from the initial zero value in a non-linear model. Secondly, the density of observations with arc spacing of about half anomaly block size is adequate for the anomaly recovery. Thirdly, we conclude that the effect of re-

sidual anomalies farther than 2 anomaly blocks, i.e. 20°, is very small on the summed range rate observations.

To confirm the above conclusion, a reduced set of observations with latitudinal extent from 10° N. to 50° N were extracted from the previous observations, covering the latitudinal extent from 10° S. to 60° N.

The longitudinal extent of this reduced set of observations was so kept that these observations covered only 16 anomalies numbered 6 to 8; 10 to 13; 15 to 19; and 21 to 24. These anomalies and arcs alongwhich observations were used are shown in Figure 4.8.

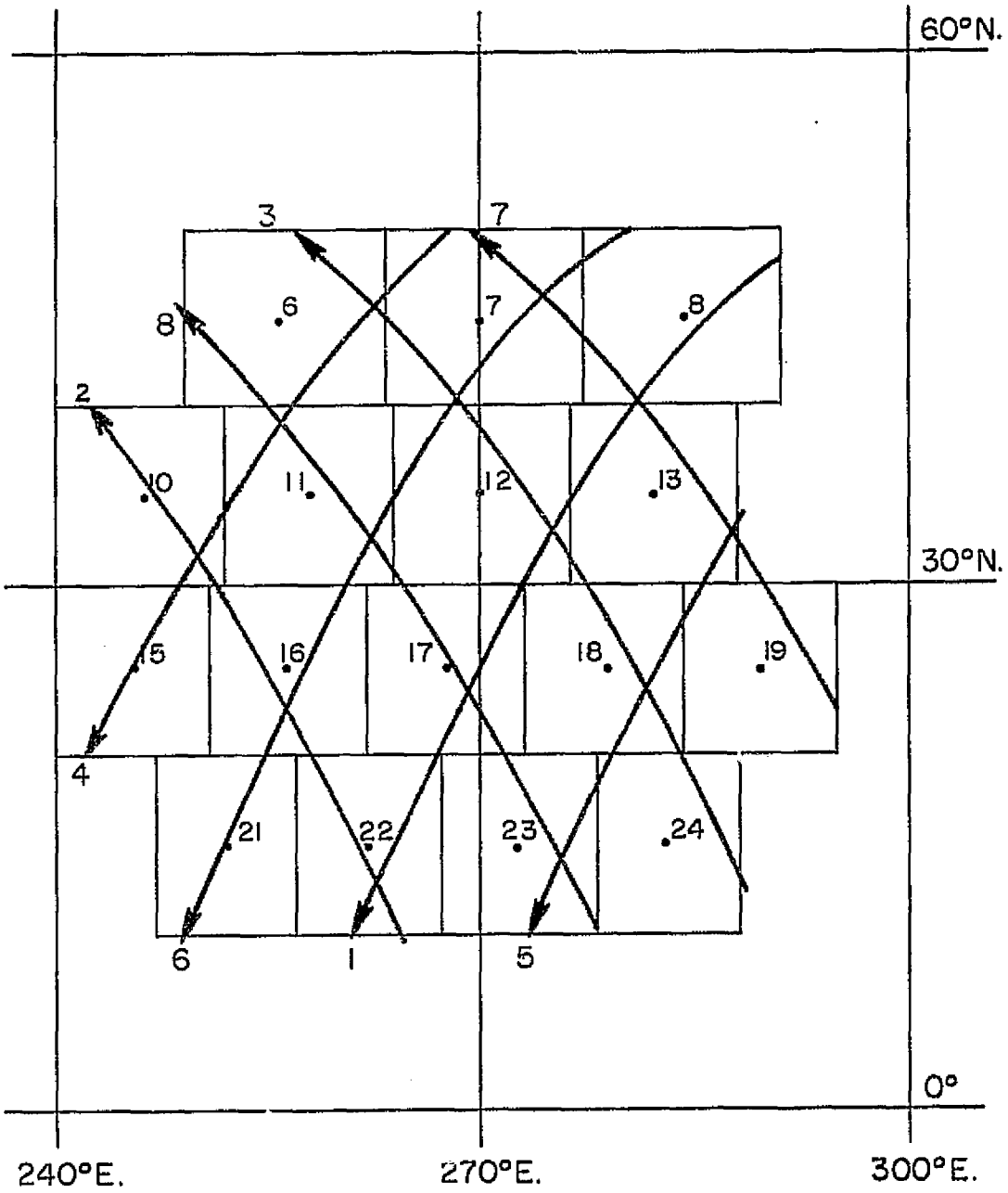

Figure 4.8 Reduced Set of Observations - Arcs 1 to 8.

These extracted observations had thus been generated using anomalies up to a spherical distance of at least 40° beyond the limit of this area, and these observations were now used to recover 16 anomalies of interest along with 2 anomaly blocks all around the periphery. Observations were used only along 8 arcs, Arcs 1 to 8, i.e. at arc spacing roughly same as the size of anomaly block, and therefore with this sparser density of observations, the anomaly recovery could not be expected to have as close agreement as reported in the last column of Table 4.11 for Solution 10-3. However, the R.M.S. value of anomaly discrepancy for the 16 anomalies of interest was only 0.9 mgals, and the correlation coefficient between the recovered value and the expected value of anomalies was 0.988. As these results confirm the conclusion that the effect of residual anomalies farther than 2 anomaly blocks is negligibly small on the summed range rate observations, this test for 16 anomalies of interest was not repeated with 14 arcs.

We may now elaborate on the remark after Table 4.11 that anomalies were not recovered in Solution 10-3. Firstly, the correlation coefficients between the 37 recovered anomalies, as obtained from the variance covariance matrix of Solution 10-3, were very high. The average value of this correlation coefficient for anomalies in the same latitude zone between 2 adjacent anomalies and between 2 anomalies separated by 1, 2 and 3 anomaly blocks between them was about 0.9. Its value between two recovered anomalies in 2 adjacent latitude zones and between 2 anomalies separated by 1 and 2 latitude zones was also about 0.9. In short, the different anomalies were not being recovered individually. Secondly, the std. devn. of the 37 recovered anomalies were also large; the minimum, maximum and R.M.S. value being 41.4, 63.1 and 52.8 mgals respectively. When we note that minimum, maximum and R.M.S. value of std. devn. for the 37 anomalies in Solution 10-2 were 3.4, 23.4 and 7.5 mgals respectively, we have to conclude that Solution 10-3 has to be rejected, and Solution 10-2 accepted. Solution 10-2 will be examined in greater detail in the following Sec. 4.1.9.

4.1.9 Recovery Model for 10° Equal Area Mean Anomalies

The statistics for Solution 10-2 have been presented in Table 4.11 for the 37 anomalies of interest covered by the observations. We may also record here the improvement in anomaly recovery, with the increase in density of observations from arc-spacing of roughly same as anomaly block size (8 Arcs) to arc spacing of roughly half of anomaly block size (14 Arcs). The number of recovered anomalies in both cases were 64, i.e. 37 anomalies of interest and an additional anomaly all around the area covered by observation; and the spacing of observations along the arc was 1 min. The statistics for the 37 anomalies of interest are given in Table 4.12.

Table 4.12

Effect of Reduction in Spacing of Arcs for Solution 10-2
for 37 10° Equal Area Mean Anomalies

	Soln. 10-2 14 Arcs	8 Arcs
R.M.S. value of anomaly discrepancy (mgals)	0.3	1.3
Mean value of anomaly discrepancy (mgals)	-0.1	0.2
Minimum value of anomaly discrepancy (mgals)	-0.7	-2.4
Maximum value of anomaly discrepancy (mgals)	0.8	6.3
Sum of Squares of anomaly discrepancy $(mgals)^2$	4.3	59.9
R.M.S. value of recovered anomalies (mgals)	5.5	5.5
R.M.S. value of expected anomalies (mgals)	5.4	5.4
Correln. coeff. (ρ) of recovered anom. with expected anom.	0.998	0.973
R.M.S. value of std. devn. of recovered anom. (mgals)	7.5	43.0

The correlation coefficients between the 37 recovered anomalies obtained from the variance-covariance matrix of Solution 10-2 are shown in Figure 4.9. The figure shows the correlation coefficients between adjacent anomalies both in the east-west direction in the same latitude zone, as well as in the north-south direction between two adjacent anomalies in two adjacent latitude zones. We first note that the magnitude of the correlation coefficients is low; average value in the east-west direction is -0.32, and average value in the north-south direction is -0.44, which indicates that the individual 10° equal area anomalies are being recovered. Secondly, the correlation coefficients are lower in the center, where the density of observations is large because of the presence of both ascending and descending arcs. Thirdly, in the north half of the area, the magnitude of the east-west correlation coefficient is higher (average -.40) than the magnitude of the north-south correlation coefficient (average -.26); while in the south-half of area the east-west correlation coefficient is lower (average -.28) than the north-south correlation coefficient (average -0.61). This is due to larger spacing between arcs in the south as compared to the north, as would be clear from Figure 4.2. A high correlation coefficient appears as a sign of weak anomaly recovery.

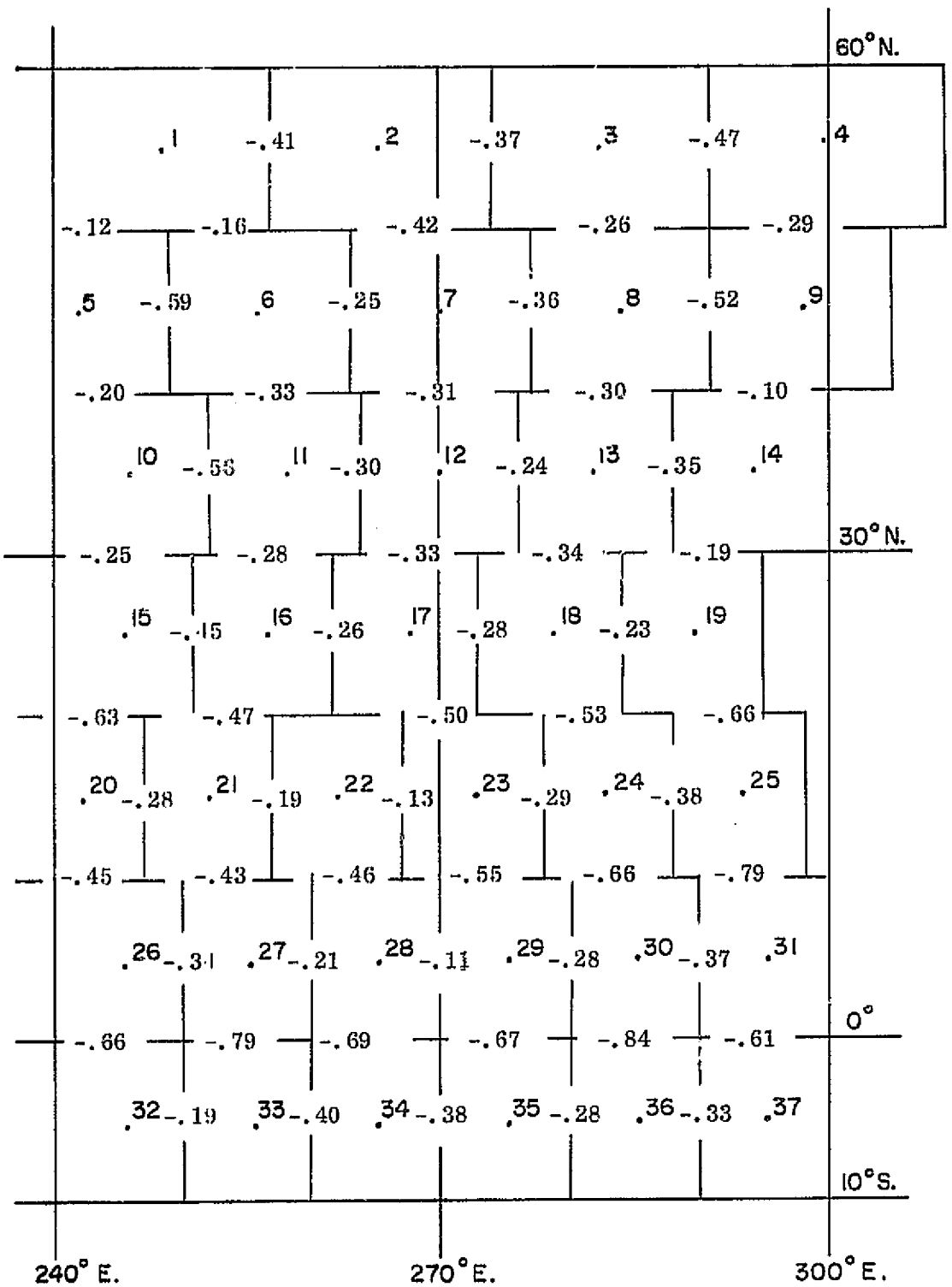

Figure 4.9 Correlation Coefficients between Recovered Anomalies in Solution 10-2.

We may now consider the std. devns. of the recovered anomalies for the 37 anomalies of interest in Solution 10-2. These have been tabulated in Table 4.13. We find that the std. devns. are lowest in the center of the area. Further, the std. devns. of anomalies in the north of the area are lower as compared to the anomalies in the south of the area; and finally, std. devns. of anomalies in the east of area are lower than for the anomalies in the west of area in each latitude zone.

Table 4.13

Variation in Standard Deviation of
37 10° Equal Area Mean Anomalies in Solution 10-2

Anomaly No.	Latitude Zone	Std. Devn. of Anomalies Sequentially from W. to E. (mgals)					
1 - 4	50° - 60° N.	9.5,	6.1,	4.6,	6.1		
5 - 9	40° - 50° N	10.3,	4.6,	3.9,	4.3,	7.8	
10 - 14	30° - 40° N	11.2,	4.0,	3.6,	3.4,	7.3	
15 - 19	20° - 30° N.	7.2,	4.4,	3.5,	3.9,	4.8	
20 - 25	10° - 20° N.	7.4,	5.5,	4.0,	3.5,	4.8,	5.4
26 - 31	0° - 10° N.	11.3,	6.9,	4.8,	4.3,	6.0,	5.9
32 - 37	10° S - 0°	23.4,	15.6,	10.4,	5.5,	7.0*,	5.2

*perhaps caused by Arc. No. 8 not going up to the edge of the area. See remarks before Table 4.1.

The std. devns. decrease in the center of the area clearly because of the increased density of observations because of the presence of both ascending and descending arcs. It may therefore be better to consider the recovery of anomalies in an area shaped like a rhombus with the diagonals roughly east-west and north-south so that most of the area is covered by both ascending and descending arcs. This has been done in Sec. 4.2 and Chapter 5. The increase in std. devns. in the south of area as compared to the north of area is due to the increase in the spacing of arcs as we go towards the equator as may be seen from Figure 4.2. It may therefore be appropriate, if it can be so arranged, to consider recovery in equatorial areas separately from mid-latitudes.

The reason for the increase in std. devn. from east to west in a latitude zone is due to the fixing of starting coordinates of each arc, as observations of about 20 minutes duration could not solve for the starting coordinates, as discussed in Sec. 2.3.3. The misclosures of 'observed value' - 'computed value' of summed range rate are therefore zero in the north-east for descending arcs and in the south-east for ascending arcs, and increase as we proceed along the arcs to south-west and north-west respectively. As outlined later in Sec. 6.1, while working with actual observational data over entire usable portion of the arc, say, 40 minutes, and in conjunction with other tracking data, it may be

possible to adjust the starting coordinates of the arc (or portions of the arc) to fit the whole data, and there may not then be any large change in std. devn. of anomalies in a latitude zone towards one edge.

We may now examine the question of 'goodness' of solution, as we have already considered this for Solution 10-2. For simulated observations, not burdened with observational errors, the anomaly discrepancies should be small, about 1/2 to 1/3 of the R.M.S. value of the expected anomalies. The R.M.S. value of the recovered anomalies should be comparable to the R.M.S. value of the expected anomalies, with a high value, say 0.9, of the correlation coefficient of recovered with expected anomalies, as defined by ρ in equation (4.1). These statistics may be seen for Solution 10-2 in Table 4.11.

The correlation coefficient between the recovered anomalies, as obtained from the variance-covariance matrix should be small, say about 0.5 or less; see Figure 4.9. The std. devn. of recovered anomalies should be comparable to, or less than, the std. devn. of the expected anomalies, which may be obtained as the R.M.S. value of the expected anomalies. We may note here that the std. devn. of recovered anomalies would be decreased by a factor by which the std. devn. of observations is reduced, as the observations were considered to be independent, and having the same std. devn.; see equation (4.2) in Sec. 4.1.5. The std. devn. of summed range rate observations in Sec. 4.1 was taken as .08 cm/sec., which is based on an integration interval of 10 sec. However, as we have used observations at 1 minute interval, we may consider their std. devn. as .03 cm/sec. based on an integration interval of 1 minute. The std. devn. of recovered anomalies in Solution 10-2 would thus become 2.8 mgals instead of 7.5 mgals. We have already discussed the increased std. devn. of recovered anomalies on the south and west edges of the area because of reduced number of observations. If we then consider the remaining anomalies, i.e. except Anomaly No. 5, 10, 26, 32, 33, 34 on the edges of the area (see Table 4.13 and Figures 4.1 and 4.2) having std. devn. larger than 10 mgals, the R.M.S. value of 31 recovered anomalies in Solution 10-2 would become 5.2 mgals considering std. devn. of summed range rate observations as .08 cm/sec. This will be reduced to 2.0 mgals, if we consider the std. devn. of summed range rate observations as .03 cm/sec. This R.M.S. value of the std. devn. of recovered anomalies, 2.0 or 2.8 mgals, may then be compared for judging the 'goodness' of anomaly recovery with the std. devn. of expected anomalies of 5.4 mgals, obtained as the R.M.S. value of the 37 expected anomalies.

We may also recall the discussion in Sec. 4.1.3 about computing the std. devn. of recovered anomalies when the spacing of observations along the arc is about the same as spacing of observations between adjacent arcs. We have ensured this in Solution 10-2, where the spacing of arcs was about half anomaly block size by considering observations along the arc at 1 minute interval; see Figure 4.2. However, if we had considered observations along the arc at closer time interval, say n times the spacing of observations between the arcs, then the

resulting std. devn. of the recovered anomalies need to be multiplied by $\sqrt{n}$. This was demonstrated in Table 4.3, but those results were based on a recovery model which solved only for the anomalies covered by observations, and the observations were also grossly inadequate, as we considered only 2 arcs. Now that we have decided on the optimum recovery model by solving for an additional anomaly all around the border of area covered by observations, we may examine the change in std. devns. with increased along-arc observations for this model. We have already reported in Table 4.12 the results of recovering 37 anomalies of interest, using observations along 8 arcs at 1 minute interval to solve for 64 anomalies. Another solution was then obtained using the same model, but with observations at 30 sec. interval along 8 arcs. The difference between anomaly recovery for the 37 anomalies of interest between these 2 runs was nominal, the R.M.S. value of the difference being 1.4 mgals. However, the std. devns. of recovered anomalies of the two solutions bore an almost constant ratio, whose mean value was 0.70, which agrees with the factor $1/\sqrt{2} = 0.71$. These results then confirm the conclusions of Sec. 4.1.3.

We have thus described the criteria for judging the 'goodness' of anomaly recovery and illustrated it with Solution 10-2 of 37 10° equal area mean anomalies. We now describe in Sec. 4.2 the anomaly recovery of 5° equal area mean anomalies using a close satellite of height 250 km.

4.2 Recovery of 5° Equal Area Mean Anomalies from Close Satellite at Height of 250 km

4.2.1 Area of Investigation and Satellite Arcs

The area for the recovery of 5° equal area anomalies was also centered on latitude 30°N. and longitude 265°E. Two changes were, however, made in the shape and the extent of the area as per the discussion before Table 4.13 in Sec. 4.1.9. First, the shape of the area was changed from a roughly rectangular one, as in Figure 4.1 to nearly like a rhombus with the diagonals roughly east-west and north-south. This change resulted in most of the anomalies being covered by both ascending and descending arcs (see Figure 4.10), thereby increasing the density of observations and making it more uniform over a much larger portion of the area than what was possible with a rectangular shape of the area as in Figure 4.1. The second change was to reduce the latitudinal extent of the area so that the spacing between two adjacent arcs was more nearly the same over anomalies in the north edge of the area as compared to the spacing over anomalies in the south edge of the area (see Figure 4.11 a,b). The wide latitudinal extent of 70° for the area for the recovery of 10° anomalies had resulted in the spacing between the arcs to be nearly halved over anomalies in the south edge as compared to the north edge of the area, as may be seen from Figures 4.2a and 4.2d. However, the present latitudinal extent of 20° for the area for the recovery of 5° anomalies was merely for the computational convenience of having a smaller number of arcs to be simulated. This will become more apparent in Sec. 5.1, where the same area of investigation was retained to enable comparison, but we needed to consider up to 28 arcs. From the consideration of nearly uniform spacing between the arcs from the north edge to the south edge of the area, we may have as well increased the latitudinal extent to 40°.

The area of investigation and the satellite arcs have been shown in Figure 4.10. As discussed, the anomalies to be recovered were chosen so that their location and extent would result in the shape of the area being more nearly a rhombus. The total number of anomalies with these considerations came out to be 12. The satellite arcs were selected so that the spacing between adjacent arcs was roughly half of the longitudinal extent of the 5° anomaly block; and that all the arcs taken together were positioned symmetrically over the area of investigation. The total number of arcs selected from these considerations were 12. The inter-se numbering of arcs was according to the starting time of the arc. The starting time, the duration of arc and the coordinates for the first and last sub-satellite point for the close satellite are given in Table 4.14.

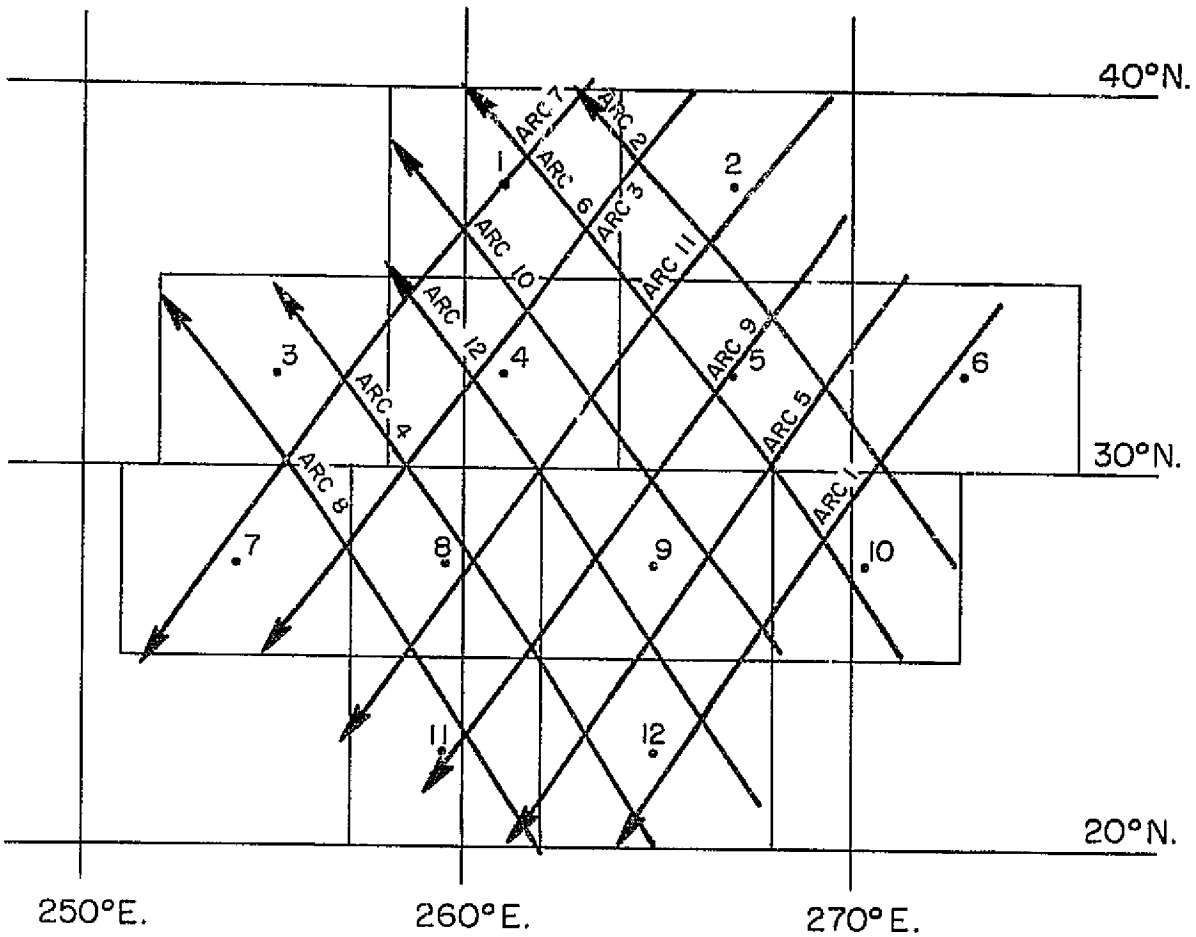

Figure 4.10 Satellite Arcs for Recovery of 5° Equal Area Mean Anomalies. Height of Close Satellite ≈ 250 km.

Table 4.14

Satellite Arcs Used for Recovery of 5° Equal Area Mean Anomalies
Height of Close Satellite ≈ 250 km

Arc No.	Ascending/ Descending Arc	Starting Time* Day	Hour	Min.	Sec.	Duration of Arc Min.	Sec.	First & Last Subsatellite Pts. for Close Sat. φ°	λ°	φ°	λ°
1	↙	0	12	31	00	4	00	34.4	273.9	20.2	264.2
2	↖	0	22	29	40	3	40	27.5	272.8	40.2	262.8
3	↙	2	13	42	00	4	10	39.8	265.9	25.3	254.8
4	↖	2	23	40	10	4	10	20.1	265.0	34.8	254.9
5	↙	4	13	26	30	4	10	35.1	271.4	20.3	261.2
6	↖	4	23	24	40	4	20	25.0	271.5	40.1	259.9
7	↙	6	14	37	40	4	20	39.9	263.0	24.8	251.4
8	↖	7	00	35	50	4	10	19.9	262.0	34.7	252.0
9	↙	8	14	21	40	4	20	36.9	269.9	21.6	259.0
10	↖	9	00	20	30	3	50	25.5	268.1	38.9	258.0
11	↙	12	15	16	30	4	50	39.8	269.5	22.9	256.8
12	↖	13	01	15	00	4	00	21.2	267.8	35.4	258.0

*in elapsed time from 21 Sept. 69 01 hr. 33 min. 36.3 sec. (see Sec. 1.1)

The observations along each arc were simulated at a time interval of 10 seconds. The observations corresponding to the position of sub-satellite points of the close satellite over 4 anomaly blocks have been shown in Figures 4.11a to d, the longitudinal scale having been reduced to achieve an equal area representation. The observations have been shown in Figure 4.11 at time interval of every 30 seconds only. We notice from Figure 4.11a that the spacing of along-arc observations at 30 seconds time interval is slightly larger in anomaly block No. 1 at the north edge of the area, as compared to the spacing of observations between adjacent arcs. But, as we proceed to the south edge of the area through anomaly blocks No. 4, 9, 12, the along-arc spacing of observations becomes slightly smaller than the across-arc spacing of observations. However, considering the whole area, if we achieve satisfactory anomaly recovery with 12 arcs giving across-arc spacing of half anomaly block size, we ought to utilize the corresponding along-arc spacing of observations as 30 sec. And, in that case, as we have used the observations at time interval of 10 seconds, we need to multiply the resulting std. devns. of the recovered anomalies by a factor of $\sqrt{3}$. The std. devns. in Sec. 4.2 have been quoted throughout as obtained from the observations at 10 seconds time interval without multiplying by the factor of $\sqrt{3}$, and this has been done only finally in the end of Section 4.2.3.

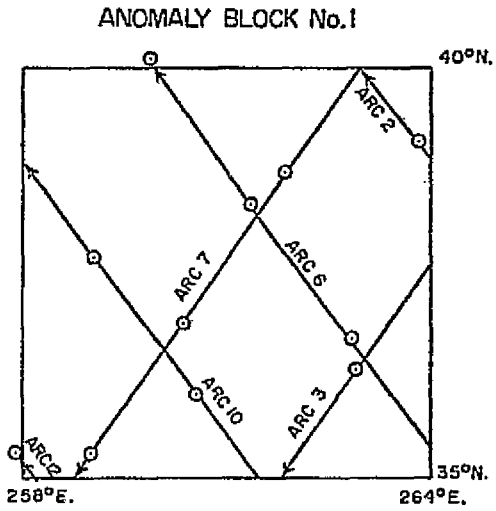

Figure 4.11a

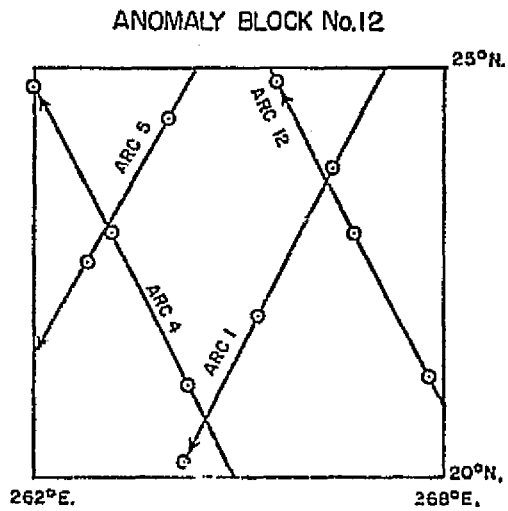

Figure 4.11b

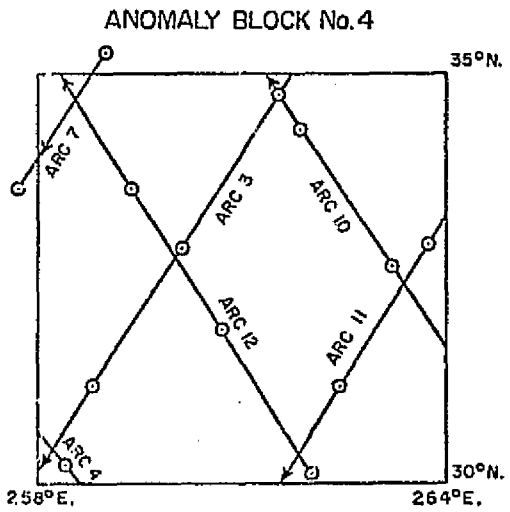

Figure 4.11c

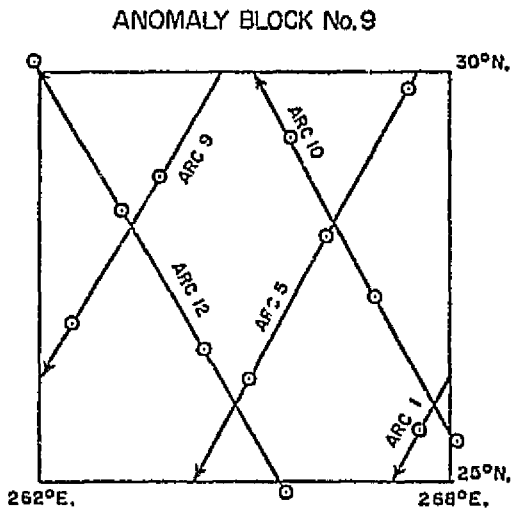

Figure 4.11d

Figure 4.11 Typical Spacing of Observations over 5° Equal Area Mean Anomaly Blocks.
Height of Close Satellite ≈ 250 km.
Arc Spacing ≈ 3°, Time Interval Along Arc = 30 sec.

4.2.2 Relative Location of Anomalies and Arcs

We have already noticed in Sec. 4.1.8, particularly in the remarks following Table 4.11, that the anomaly recovery improves for the anomalies covered by observations if additional anomalies all around the anomalies of interest are included in the solution. We would thus discuss 3 solutions, Solutions 250-5-1, 250-5-2, 250-5-3 indicating the 3 solutions for 5° anomalies using close satellite at a height of about 250 km. The statistics will be quoted only for the 12 anomalies of interest, as in Figure 4.10, but the number of anomalies solved for in the 3 solutions would be 12, 24 and 40 respectively. The layout of these 12, 24 and 40 anomalies has been shown in Figure 4.12.

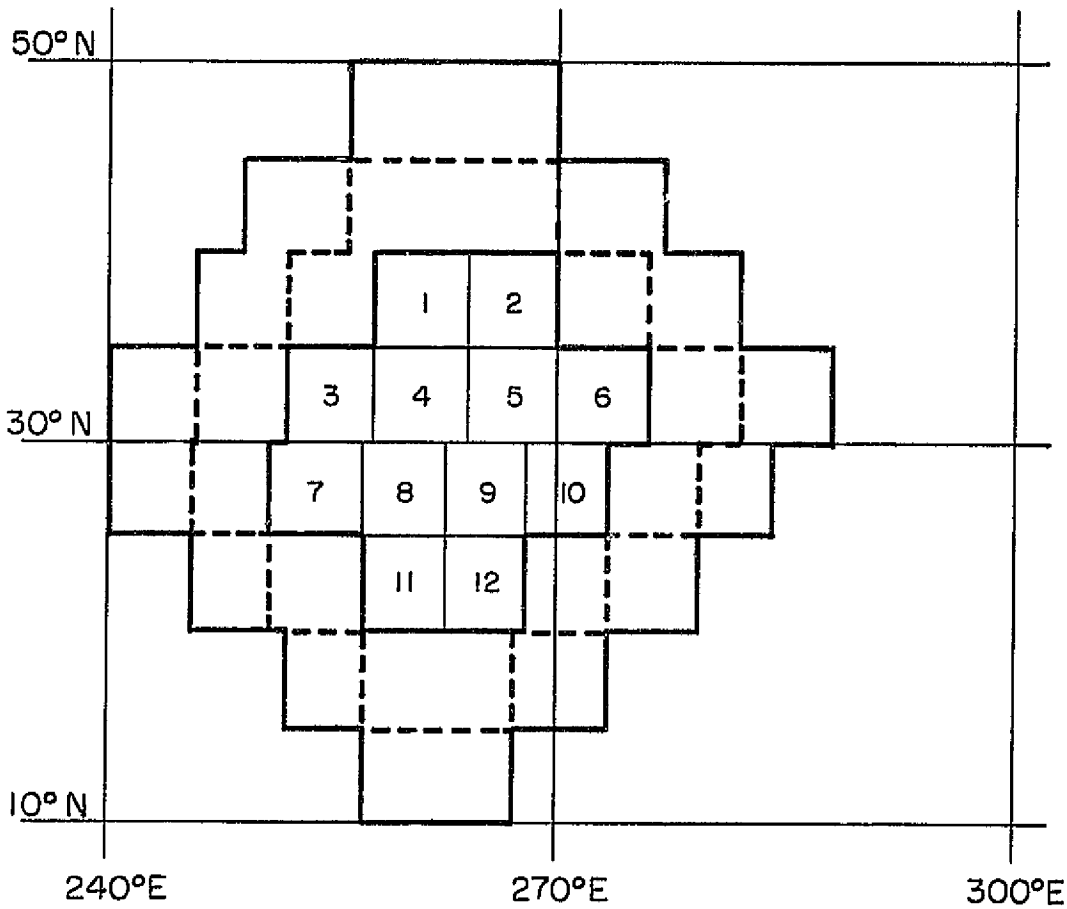

Figure 4.12 Layout of Anomalies for Solutions 250-5-1, 250-5-2, 250-5-3. No. of Anomalies Solved for Were 12, 24, 40 respectively.

Summed range rate observations with std. devn. of .08 cm/sec., and time interval of 10 seconds along an arc, were used for 12 arcs as in Figure 4.10 for all the three solutions, 250-5-1, 2, 3.

We will first report the anomaly discrepancies using 6 arcs, i.e. arc spacing roughly same as anomaly block size. Two different sets of 6 arcs were used. The location of these two sets of arcs are shown in Figures 4.13 a, b respectively.

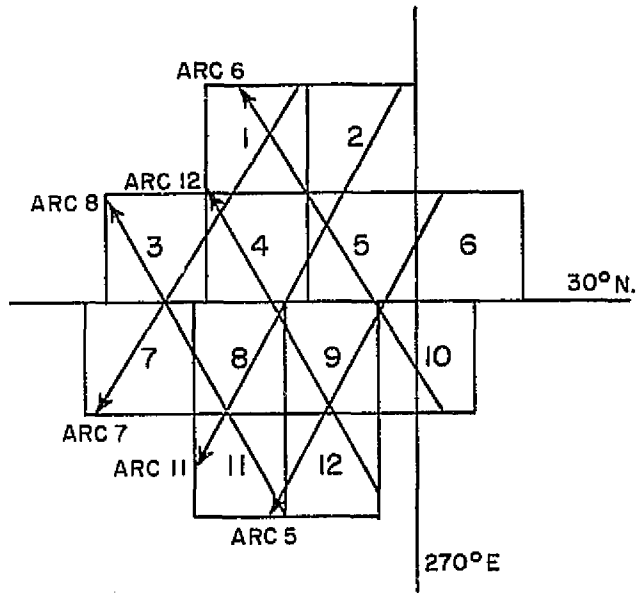

Figure 4.13a Case 1. Arcs 5 to 8, 11, 12.

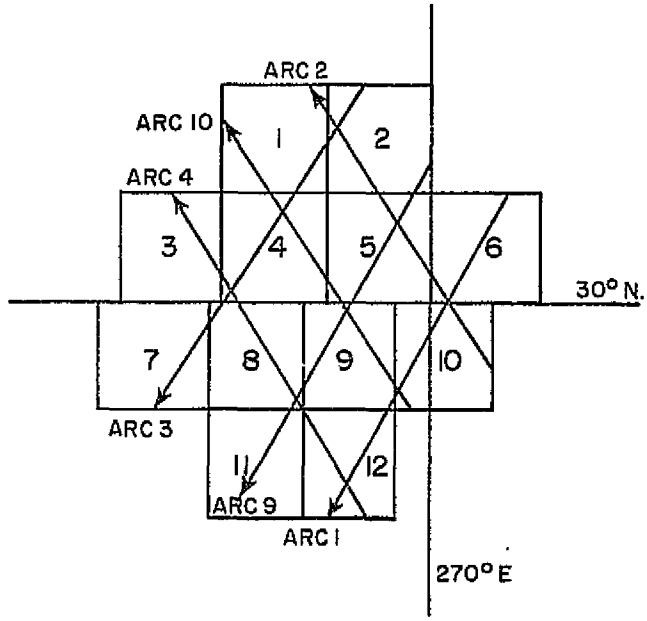

Figure 4.13b Case 2. Arcs 1 to 4, 9, 10.

Figure 4.13 Relative Location of Anomaly Blocks and 6 Arcs.

The spacing of arcs is the same in both cases, but in the first case the peripheral anomaly blocks on the west are better covered by observations as compared to the second case, while the reverse is true for the peripheral anomaly blocks on the east. However, as the misclosures of summed range rate are zero on the north-east and south-east edges because of fixing of the starting coordinates of each arc, as discussed in Sec. 2.3.3, and the misclosures increase as we proceed towards the west edge of the area, Case 2 is likely to give a worse anomaly recovery than Case 1. The anomaly discrepancies are given in Table 4.15 for Cases 1, 2 and also for their combination, i.e. using all the 12 arcs. To enable comparison of these cases, 40 anomalies, i.e. 2 additional anomalies all around the 12 anomalies of interest, were solved for in all the 3 cases, but anomaly discrepancies have been tabulated for only the 12 anomalies of interest.

Table 4.15

Relative Location of Anomaly Blocks and Arcs
Summed Range Rate Observations at 10 sec. Time Interval

Anom. No.	Anomaly Discrepancy in mgals Case 1. - 6 Arcs Arc No. 5 to 8, 11, 12	Case 2. - 6 Arcs Arc No. 1 to 4, 9, 10	12 Arcs Solution 250-5-3
1	-0.5	2.3	0.0
2	-0.1	1.3	-0.2
3	0.9	6.8	0.9
4	0.4	2.1	0.2
5	0.1	0.8	0.0
6	1.8	1.0	-0.5
7	3.6	9.9	2.5
8	1.4	0.3	0.9
9	0.5	0.7	0.4
10	1.0	0.7	0.1
11	1.4	-0.9	0.4
12	0.5	-0.3	0.4
R.M.S. Value	1.4	3.6	0.8

The largest change in anomaly discrepancies between Cases 1 and 2 occurs for Anomaly No. 3 and 7 on the west edge of the area. With reference to Figure 4.13, we find that this change is only due to the observations in Case 1

being positioned centrally over these anomalies as compared to Case 2. The difference in anomaly discrepancies between Cases 1 and 2 for the other 10 anomalies is only marginal, the R.M.S. value for these 10 anomaly discrepancies being 1.0 and 1.2 mgals respectively. If we now compare the anomaly discrepancies between Case 1 with Solution 250-5-3, we find that the anomaly discrepancies have been reduced for all anomalies because of decreased spacing of arcs. The reduction is noticeable not only for Anomalies No. 6, 10 on the east edge, but also for Anomalies No. 1, 7, 11 on the west edge. However, the anomaly discrepancy for Anomaly No. 7 continues to be large in Solution 250-5-3 as compared to other anomalies, exceeding 3 times the R.M.S. value of the 12 anomaly discrepancies. In view of the sharp reduction in anomaly discrepancies for Anomaly No. 3 and 7 in going from Case 2 to Case 1, it appears likely that we may achieve a still better anomaly recovery if the density of observations over peripheral anomalies is increased still further over the design of arcs in Figure 4.10, which we may recall, was already an improvement over the design of arcs in Figure 4.1 for 10° anomaly recovery. This aspect will be examined further in Sec. 5.1.3.

We may, however, emphasize as we discussed for Solution 10-3 in the end of Sec. 4.1.8, that Solution 250-5-3 does not fit as a suitable recovery model for 5° anomalies. As mentioned in Sec. 3.4 and shown in Figure 4.14, the summed range rate 'observations' were simulated using 52 5° anomalies, i.e. two 5° anomalies all around the area of investigation, and 37 10° anomalies, i.e. two 10° anomaly all around the periphery of 52 5° anomalies, thus taking into account the contribution of residual anomalies up to 30° around the area of investigation besides the global gravity field defined by potential coefficients up to degree and order 12. In Solution 250-50-3, we have now used these 'observations' to solve for 40 5° anomalies, i.e. two 5° anomalies all around the 12 anomalies of interest, thereby virtually repeating the process in reverse order. In Solution 10-3, we found an almost constant anomaly discrepancy of 0.3 mgals due to the effect of residual anomalies beyond 20° from the area of investigation being very little. The anomaly discrepancies are slightly larger in Solution 250-5-3, as we have gone up to 10° only from the area of investigation. But, as pointed out in remarks after Table 4.11 in Sec. 4.1.8, these discrepancies are small enough to show the adequacy of the computations of the partials matrix of observations with respect to unknown 5° anomalies, and the adequacy of the density of observations.

To elaborate further on Solution 250-5-3, the correlation coefficients between the 12 recovered anomalies as obtained from the variance-covariance matrix were very high. The average value of this correlation coefficient for anomalies in the same latitude zone between 2 adjacent anomalies was 0.78, and even between 2 anomalies separated by one anomaly block between them, it was 0.61. Its average value between two anomalies in adjacent latitude zones was 0.72, and between 2 anomalies separated by 2 latitude zones, it was still 0.55. The std. devn. of the 12 recovered anomalies were also large, the minimum, maximum and R.M.S. value being 6.9, 43.8, 20.5 mgals respectively.

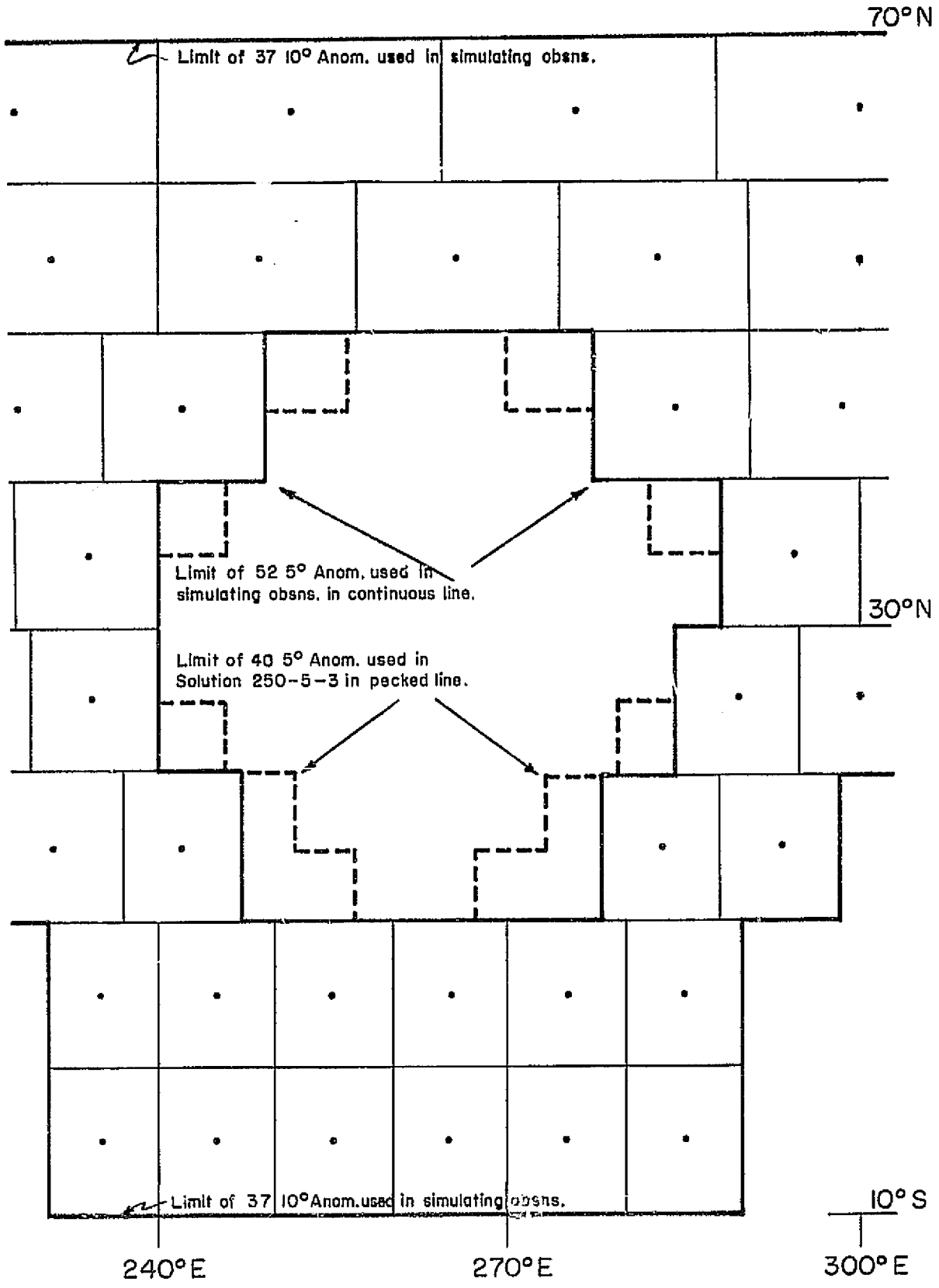

Figure 4.14 Limit of 40 5° Anomalies Used in Solution 250-5-3 in Relation to Anomalies used for Simulating Observations.

The anomaly discrepancy and std. devns. for 12 anomalies of interest in Solution 250-5-2 are given in Table 4.16, though, as already mentioned, 24 anomalies were solved for. This solution has been discussed further in Sec. 4.2.3.

Table 4.16

Solution 250-5-2.
Summed Range Rate Observation at 10 sec. Time Interval for 12 Arcs

Anom. No.	Expected Anomaly	Solution 250-5-2 Anomaly	Std. devn.	Anom. Discrep.
1	-21.8	-24.1	2.7	-2.3
2	-14.8	-12.2	1.5	2.6
3	-1.5	-4.9	4.3	-3.4
4	-12.9	-12.5	1.7	0.4
5	-9.6	-9.7	1.5	-0.1
6	3.2	-1.8	6.0	-5.0
7	16.8	17.7	5.0	0.9
8	1.0	1.8	2.2	0.8
9	-20.4	-20.6	1.4	-0.2
10	-0.3	3.3	1.7	3.6
11	22.4	22.2	5.2	-0.2
12	-9.1	-8.4	2.2	0.7
R.M.S. Value	13.7	13.9	3.4	2.3

Units are mgals.

In view of the discussion in Sec. 4.1, we need only mention that the minimum, maximum and the R.M.S. value of anomaly discrepancy in Solution 250-5-1, when only the 12 anomalies covered by observations were solved for, was -3.5, 13.9 and 6.8 mgals, i.e. the anomaly recovery was worse than Solution 250-5-2. We will thus examine only the Solution 250-5-2 for how good the anomaly recovery has been with respect to the criteria discussed in Sec. 4.1.9.

4.2.3 Recovery Model for 5° Equal Area Mean Anomalies

We again note that the std. devns. of the anomalies in Table 4.16, generally follow the same pattern as discussed before Table 4.13 in Sec. 4.1.9. The correlation coefficients between the 12 recovered anomalies obtained from the variance-covariance matrix of Solution 250-5-2 are shown in Figure 4.15.

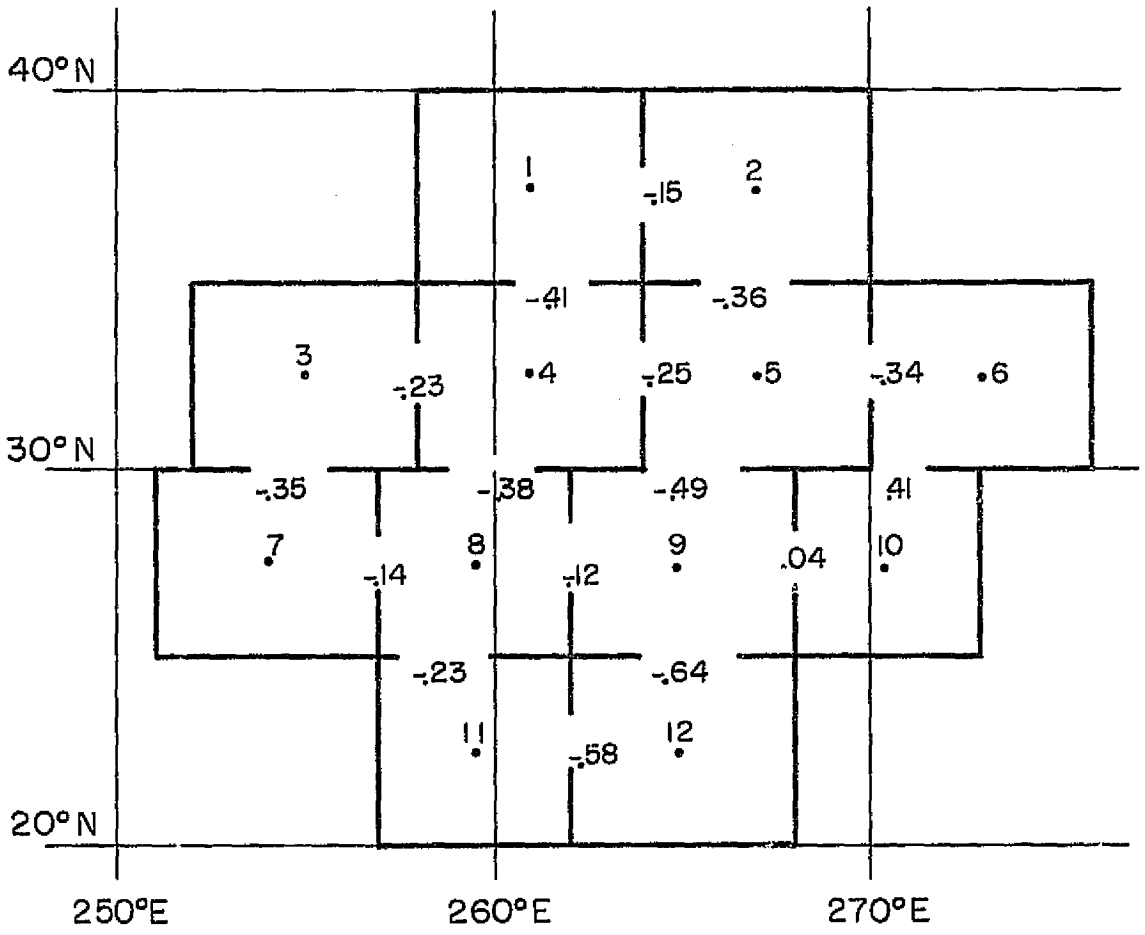

Figure 4.15 Correlation Coefficients Between Recovered Anomalies in Solution 250-5-2.

The correlation coefficients are shown between 2 adjacent anomalies both in the east-west and in the north-south direction. We note that the magnitude of the correlation coefficients is low; average value in the east-west direction is -.26, and average value in the north-south direction is -.41, which indicates that the individual 5° anomalies are being recovered.

We may now put together in Table 4.17 the statistics discussed in the end of Sec. 4.1.9 to examine the 'goodness' of anomaly recovery in Solution 250-5-2 for the 12 anomalies of interest.

Table 4.17

Statistics for 5° Anomaly Recovery in Solution 250-5-2
Summed Range Rate Observations at 10 sec. Time Interval for 12 Arcs

No. of anomalies recovered	24
No. of anomalies of interest	12
R.M.S. value of anomaly discrepancy (mgals)	2.3
R.M.S. value of expected anomalies (mgals)	13.7
R.M.S. value of recovered anomalies (mgals)	13.9
Correln. coeff. (ρ) of recovered anom. with expected anom.	0.986
Mean correln. coeff. of adjacent recovered anom. (E.W. direction)	-0.26
Mean correln. coeff. of adjacent recovered anom. (N.S. direction)	-0.41
R.M.S. value of std. devn. of recovered anom. (mgals)	3.4
Along-arc/Across-arc spacing of observations	3
R.M.S. value of std. devn. of recovered anom. corrected for spacing of observations (mgals)	5.9

We thus find that the anomaly recovery in Solution 250-5-2 is satisfactory, but the along-arc spacing of observations at 10 sec. time interval is about 3 times the across-arc spacing of observations with 12 arcs, as pointed out in the end of Sec. 4.2.1 after examination of Figure 4.11. The R.M.S. value of std. devn. of recovered anomalies should then be increased by a factor of $\sqrt{3}$ in view of the discussion in the end of Sec 4.1.9, and this has therefore been done in the last line of Table 4.17.

4.3 Recovery of Gravity Anomalies from Strong Signal

We will summarize here the recovery of 10° and 5° equal area mean anomalies, as obtained respectively in Solution 10-2 (Tables 4.11, 4.13, Figure 4.9) and Solution 250-5-2 (Tables 4.16, 4.17, Figure 4.15).

We have already summarized the criteria for examining the 'goodness' of anomaly recovery at the end of Sec. 4.1.9. To recapitulate briefly, for simulated observations not burdened with observational errors, the R.M.S. value of the anomaly discrepancy should be small, about 1/2 to 1/3 of the R.M.S. value of the expected anomalies. The R.M.S. value of the recovered anomalies should be comparable to the R.M.S. value of the expected anomalies, with a high value, say, about 0.9, of the correlation coefficient between the recovered and expected anomalies. The correlation coefficients between adjacent recovered anomalies, as obtained from their variance-covariance matrix, should be small, say less than 0.5, both in the east-west and in the north-south directions.

The R.M.S. value of the std. devn. of the recovered anomalies should be comparable to, or less than, the std. devn. of the expected anomalies, which may be obtained as the R.M.S. value of the expected anomalies. The std. devn. of the recovered anomalies should be computed for that spacing of along-arc observations, which is roughly equal to the spacing of observations between adjacent arcs. The optimum spacing of arcs was found to be half anomaly block size, i.e. roughly 6° and 3° respectively for the recovery of 10° and 5° equal area anomalies. The corresponding along-arc spacing is obtained when the time interval of observations along the arc is 1 minute and 30 seconds respectively (Figures 4.2 and 4.11). If the along-arc observations are closer, e.g. every 10 seconds in Solution 250-5-2, which is 3 times closer than the desired across-arc spacing of observations, then the resulting std. devns. of the recovered anomalies should be multiplied by $\sqrt{3}$ (Table 4.17 in Sec. 4.2.3).

The time interval of along-arc observations in Solution 10-2 was 1 minute, which was roughly the same as the across-arc spacing of observations of half anomaly block size, i.e. about 6°. However, in this case, we should have used the std. devn. of summed range rate observations as .03 cm/sec based on an integration interval of 1 minute, instead of .08 cm/sec based on an integration interval of 10 seconds. As all observations were considered to be independent and with the same std. devn., the resulting std. devn. of recovered anomalies in Table 4.13 should then be multiplied by a factor of 3/8. This has been done in Table 4.18 below, which gives the statistics for the anomaly recovery of 10° and 5° equal area mean anomalies for Solutions 10-2 and 250-5-2 respectively.

Table 4.18

Statistics for Recovery of 10° and 5° Equal Area Mean Anomalies from Strong Signal

Approximate height of close satellite (km)	900	250
Size of equal area mean anomaly blocks	10°	5°
Solution No.	10-2	250-5-2
Latitudinal extent of the area of investigation	70°	20°
Longitudinal extent of the area of investigation (approx.)	60°	25°
No. of anomalies of interest, covered by observations	37	12
No. of anomalies estimated	64	24
No. of anomaly blocks all around the area of investigation, not covered by obsns.	1	1
Spacing of Satellite arcs in terms of anomaly block size	1/2	1/2
Longitudinal spacing of satellite arcs (approx.)	6°	3°
No. of satellite arcs used in the solution	14	12
R.M.S. value of expected anomalies (mgals)	5.4	13.7
R.M.S. value of recovered anomalies (mgals)	5.5	13.9
Correln. coeff. of recovered anom. with expected anom.	0.998	0.986
R.M.S. value of anomaly discrepancy (mgals)	0.3	2.3
Mean " " "	-0.1	-0.2
Minimum " " "	-0.7	-5.0
Maximum " " "	0.8	3.6
Time interval of observations along an arc	1 min.	10 sec.
R.M.S. value of std. devn. of recovered anomalies (mgals)	5.2*	3.4
" " " , corrected for integration interval of observations	2.0	3.4
Ratio of along-arc to across-arc spacing of observations	1	3
R.M.S. value of std. devn. of recovered anomalies, corrected for integration interval and along-arc spacing of observations	2.0	5.9
Average correln. coeff. between adjacent recovered anom. (E.W. direction)	-0.32	-0.26
Average correln. coeff. between adjacent recovered anom. (N.S. direction)	-0.44	-0.41
Results tabulated in Chapter 4	Tables 4.11, 4.13 Figure 4.9	4.16, 4.17 4.15

*R.M.S. value for 31 anomalies, after leaving out 6 anomalies on the south and west edges of the area, not well covered with observations (see remarks after Table 4.13 in Sec. 4.1.9).

5. RECOVERY OF GRAVITY ANOMALIES FROM WEAK SIGNAL

We discuss in this Chapter the recovery of 5° equal area mean residual anomalies from the close satellite at a height of about 900 km, and the recovery of 2°.5 equal area mean residual anomalies from the close satellite at a height of about 250 km. The effect of anomalies in 5° blocks will obviously be felt less than the effect of anomalies in 10° blocks, on the close satellite at height of 900 km, and similarly, the effect of 2°.5 anomalies will be weaker than that of 5° anomalies on the close satellite at height of 250 km. The signal to be recovered from the summed range rate measurements is then weaker than the cases discussed in Sec. 4.1 and Sec. 4.2.

5.1 Recovery of 5° Equal Area Mean Anomalies from Close Satellite at Height of 900 km

5.1.1 Area of Investigation and Satellite Arcs

The area of investigation for the recovery of 5° anomalies from close satellite at height of 900 km, was retained to be the same as in Sec. 4.2. The location of the area, its shape, and the numbering of 5° anomalies to be recovered were also the same as in Sec. 4.2. The satellite arcs were selected to achieve symmetrical positioning over the area, and to achieve spacing of roughly 1/2 the anomaly block size. 13 arcs were chosen initially as compared to 12 arcs in Sec. 4.2 (see Figure 4.10). However, as discussed in Sec. 4.2.2, 4 more arcs were also selected, one in each corner of the area, to examine the effect of progressively increasing the density of observations directly over the peripheral anomaly blocks.

The location of the arcs with respect to the anomalies to be recovered is shown in Figure 5.1. The numbering of arcs from 1 to 13 was according to the starting time of the arc. The numbering of the corner arcs was in accordance with the examination of the effect on the anomaly recovery made from 13 arcs, as the additional arcs were added to the solution one at a time; and this order was arcs 14, 15, 14A and 15A respectively. Later, in Sec. 5.1.4, we will further investigate the effect of increasing the density of arcs from 1/2 anomaly block size to 1/4 anomaly block size. These arcs would be numbered 16 to 28. The particulars for Arcs 1 to 13, and for Arcs 14, 15, 14A, 15A, have been given in Table 5.1.

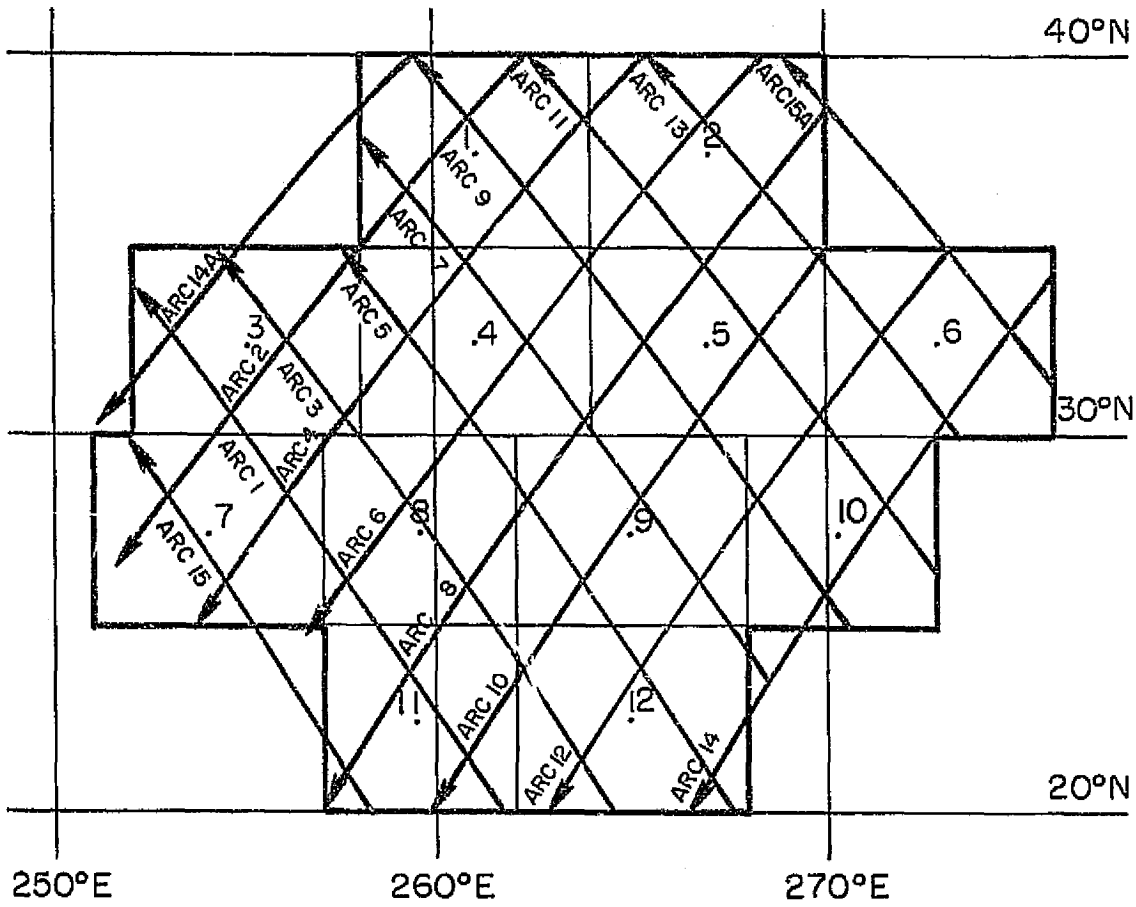

Figure 5.1 Satellite Arcs for Recovery of 5° Equal Area Mean Anomalies.
Arc Spacing ≈ $\frac{1}{2}$ Anomaly Block Size.
Height of Close Satellite ≈ 900 km.

Table 5.1

Satellite Arcs Used for Recovery of 5° Equal Area Mean Anomalies.
Height of Close Satellite ≈ 900 km

Arc No.	Ascending/ Descending Arc	Starting Time*				Duration of Arc		First & Last Subsatellite Pts. for Close Sat.			
		Day	Hour	Min.	Sec.	Min.	Sec.	φ°	λ°	φ°	λ°
1	↖	1	20	29	50	4	30	20.0	261.4	34.1	251.7
2	↙	2	10	41	20	4	30	40.5	262.6	27.0	251.8
3	↖	2	20	24	00	5	00	19.7	264.7	35.3	253.8
4	↙	3	10	35	40	5	10	40.3	265.5	24.7	253.4
5	↖	3	20	18	20	4	50	20.0	267.7	35.1	257.2
6	↙	4	10	30	00	5	10	40.1	268.5	24.5	256.4
7	↖	4	20	13	50	4	40	23.9	268.3	38.3	257.6
8	↙	5	10	24	40	6	10	38.9	270.5	20.2	256.8
9	↖	5	20	08	20	5	00	24.7	271.0	40.0	259.1
10	↙	6	10	20	00	5	10	35.7	270.9	19.9	259.8
11	↖	6	20	03	00	4	40	26.0	273.3	40.2	262.0
12	↙	7	10	14	20	5	10	35.5	273.8	19.6	262.7
13	↖	7	19	58	30	3	20	29.8	273.7	40.0	265.4
14	↙	0	09	12	40	4	30	33.7	275.9	19.9	266.5
15	↖	0	20	35	30	3	10	19.8	258.4	29.8	251.9
14A	↙	1	10	47	00	3	20	40.7	259.7	30.8	251.4
15A	↖	0	18	56	30	3	20	30.6	276.7	40.7	268.3

* in elapsed time from 21 Sept. 69 01 hr. 33 min. 36.3 sec. (See Sec. 1.1)

The time interval between observations along an arc in Sec. 5.1 was kept as 10 sec., as in Sec. 4.2. Hence, we would need to multiply the std. devns. of the recovered anomalies by $\sqrt{3}$, when we finally obtain a solution using satellite arcs shown in Figure 5.1. This has thus been taken into account only in Table 5.6 at the end of Sec. 5.1.3.

5.1.2 Relative Location of Anomalies and Arcs

We have already seen in Chapter 4 that the anomaly recovery in the area of investigation covered by satellite arcs, is 'good', when we include in the estimation process an additional anomaly all around the anomalies of interest. If we include in the estimation process two additional anomalies all around the anomalies of interest, the solution get worse as evidenced by large std. devns. and high correlation coefficients of the recovered anomalies. However, in this case, the anomaly discrepancies are much reduced due to a much larger sub-

set of anomalies being solved for, out of the total anomalie u ed in the simulation of 'observations'.

Hence, before we examine in detail the 'goodness' of anomaly recovery with a particular design of arcs, by the statistics discussed in the end of Sec. 4.1.9, it will be adequate, as an initial test, to examine the anomaly discrepancies for the 12 anomalies of interest in a solution, where 40 anomalies have been solved for. We will adopt this procedure in testing the improvement in anomaly recovery, as we consider the increase in density of observations over the area of investigation, and, in particular, over the peripheral anomalies. The std. devns. and anomaly discrepancies of the 12 anomalies of interest, will also be examined for the solutions, in which 24 anomalies, i.e. after inclusion of an additional anomaly all around the anomalies of interest, have been estimated. These two criteria of anomaly discrepancy, and std. devns. of the recovered anomalies, would be clarified when the results are presented.

We first present in Table 5.2 the anomaly discrepancies for the 12 anomalies of interest, both when 40 and 24 anomalies were solved for respectively, using Arcs 1 to 13 giving arc spacing of roughly half of anomaly block size. We may call these solutions as Solution 900-5-3 and Solution 900-5-2, 900 km being the height of close satellite, 5° being the anomaly block size, and suffixes 3 and 2 denote, as in Chapter 4, that respectively 2 or 1 additional anomalies all around the area of investigation have been included in the solution. The last column in Table 5.2 gives the std. devns. of the recovered anomalies in Solution 900-5-2.

Table 5.2

Anomaly Discrepancies and Std. Devns. for 12 5° Equal Area Mean Anomalies for Arc Spacing Roughly Half Anomaly Block Size.
Summed Range Rate Observations at 10 sec. Time Interval for 13 Arcs (Arcs 1 to 13).
Height of Close Satellite $\approx$ 900 km

Anom. No.	Anomaly Discrepancy in mgals Soln. 900-5-3	Soln. 900-5-2	Std. Devn. (mgals) Soln. 900-5-2
1	6.0	-3	72
2	0.2	-21	79
3	3.4	-11	86
4	-1.5	5	65
5	-1.8	12	69
6	3.4	-34	90
7	-0.8	10	88
8	-0.6	2	80
9	3.0	-16	63
10	-5.8	18	63
11	-4.8	0	121
12	2.5	18	98
R.M.S. value	3.4	15.6	83

The anomaly discrepancy in column 2 of Table 5.2 is much higher than the values in the last column of Table 4.15, in Sec. 4.2, when 5° recovery was being attempted with close satellite at height of 250 km. We have thus not been able to recover the 5° anomalies with close satellite at height of 900 km even when the spacing of arcs was roughly half of anomaly block size. This is still more evident from columns 3 and 4 of Table 5.2.

5.1.3 Satellite Arcs Over Peripheral Anomalies

Before we consider increasing the density of arcs further to roughly 1/4th of the anomaly block size, we would investigate the effect of considering greater density of observations over the peripheral anomalies. The arc spacing is still retained at roughly half anomaly block size, but we progressively add to the solution obtained with 13 arcs the observations of Arcs 14, 15, 14A and 15A. The number of anomalies solved for was 40 in all these 4 solutions. We report in Table 5.3 the anomaly discrepancies, as we add the observations in Arc 14 and Arc 15. The improvement or worsening of anomaly recovery, denoted by + and - signs respectively, has also been shown. The effect on the std. devns. of the recovered anomalies, as more arcs are included in the solution, will be examined later.

Table 5.3

Effect of Increasing the Density of Observations Over Peripheral Anomalies. Summed Range Rate Observations with Arc Spacing Roughly Half Anomaly Block Size. Height of Close Satellite ≈ 900 km

Anom. No.	Anom. Discrep. in mgals Arcs 1-14	Arcs 1-15	Improvement(+) or Worsening(-) of Anom. Discrep. (mgals) 13 to 14 Arcs	14 to 15 Arcs	13 to 15 Arcs
1	2.9	2.0	3.1	0.9	4.0
2	1.9	2.2	-1.7	-0.3	-2.0
3	4.7	4.0	-1.3	0.7	-0.6
4	-2.0	-1.9	-0.5	0.6	0.1
5	-1.0	-1.4	0.8	-0.4	0.4
6	1.0	1.4	2.4	-0.4	2.0
7	-3.6	0.5	-2.8	3.1	0.3
8	0.6	-1.0	0.0	-0.4	-0.4
9	1.7	2.2	1.3	-0.5	0.8
10	-2.4	-2.8	3.4	-0.4	3.0
11	-2.9	-0.9	1.9	2.0	2.9
12	1.6	0.8	-0.9	0.8	1.7
R.M.S. value of col (2),(3)	2.5	2.0	0.5	0.5	1.1
Mean value of col. (4) to (6)					

If we now examine the location of the arc added to the solution, with respect to the improvement in anomaly discrepancies, we find that the pronounced changes are in the peripheral anomalies; those below the arc show improvement, while those away from the arc get worse, but the latter's magnitude is slighly less than the improvement in the anomalies below the arc. When we consider the effect of additing both Arcs 14 and 15 to the solution obtained from 13 arcs, we find that almost all anomaly discrepancies improve with a mean value of 1.1 mgals. The single noticeable worsening by 2.0 mgals of anomaly No. 2 can perhaps be also overlooked as we find that the final anomaly discrepancy is still only 2.2 mgals compared to the R.M.S. value of 2.0 mgals.

It therefore appears that the increase in density of observations over the peripheral anomaly blocks improves the solution, even though small portions of Arcs 14 and 15 lie outside the area of investigation. It also appears that it is better to have symmetrical positioning of the Arcs i.e. with both Arcs 14 and 15 added to the 13 arcs.

We now present in Table 5.4 the effect on anomaly discrepancies of the 12 anomalies of interest, as we add Arcs 14A and 15A to the solution obtained by 15 arcs. The layout of Table 5.4 follows that of Table 5.3, and 40 anomalies were solved for, as before.

Table 5.4

Effect of Anom. Discrep. by Increasing the Density of Obsns. Over Peripheral Anomalies. Summed Range Rate Obsns. Using 16 and 17 Arcs. Height of Close Satellite ≈ 900 km.

Anom. No.	Anom. Discrep. in mgals 16 Arcs	17 Arcs	Improvement(+) or Worsening(−) of Anom. Discrep. (mgals) 15 to 16 Arcs	16 to 17 Arcs	15 to 17 Arcs
1	0.3	0.1	1.7	0.2	1.9
2	2.5	2.3	-0.3	0.2	-0.1
3	3.5	6.0	0.5	-2.5	-2.0
4	-0.9	-2.0	0.5	-1.1	-0.6
5	-1.3	0.4	0.1	0.9	1.0
6	1.4	-1.4	0.0	0.0	0.0
7	0.3	-0.5	0.2	-0.2	0.0
8	-1.0	-0.8	0.0	0.2	0.2
9	1.9	1.5	0.3	0.4	0.7
10	-2.6	-2.0	0.2	0.6	0.8
11	-0.9	-0.2	0.0	0.7	0.7
12	1.0	0.6	-0.2	0.4	0.2
R.M.S. value of cols (2),(3)	1.7	3.1	0.2	0.0	0.1
Mean value of cols. (4) to (6)					

From the last row in columns 4 to 6 of Table 5.4, we notice that the mean value of improvement of 0.2, 0.0, 0.1 mgals, by the addition of Arcs 14A and 15A is nearly zero; and is in any case less than the corresponding values of 0.5, 0.5 and 1.1 mgals in Table 5.3, when Arcs 14 and 15 were added to the solution obtained from 13 arcs. This may be explained by the geometry of the arcs in relation to the area of investigation, as may be seen from Figure 5.1. A much larger portion of Arcs 14 and 15 lie over the area, while only a smaller portion of arcs 14A and 15A lie over the area.

The reduction of std. devns. of the 12 anomalies of interest, with the addition of Arcs 14, 15, 14A and 15A was also examined. It was found that the reduction primarily occurs for the anomalies directly covered by the observations. This is, however, also accompanied by a slight reduction in the std. devns. of all other anomalies. We will designate the solution using 15 (Arcs 1 to 15) and 17 arcs (Arcs 1 to 15, 14A and 15A), and solving for 24 anomalies, as Solution 900-5-2A and Solution 900-5-2B respectively. The anomaly discrepancies and the std. devns. of the 12 anomalies of interest in these solutions are given in Table 5.5.

Table 5.5

Anom. Discrep. and Std. Devn. for 12 5° Equal Area Mean Anomalies for
Arc Spacing Roughly Half Anomaly Block Size
Summed Range Rate Obsns at 10 sec. Time Interval for 15 and 17 Arcs.
Height of Close Satellite ≈ 900 km

Anom. No.	Solution 900-5-2A		Solution 900-5-2B	
	Anom. Discrep.	Std. Devn.	Anom. Discrep.	Std. Devn.
1	-2.3	69	0.6	49
2	-24.7	73	-31.3	60
3	-13.3	77	-9.8	53
4	7.7	55	7.8	45
5	11.2	57	13.8	52
6	-29.6	46	-34.5	35
7	7.8	77	6.5	67
8	2.7	75	1.4	70
9	-19.5	57	-20.9	53
10	22.6	55	22.9	50
11	-8.9	93	-12.4	86
12	28.0	71	23.9	85
R.M.S. value	17.5	68	18.8	59

Units are mgals.

The results of Solutions 900-5-2A and 900-5-2B in Table 5.5 may be compared with the results of Solution 900-5-2 (13 Arcs) in Table 5.2. The R.M.S. value of the std. devn. decreases as we consider the solution with 13, 15 and 17 arcs to 83, 68 and 59 mgals respectively. We expect this to occur, as the density of observations over peripheral anomalies is increased to be nearly the same as over the anomalies in the center of the area. The reduction is more pronounced as we go from 13 to 15 arcs, but becomes less pronounced as we go from 15 to 17 arcs, which is also what we expect, as a smaller portion of the Arcs 14A and 15A lies over the area of investigation as compared to Arcs 14 and 15 (see Figure 5.1). However, when we consider the R.M.S. value of the anomaly discrepancies, it rises from 15.6 to 17.5, and then to 18.8 mgals, as we consider the solution with 13, 15 and 17 arcs, respectively. It is not clear why this should occur, except perhaps to indicate that 5° anomalies are not being recovered from the close satellite at height of 900 km. A greater density of observations increases the reliability, as evidenced from the reduction in std. devns. of the recovered anomalies. But as the R.M.S. value of the std. devns. is still so large, the anomaly discrepancies cannot be very meaningful.

We may now put together the statistics for examining the 'goodness' of recovery of the 5° anomalies, as discussed at the end of Sec. 4.1.9. This has been done in Table 5.6 for Solution 900-5-2A, using 15 arcs, which appears to be the optimum solution obtainable from arc spacing of half anomaly block size.

Table 5.6

Statistics for 5° Anomaly Recovery in Solution 900-5-2A.
Summed Range Rate Observations at 10 sec. Time Interval for 15 Arcs

No. of anomalies recovered	24
No. of anomalies of interest	12
R.M.S. value of anomaly discrepancy (mgals)	17.5
R.M.S. value of expected anomalies (mgals)	13.7
R.M.S. value of recovered anomalies (mgals)	23.0
Correln. coeff. (ρ) of recovered anom. with expected anom.	0.65
Mean correln. coeff. of adjacent recovered anom. (E.W. direction)	-0.54
Mean correln. coeff. of adjacent recovered anom. (N.S. direction)	-0.60
R.M.S. value of std. devn. of recovered anom. (mgals)	68
Along-arc/Across-arc spacing of observations	3
R.M.S. value of std. devn. of recovered anom. corrected for spacing of observations (mgals)	118

When we compare Table 5.6 with Table 4.17 of Sec. 4.2.3 for the recovery of 5° anomalies from close satellite at height of 250 km., it is obvious that we are not able to recover 5° anomalies from close satellite at height of 900 km with arc spacing of roughly half anomaly block size. In fact, all the criteria discussed at the end of Sec. 4.1.9 for examining the 'goodness' of anomaly recovery fail for Solution 900-5-2A in Table 5.6. We may now only check whether the anomaly recovery could be significantly improved by making the density of arc-spacing to 1/4th anomaly block size. This will be examined in Sec. 5.1.4.

5.1.4 Increased Density of Satellite Arcs

Thirteen additional satellite arcs were used in this investigation, which together with the 15 arcs in Sec. 5.1.1, gave the arc spacing as 1/4th anomaly block size, i.e. the longitudinal spacing of roughly $1\frac{1}{2}^{\circ}$. These 13 additional arcs have been shown by a dashed line in Figure 5.2, along with 15 arcs of Figure 5.1 which have been shown by a continuous line.

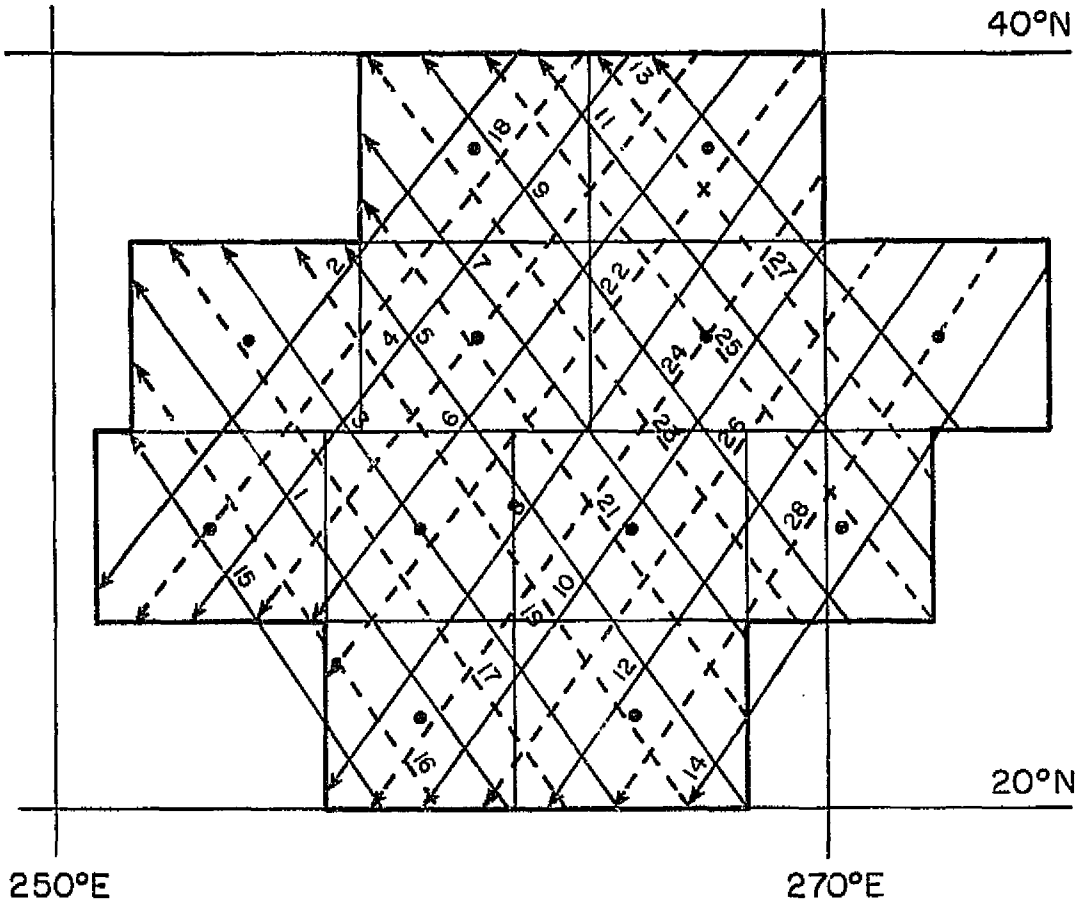

Figure 5.2 Satellite Arcs for Recovery of 5° Equal Area Mean Anomalies.
Arc Spacing ≈ 1/4 Anomaly Block Size.
Height of Close Satellite ≈ 900 km.

The numbering of the additional arcs was from 16 to 28 according to the starting time of the arc. The particulars of these arcs have been given in Table 5.7.

Table 5.7

Additional Satellite Arcs Used for Recovery of 5° Equal Area Mean Anomalies. Height of Close Satellite ≈ 900 km

Arc No.	Ascending/ Descending Arc	Starting Time*				Duration of Arc		First & Last Subsatellite Pts. for Close Sat.			
		Day	Hour	Min.	Sec.	Min.	Sec.	φ°	λ°	φ°	λ°
16	↖	25	23	19	20	3	50	19.7	260.2	31.7	252.2
17	↖	26	23	13	40	4	50	19.9	263.2	35.0	252.7
18	↙	27	13	25	20	5	00	40.3	264.1	25.2	252.3
19	↖	27	23	08	00	4	50	20.1	266.2	35.2	255.7
20	↙	28	13	19	40	5	00	40.1	267.0	25.0	255.3
21	↖	28	23	02	50	4	40	22.0	268.2	36.4	257.8
22	↙	29	13	14	00	5	40	39.9	270.0	22.7	257.0
23	↖	29	22	58	00	4	50	24.8	269.5	39.7	258.1
24	↙	30	13	09	30	5	20	36.2	269.9	19.9	258.3
25	↖	30	22	52	20	4	50	25.1	272.5	39.9	261.0
26	↙	31	13	04	10	4	50	35.0	272.0	20.2	261.6
27	↖	31	22	47	50	3	40	28.9	273.0	40.1	263.9
28	↙	32	12	58	30	4	50	34.8	274.9	20.0	264.4

* in elapsed time from 21 Sep. 69 01 hr. 33 min. 36.3 sec. (see Sec. 1.1)

The time interval between observations along an arc was again kept as 10 seconds. The arc spacing of 1/4th anomaly block size is now very nearly equal to the along-arc spacing of observations, or at most 1.5 times. We thus need not change the std. devns. of the recovered anomalies with 10 seconds time interval between observations, or if we wish to take a conservative view, multiply them by a factor of $\sqrt{1.5} = 1.2$.

We first present in Table 5.8 the anomaly discrepancies for the 12 anomalies of interest using the 13 additional arcs, both when 40 and 24 anomalies were solved for, and the std. devns for the latter case. The information in Table 5.8 for Arcs 16-28, may then be compared to that given in Table 5.2 for Arcs 1-13.

Table 5.8

Anom. Discrep. and Std. Devns. for 12 5° Equal Area Mean Anomalies for
Arc Spacing Roughly Half Anomaly Block Size.
Summed Range Rate Observations at 10 sec. Time Interval
Using 13 Additional Arcs (Arcs 16-28)
Height of Close Satellite ≈ 900 km

Anom. No.	# Anom. Solved →	Anom. Discrep. in mgals 40	24	Std. Devn. in mgals 24
1		1.0	2	107
2		-3.7	-28	87
3		3.1	-14	109
4		-2.3	-3	80
5		3.6	18	65
6		-5.4	-35	61
7		1.8	10	115
8		0.1	9	97
9		-0.9	-14	78
10		1.3	12	82
11		-0.8	-13	109
12		-1.1	20	100
R.M.S. value		2.6	17.4	92

The purpose of Table 5.8 was to assure ourselves that the normals and constant vector for the 13 additional arcs have been computed correctly, before we combine them with those obtained earlier to get a final solution with arc spacing of 1/4th anomaly block size, instead of the arc spacing of 1/2 anomaly block size attempted so far. This purpose is roughly met as may be seen by comparing the last rows of Tables 5.8 and 5.2.

We now present in Table 5.9 the anomaly discrepancies and std. devns. for the 12 anomalies of interest, for arc spacing of 1/4th anomaly block size for both 28 and 26 arcs (i.e. without arcs 14 and 15). In both cases, the anomaly discrepancy has first been given for the solution in which 40 anomalies have been estimated. This is then followed by the anomaly discrepancy and std. devn. when 24 anomalies have been estimated.

Table 5.9

Anom. Discrep. and Std. Devns. for 12 5° Equal Area Mean Anomalies
for Arc Spacing 1/4 Anomaly Block Size.
Summed Range Rate Obsns. at 10 sec. Time Interval for 28 and 26 Arcs.
Height of Close Satellite ≈ 900 km

	Arcs 1 to 28			Arcs 1 to 13, 16 to 28		
# Anom. Solved	40	24	24	40	24	24
Anom. No.	Anom. Discrep.	Anom. Discrep.	Std. Devn.	Anom. Discrep.	Anom. Discrep.	Std. Devn.
1	-3.0	1.1	54	-4.2	2.9	55
2	-2.9	28.2	52	-2.7	24.4	55
3	-3.5	14.9	56	-3.0	11.3	60
4	1.5	-6.1	43	1.7	-2.3	46
5	1.6	-13.5	42	1.9	-16.4	44
6	-1.5	30.1	35	-2.3	35.7	44
7	0.0	-7.0	58	0.4	-8.7	67
8	0.8	-6.3	56	0.5	-4.7	58
9	-2.1	21.2	42	-2.3	17.3	46
10	2.9	-21.9	41	3.7	-17.0	47
11	1.7	11.3	67	2.5	8.8	74
12	-1.1	-28.7	54	-1.6	-23.7	63
R.M.S. value	2.1	18.5	51	2.5	17.3	56

Units are mgals.

The effect of incorporating the 13 additional arcs in the solution obtained from Arcs 1 to 15 or in the solution obtained from Arcs 1 to 13 may now be examined by comparing Table 5.9 with Tables 5.5 and 5.2 respectively. In going from the solution with 15 arcs to the solution with 28 arcs, the R.M.S. value of the std. devn. falls from $68\sqrt{3} = 118$ mgals to $51\sqrt{1.5} = 62$ mgals, but the R.M.S. value of anomaly discrepancy goes up slightly from 17.5 mgals to 18.5 mgals. In the case of going from the solution with 13 Arcs to the solution with 26 Arcs, the R.M.S. value of std. devn. falls from $83\sqrt{3} = 144$ mgals to $56\sqrt{1.5} = 69$ mgals, but the R.M.S. value of anomaly discrepancy shows a slight rise from 15.6 mgals to 17.3 mgals. It may also be noticed that the difference between the solutions with 28 and 26 arcs in Table 5.9 is less marked than the difference between the solutions with 15 and 13 arcs in Tables 5.5 and 5.2.

It is however, clear that even by increasing the density of arcs to 1/4th anomaly block size, the R.M.S. value of the anomaly discrepancy remains about 15 to 20 mgals and R.M.S. value of the std. devn. of the recovered anomalies remains about 50 to 70 mgals. These appear to be the limiting values obtainable in the recovery of 5° anomalies using a close satellite at height of about 900 km, without using any a-priori information from terrestrial gravity data.

The recovery model for 5° anomalies has therefore to be re-examined. This will be done in Sec. 5.3, after investigating the recovery model for $2^\circ.5$ anomalies from close satellite at height of 250 km.

5.2 Recovery of 2°.5 Equal Area Mean Anomalies from Close Satellite at Height of 250 km

5.2.1 Area of Investigation and Satellite Arcs

The area of investigation for the recovery of 2°.5 anomalies from close satellite at height of 250 km, comprised of a total of 20 2°.5 equal area blocks. A total of 20 satellite arcs were selected to achieve symmetric positioning over the area, adequate coverage of the peripheral anomalies, and to achieve an arc spacing of about half anomaly block size, i.e. a longitudinal spacing of about 1½°. The limits of the 2°.5 anomaly blocks, and the satellite arcs, have been shown in Figure 5.3.

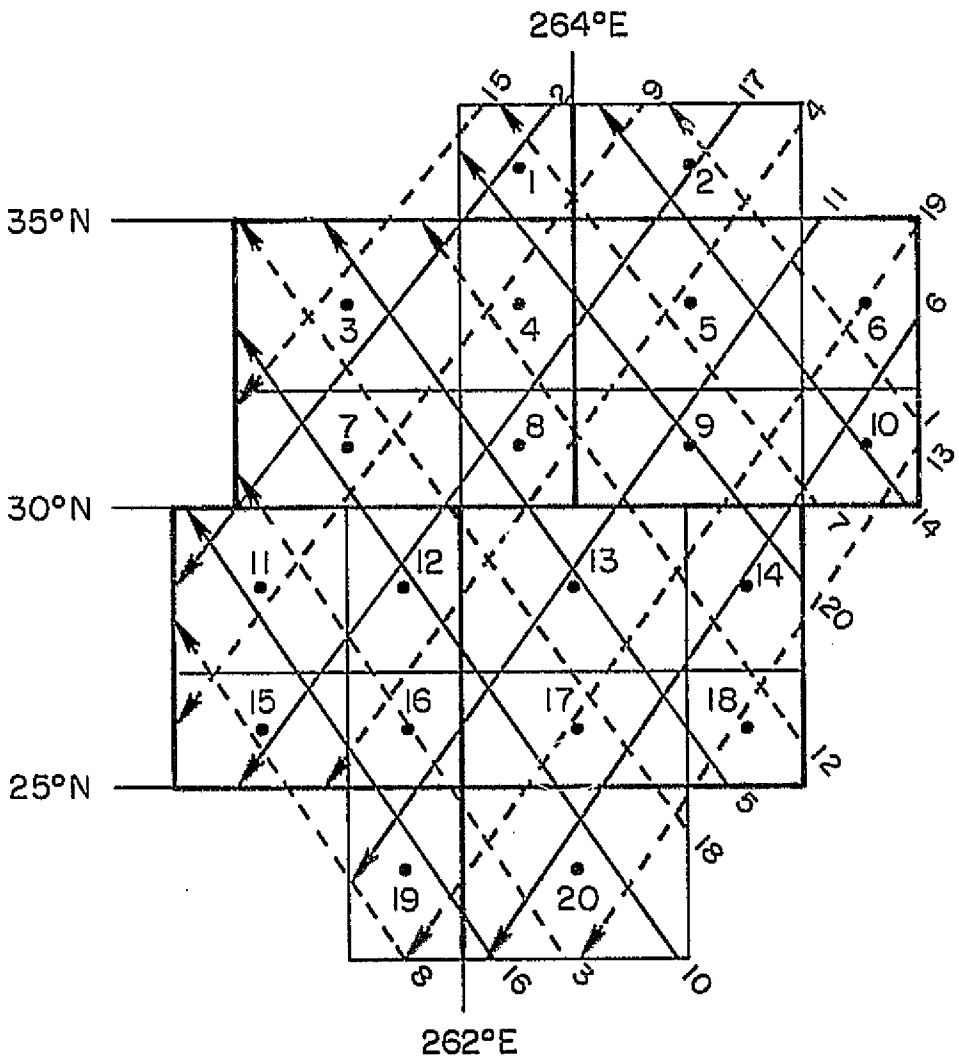

Figure 5.3 Satellite Arcs for Recovery of 2°.5 Equal Area Mean Anomalies. Arc Spacing = ½ Anomaly Block Size. Height of Close Satellite = 250 km.

as anomaly block size, we may either take 9 arcs shown by continuous lines in Figure 5.3, or else, we may take the 11 arcs shown by dashed lines. These 11 arcs cover some of the peripheral anomalies better, but have comparatively a small number of observations over the area of investigation. If we wish to consider the arc spacing of half anomaly block size, we may consider 16 arcs, i.e. excluding the 4 corner arcs. Or else, we may consider 18 arcs including the arcs No. 13 and 1, which have slightly larger number of observations over the area than arcs No. 8 and 15; finally we may consider all the 20 arcs shown in Figure 5.3. We will refer to the groups of arcs described above as 9, 11, 16, 18 and 20 arcs.

The number of $2^{\circ}.5$ anomalies, which we are considering for recovery, is 20. If we consider 1 or 2 additional anomalies all around them during the estimation process, the total number of anomalies becomes 36 and 56 respectively. The limits of these 20, 36 and 56 $2^{\circ}.5$ anomalies have been shown in Figure 5.4.

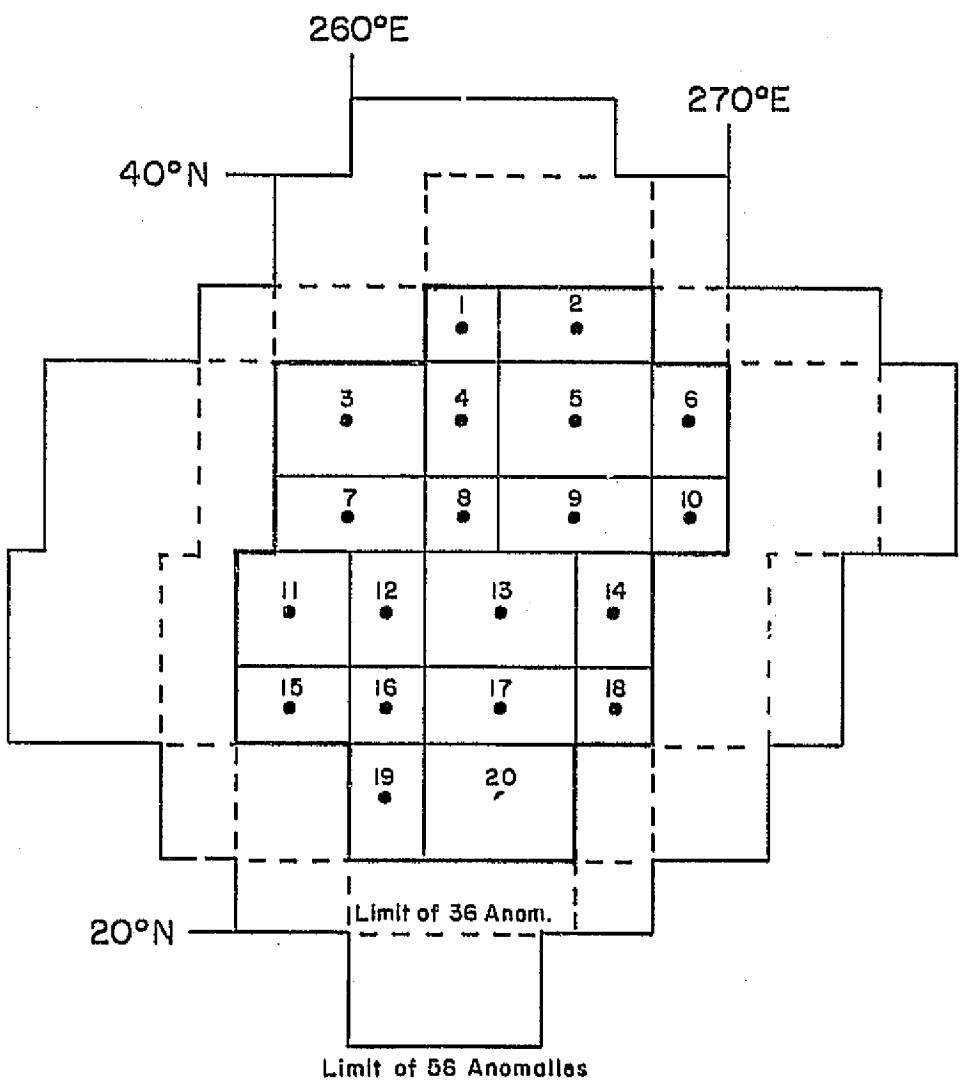

Figure 5.4 Limits of 20, 36 and 56 $2^{\circ}.5$ Equal Area Mean Anomalies.

Alternate arcs have been shown by a dashed line for convenience of reference. The numbering of the satellite arcs from 1 to 20 was again according to the starting time of the arc. The particulars for these arcs have been given in Table 5.10. The time interval between observations along an arc was kept as 10 seconds. The along-arc spacing of observations was then roughly equal to the across-arc spacing, when we consider it to be about half anomaly block size.

Table 5.10

Satellite Arcs Used for Recovery of 2°.5 Equal Area Mean Anomalies.
Height of Close Satellite ≈ 250 km

Arc No.	Ascending/ Descending Arc	Starting Time*				Duration of Arc		First & Last Subsatellite Pts. for Close Sat.			
		Day	Hour	Min.	Sec.	Min.	Sec.	φ°	λ°	φ°	λ°
1	↖	0	22	30	50	1	30	31.6	269.9	36.8	265.8
2	↙	2	13	42	50	2	30	37.0	263.4	28.2	256.8
3	↖	2	23	40	40	2	30	21.9	263.9	30.8	258.0
4	↙	3	13	34	30	3	20	36.6	267.9	24.9	259.3
5	↖	3	23	33	10	2	50	25.2	266.5	35.2	259.4
6	↙	4	13	27	00	3	10	33.3	270.0	22.1	262.4
7	↖	4	23	26	00	2	10	29.8	268.3	37.3	262.4
8	↖	7	00	36	20	1	40	21.7	260.9	27.7	257.1
9	↙	7	14	30	00	3	10	37.3	265.4	26.2	257.2
10	↖	8	00	28	00	3	10	22.1	265.5	33.4	257.8
11	↙	8	14	22	10	3	20	35.2	268.5	23.4	260.2
12	↖	9	00	20	30	2	40	25.5	268.1	34.9	261.4
13	↙	9	14	15	00	2	30	30.7	269.9	21.8	264.0
14	↖	10	00	13	20	2	00	30.0	269.8	37.0	264.5
15	↙	11	15	25	50	1	30	36.8	262.0	31.6	257.9
16	↖	12	01	23	40	2	20	22.0	262.6	30.3	257.0
17	↙	12	15	17	20	3	30	37.0	267.0	24.7	258.0
18	↖	13	01	15	50	3	00	24.2	266.0	34.8	258.4
19	↙	13	15	09	30	3	40	34.9	270.0	21.9	261.0
20	↖	14	01	08	30	2	20	28.2	268.1	36.3	262.0

* in elapsed time from 21 Sep. 69 01 hr. 33 min. 36.3 sec. (see Sec. 1.1)

5.2.2 Relative Location of Anomalies and Arcs

We will first describe the groups of arcs that may be considered for examining the anomaly recovery. If we consider arc spacing roughly the same

As per the discussion in Sec. 5.1.2, we will first examine the anomaly discrepancies for the 20 anomalies of interest when we have solved for 56 anomalies. This has been given in Table 5.11, when 9, 11, 16, 18 and 20 arcs were used in the solution. We will later consider the recovery of 20 anomalies from solution in which 36 anomalies have been solved for. We will use throughout Sec. 5.2 summed range rate observations with uniform std. devn. of .08 cm/sec., based on an integration interval of 10 seconds.

Table 5.11

Anom. Discrep. for 20 $2^{\circ}.5$ Equal Area Mean Anomalies
for 9, 11, 16, 18 and 20 Arcs.
2 Additional Anomalies All Around the Area Included in the Solution.
Height of Close Satellite $\approx$ 250 km

Anom. No.	Expected Anomaly	Anomaly Discrepancy in mgals 9 Arcs	11 Arcs	16 Arcs	18 Arcs	20 Arcs
1	-9.7	22.6	4.2	21.0	30.8	4.4
2	-10.0	-3.6	9.8	-1.9	-2.4	20.8
3	-31.0	-1.1	16.1	4.8	5.3	3.9
4	1.4	-9.4	1.3	-0.6	-3.1	4.8
5	-9.2	7.6	4.2	-0.3	-2.6	-5.0
6	3.8	-30.3	-3.5	7.8	11.7	18.0
7	2.1	-1.8	14.2	-0.3	-1.2	7.6
8	-11.3	14.2	7.0	3.4	6.8	4.7
9	-21.2	-0.9	9.8	4.1	3.2	7.1
10	-7.4	9.7	-0.1	6.1	0.9	1.6
11	4.4	-16.6	-26.5	6.9	8.4	-0.7
12	-17.3	12.2	11.7	1.2	5.6	11.2
13	-21.9	-2.2	6.7	3.5	0.8	1.7
14	5.1	1.8	5.8	-7.5	3.9	4.4
15	28.1	20.5	85.9	10.4	3.2	2.5
16	-20.5	-16.0	-3.9	9.0	7.4	11.4
17	-33.0	10.4	10.8	5.1	11.6	11.5
18	-28.6	-28.3	-24.9	-19.9	-29.2	-24.8
19	10.6	-5.6	85.1	20.5	17.0	20.5
20	-27.3	-9.6	-15.4	-4.8	-2.9	-5.4
R.M.S. value	18.3	14.2	29.4	9.4	11.5	11.1

We notice that the anomaly discrepancies are large in all cases, and the solutions are unstable. The R.M.S. value of anomaly discrepancies for the 20 anomalies, would only get worse in the solutions when we solve for 36 anomalies. This was discussed in Sec. 5.1.2, and is again found in Table 5.12.

Table 5.12

R.M.S. Value of Anomaly Discrepancies for 20 $2^{\circ}.5$ Equal Area Mean Anomalies for 9, 11, 16, 18 and 20 Arcs.
1 Additional Anomaly All Around the Area Included in the Solution.
Height of Close Satellite $\approx$ 250 km

No. of Arcs Used	R.M.S. Value of Anom. Discrep. (mgals)
9	17.8
11	28.3
16	32.3
18	34.0
20	26.7

We notice, in particular, the small increase in the R.M.S. value of anomaly discrepancy in the solution using 9 arcs, when we solve for 56 anomalies and 36 anomalies, the value being 14.2 and 17.8 mgals respectively. However, the instability of the solution is apparent, when we compare the values in the last line of Table 5.11 with the corresponding values in Table 5.12. To examine this in greater detail, the anomaly discrepancies and std. devns. using 9 arcs and 20 arcs, and solving for 36 anomalies in each case, has been shown in Table 5.13.

Table 5.13

Anom. Discrep. and Std. Devns. for 20 2°.5 Equal Area Mean Anomalies. Arc Spacing Roughly Same and Half Anomaly Block Size (9 & 20 Arcs respectively) Height of Close Satellite ≈ 250 km

Anom. No.	9 Arcs Anom. Discrep.	9 Arcs Std. Devn.	20 Arcs Anom. Discrep.	20 Arcs Std. Devn.
1	25.5	120.7	-38.3	31.1
2	-21.4	29.3	3.4	14.1
3	7.8	38.7	6.3	15.3
4	-10.6	77.7	-7.0	21.9
5	9.8	41.8	7.6	9.8
6	-36.0	112.4	-50.5	13.7
7	12.6	58.9	-13.1	19.2
8	-9.3	88.7	18.3	29.8
9	0.7	34.3	1.4	14.2
10	-1.2	80.4	-15.0	29.7
11	9.2	59.9	4.3	23.7
12	-11.5	50.6	0.1	21.3
13	7.9	25.3	-5.7	10.8
14	-35.6	85.5	4.2	15.4
15	24.7	128.7	2.1	39.2
16	-28.4	115.2	0.3	29.6
17	14.6	49.5	25.9	15.7
18	-11.6	100.2	-75.7	17.7
19	7.8	112.2	-53.3	20.6
20	-13.0	28.3	-7.7	12.0
R.M.S. value	17.8	79.5	26.7	21.8

Units are mgals.

The solution with 9 arcs, i.e. with arc spacing roughly same as anomaly block size is obviously unacceptable because of very large std. devns. of the recovered anomalies. The solution with 20 arcs, i.e. with arc spacing roughly 1/2 anomaly block size is also unacceptable because of large anomaly discrepancies, particularly for anomalies No. 6, 18 and 19. The large anomaly discrepancies could be caused by the increasing non-linearity of the mathematical model for the 2°.5 anomaly recovery, making it difficult to recover the anomalies from

the initial value of zero according to the procedure described in Chapter 2. We may then consider iterating the solution, and this will be discussed in Sec. 5.2.4. We may also consider using in the solution, the a-priori information about the variance of 2°.5 residual anomalies. In all solutions considered so far, we had taken the weight matrix for the anomalies, P_k in equation (2.43), to be zero. This will now be re-examined in Sec. 5.2.3.

We may also remark on the relative magnitude of the std. devns. of the recovered anomalies in the last column of Table 5.13. The scheme of subdivision of a 5° equal area block into 4 component 2°.5 blocks shown in Figure 3.1, results in the latter blocks being considerably unequal in area. From Figure 5.3, we then see that, for example, a larger number of observations fall over anomaly block No. 3 as compared to block No. 4 or 7. The number of observations over block No. 1 and 8 are still less. The std. devns. of anomalies No. 3,4,7,1 and 8 reflect this variation in the number of observations, values being 15.3; 21.9, 19.2; 31.1, 29.8 mgals respectively. The same pattern of variation in std. devn. is noticed in the last column of Table 5.13 for other 2°.5 blocks. It would be advisable, in future, to consider other schemes of formation of 2°.5 blocks to reduce this inhomogeneity of observations over neighboring blocks, but this has not been done during this study.

5.2.3 Solution Using A-Priori Variance of Residual Anomalies

The purpose of this study was to investigate the recovery of gravity anomalies from satellite to satellite tracking data alone, without using any terrestrial data. No a-priori information about terrestrial gravity anomalies and their std. devns. was thus used in any investigations reported so far. It would, however, be valid to use the a-priori information about the variance of the residual anomalies so long as it is kept the same for all anomalies being considered for recovery. We have discussed in Sec. 3.3 the formation of 2°.5 equal area residual anomalies. The variance for these 2°.5 anomalies, considering 104 anomalies in the area shown in Figure 3.4, was found to be 308 $mgals^2$. We may thus take the weight matrix of the 2°.5 residual anomalies to be a diagonal matrix with all elements on the diagonal being 1/308, instead of zero as considered so far. The initial value of all 2°.5 anomalies was still kept as zero in the adjustment scheme described in Sec. 2.2. This is therefore slightly different from a combination solution, where the a-priori estimates of the value of all terrestrial gravity anomalies, and their std. devns., may be used along with satellite to satellite summed range rate observations, to get a revised estimate of the gravity anomalies to fit all available data. We may, however, call the present procedure of using the variance of residual anomalies to form their weight matrix, also as a 'combination' solution, to differentiate it from the solutions already reported in Sec. 5.2.2. The anomaly discrepancies and std. devns. of the 20 anomalies of interest, from these 'combination' solutions using 9, 16, and 20 arcs, and solving for 36 anomalies is given in Table 5.14.

Table 5.14

Anom. Discrep. and Std. Devns. of 20 $2^{\circ}.5$ Equal Area Mean Anomalies
Using A-Priori Variance of Anomalies.
Height of Close Satellite $\approx$ 250 km

Anom No.	9 Arcs		16 Arcs		20 Arcs	
	Anom Discr	Std Devn	Anom Discr	Std Devn	Anom Discr	Std Devn
1	-13.5	15.5	-30.1	13.9	-22.7	13.1
2	5.0	10.6	13.6	9.3	9.2	9.0
3	2.6	9.2	-0.1	8.4	2.1	7.9
4	-6.8	12.1	-12.8	10.6	-12.8	10.5
5	-2.8	8.4	0.9	6.8	3.4	6.6
6	-3.6	14.2	-16.3	11.2	-33.9	8.4
7	-7.4	11.3	-5.5	9.9	-3.8	9.6
8	12.2	14.2	17.8	12.5	10.8	12.4
9	7.0	10.3	3.9	8.8	9.8	8.6
10	4.1	15.0	7.7	14.4	-6.9	13.4
11	9.6	10.7	3.0	9.4	-3.9	9.1
12	8.2	11.9	9.1	10.2	14.7	10.1
13	-3.3	7.2	-5.2	6.3	-6.4	6.2
14	-18.8	11.2	-16.7	9.6	-18.3	9.3
15	-9.1	13.9	-1.7	13.3	-11.5	12.4
16	23.1	14.7	1.5	13.1	-6.5	12.7
17	-9.6	11.4	4.7	9.4	15.7	9.1
18	8.3	14.4	18.3	11.6	-26.1	10.7
19	3.1	12.1	3.1	11.6	-25.4	10.1
20	10.2	8.6	1.4	7.6	-9.8	7.0
R.M.S. value	9.9	12.1	11.6	10.6	15.2	10.0

Units are mgals.

As the R.M.S. value of anomaly discrepancy in Table 5.14, using 20 arcs was larger than for both 16 arcs and 9 arcs, another 'combination' solution was tried for 20 arcs, in which the initial value for all 36 anomalies was retained as zero. The weight matrix was also kept as diagonal, with weights for the 20 anomalies of interest also retained as 1/308, to correspond to their std. devn. of 17.5 ($=\sqrt{308}$) mgals. However, for the remaining 16

anomalies outside the area of investigation, the weights were reduced to 1/900, corresponding to their std. devn. as 30.0 mgals. The choice of 30 mgals was arbitrary, but we do know from the results of the previous investigations, that the std. devns. of the recovered anomalies is considerably higher for the anomalies not covered by observations, as compared to those lying inside the area of investigation, and covered by observations. It may therefore be appropriate to reduce the weight in the 'combination' solution for the anomalies outside the area of investigation. However, the anomaly discrepancies in this test with 20 arcs remained large, with a R.M.S. value of 16.7 mgals. It may perhaps be argued that a 'combination' solution using 9 arcs gives lower anomaly discrepancies, as the std. devn. of 17.5 mgals is much lower than the std. devn. of the recovered anomalies, without using a-priori variance of the anomalies (see column 3 of Table 5.13). The effect of a-priori variance in the weight matrix of anomalies, is thus strongly felt in the combination solution with 9 arcs as compared to 20 arcs, as in the latter case the std. devn. of the recovered anomalies with zero weight matrix of anomalies, is already close to the value of 17.5 mgals (see last column of Table 5.13).

We cannot however justify using 9 arcs giving arc spacing roughly same as anomaly block size, in preference to 20 arcs giving arc spacing roughly half anomaly block size, in view of the experience gained so far from investigations in Chapter 4 and Sec. 5.1. We may therefore now consider a second iteration for the recovery of anomalies, in which we may use the initial value of anomalies different from zero. For the purpose of this iteration only, we may use the recovered anomalies as obtained from the combination solution using 9 arcs, as initial values instead of a zero vector. This will be investigated in Sec. 5.2.4.

5.2.4 Iteration Solution

The misclosures between 'observed' summed range rate value and the computed value was so far obtained by generating the orbits of the satellites using (12,12) potential coefficients only, and treating the residual gravity anomalies as zero. For obtaining the iteration solution, the initial value of the 20 residual gravity anomalies was taken to be as obtained from the combination solution using 9 arcs; and these were used for generating the orbits of the satellites besides the (12, 12) potential coefficients. The R.M.S. value of the misclosures of the summed range rate for the 20 arcs, when no residual gravity anomalies were used and when 20 residual gravity anomalies were used, are given in Table 5.15.

Table 5.15

R.M.S. Value of Misclosure Between Observed and Computed Value of Summed Range Rate ($\dot{R}_s$) With & Without 20 2°.5 Equal Area Residual Gravity Anoms. Height of Close Satellite ≈ 250 km

Arc No.	Misclosure in $\dot{R}_s$ in cm/sec	
	No Anomalies	20 Anomalies
1	0.434	0.714
2	1.007	0.710
3	0.459	0.237
4	0.717	0.207
5	1.330	0.077
6	0.501	0.416
7	0.331	0.491
8	0.871	1.090
9	1.029	0.641
10	0.971	0.229
11	0.724	0.025
12	0.815	0.106
13	0.397	0.797
14	0.206	0.519
15	0.791	0.690
16	0.041	0.382
17	0.836	0.395
18	1.321	0.175
19	0.643	0.246
20	0.556	0.332

We find that the misclosures were reduced in 14 out of 20 arcs. However, the reduction in the misclosure for 4 out of 14 arcs is not large. It is also marginal for arcs No. 20 and 3. The values of gravity anomalies in the iteration solution are therefore perhaps not much better as initial values, to ensure linearization of the mathematical model, as compared to the zero values used in the previous solutions in Sec. 5.2.2. The R.M.S. value of the anomaly discrepancy of 9.9 mgals (Table 5.14) for the anomalies used as initial values in the iteration solution is, in fact, slightly larger than half of the R.M.S. value of 17.5 mgals for the 2°.5 residual anomalies.

After obtaining the misclosure vector and the partial derivatives matrix as in Sec. 2.1, with initial values of gravity anomalies from 9 arcs combination solution, the correction vector to these initial values was obtained with the weight matrix of the gravity anomalies kept as zero. The anomaly discrepancy

for 20 anomalies of interest, using 9 arcs, in this iteration solution is given in Table 5.16, which may be compared with column 2 of Table 5.13. The std. devns. of the recovered anomalies were the same as in column 3 of Table 5.13.

Table 5.16

Anom. Discrep. for 20 $2^{\circ}.5$ Equal Area Mean Anomalies for 9 Arcs Iteration Soln. Height of Close Satellite $\approx$ 250 km

Anom. No.	Anom. Discrep (mgals)	Anom. No.	Anom. Discrep. (mgals)
1	29.3	11	10.8
2	-21.9	12	-12.0
3	8.0	13	7.4
4	-10.9	14	-34.8
5	9.3	15	25.0
6	-34.7	16	-30.2
7	12.2	17	16.6
8	-8.0	18	-13.8
9	0.9	19	6.3
10	-2.6	20	-13.9

On comparing Tables 5.16 and 5.13, we find that the anomaly discrepancies are almost the same in the original solution as in the iteration solution. We do not achieve any convergence from the iteration solution, as perhaps the initial values used in the iteration solution did not secure an improvement in the linearization of the mathematical model, over the zero values used in Sec. 5.2.2.

5.2.5 Recovery Model for $2^{\circ}.5$ Equal Area Mean Anomalies

The improvement in anomaly recovery by estimating an additional anomaly all around the area of investigation, which was first discussed in Sec. 4.1.8 and confirmed in later investigations, may perhaps be explained because of significant correlation between adjacent anomalies. The correlation between two anomalies, separated by one anomaly block between them, is weaker; and it is thus adequate to consider only 1 additional anomaly all around the area of investigation. This is so for 10° and 5° equal area anomalies as seen in Chapter 4. However, as the size of anomaly block is reduced to $2^{\circ}.5$ equal area, the correlation between two $2^{\circ}.5$ anomalies, separated by one anomaly block between them, may become significant. If we then allow two additional anomalies all around the area of investigation to be estimated, this correlation between every third anomaly is also taken into account. We have, in fact, already reported such solution in Table 5.11, in which 56 anomalies were estimated, i.e. 20 anomalies of interest with 2 additional anomalies all around them. These solutions were,

however not stable. We could then incorporate the information of a-priori variance of 2°.5 anomalies in a diagonal weight matrix, as in Sec. 5.2.3 instead of considering a zero weight matrix; and this 'combination' solution may make the solutions more stable. Again, as discussed after Table 5.14, the 36 anomalies outside the area of investigation may be given a lower weight as compared to the 20 anomalies of interest, lying inside the area of investigation.

The anomaly discrepancies and std. devns. determined on the above considerations, have been given for the 20 anomalies of interest in Table 5.17.

Table 5.17

Anom. Discrep. and Std. Devns. of 20 2°.5 Equal Area Mean Anomalies
Using A-Priori Variance of Anomalies.
2 Additional Anomalies All Around the Area Included in the Soln.
Arc Spacing Roughly Half Anomaly Block Size (20 Arcs)
Height of Close Satellite ≈ 250 km

Anom. No.	Expected Anomaly	Case 1. Uniform Weights Anom Discr	Std Devn	Case 2. Varying Weights Recov Anom	Anom Discr	Std Devn
1	-9.7	4.2	9.9	-4.2	5.5	14.9
2	-10.0	12.9	13.3	-1.4	8.6	10.5
3	-31.0	22.3	10.7	-20.9	10.1	9.4
4	1.4	-8.7	6.8	-7.4	-8.8	11.2
5	-9.2	-8.7	9.9	-9.8	-0.6	7.0
6	3.8	28.7	9.6	-14.2	-18.0	11.1
7	2.1	-5.8	12.7	-4.6	-6.7	10.2
8	-11.3	-0.6	8.7	-6.9	4.4	12.9
9	-21.2	9.0	13.5	-10.9	10.3	8.8
10	-7.4	35.8	11.7	-13.8	-6.4	14.2
11	4.4	-17.1	10.2	6.1	1.7	10.8
12	-17.3	-7.6	6.3	-13.1	4.2	10.5
13	-21.9	11.9	10.0	-23.9	-2.0	6.4
14	5.1	7.1	8.7	-9.3	-14.4	10.7
15	28.1	-42.0	12.9	13.7	-14.4	13.8
16	-20.5	-7.2	9.3	-11.0	9.5	13.1
17	-33.0	-2.6	11.9	-28.7	4.3	9.6
18	-28.6	31.2	11.4	-27.2	1.4	13.0
19	10.6	-41.8	7.4	4.2	-6.4	12.0
20	-27.3	11.9	11.5	-29.8	-2.5	8.1
R.M.S. value	18.3	20.3	10.5	15.5	8.5	11.1

Units are mgals.

The details of the solutions given in Table 5.17, were as follows:

All the 20 arcs were used in the solution. The initial value of all the 56 anomalies was taken as zero. The weight matrix of the anomalies was kept diagonal and two solutions were tried. In the first case, the weights for all the 56 anomalies was kept as $1/(17.5)^2$. In the second case, this weight was retained for the 20 anomalies of interest, but for the 36 anomalies outside the area of investigation, and thus not covered by observations, the weights were reduced to $1/30^2$. The expected value and the recovered value of anomalies in Case 2 have also been shown in Table 5.17.

The improvement in anomaly discrepancies for the 20 anomalies of interest, by assigning a low weight in Case 2 for the outside anomalies not covered by observations, is apparent from columns 3 and 6 of Table 5.17. This is particularly so for the peripheral anomalies, e.g., anomalies No. 3, 6, 10, 15, 18 and 19. We also notice by comparing column 3 of Table 5.17 with the last but one column of Table 5.14, that there is no improvement in the combination solution using 56 anomalies over the combination solution using 36 anomalies, if the weights of all anomalies are kept the same; the R.M.S. value of the anomaly discrepancy being 20.3 and 15.2 mgals respectively. The combination solution with uniform weights for 56 anomalies in column 3 of Table 5.17, also does not show any improvement over the original solution with zero weights for the 56 anomalies, in the last column of Table 5.11; the R.M.S. value of the anomaly discrepancy in the latter solution being 11.1 mgals. The optimum recovery model for $2^\circ.5$ equal area anomalies is therefore obtained by solving for 2 additional $2^\circ.5$ anomalies all around the area of investigation, and assigning lower weights to these outside anomalies not covered by observations. We will designate this solution as 2.5-3C; 2.5 for the size of anomaly block, 3 to indicate the inclusion of 2 additional anomalies in the solution, and C for the 'combination' solution obtained by assigning non-zero weights to the anomalies.

The statistics for examining the 'goodness' of anomaly recovery for the $2^\circ.5$ anomalies in the Solution 2.5-3C are given in Table 5.18.

Table 5.18

Statistics for $2^\circ.5$ Anomaly Recovery in Solution 2.5-3C.
Summed Range Rate Obsns. at 10 sec. Time Interval for 20 Arcs

No. of anomalies recovered	56
No. of anomalies of interest	20
A-priori std. devn. of anomalies of interest (mgals)	17.5
A-priori std. devn. of anomalies not covered by obsns. (mgals)	30
R.M.S. value of anomaly discrepancy (mgals)	8.5
R.M.S. value of expected anomalies (mgals)	18.3
R.M.S. value of recovered anomalies (mgals)	15.5
Correln. coeff. (ρ) of recovered anom. with expected anom.	0.92
Mean correln. coeff. of adjacent recovered anom. (E.W. direction)	-0.23
Mean correln. coeff. of adjacent recovered anom. (N.S. direction)	-0.39
R.M.S. value of std. devn. of recovered anom. (mgals)	11.1

5.3 Recovery Model for 5° Equal Area Mean Anomalies

We found in Sec. 5.1, with reference to the closing remarks in Sec. 5.1.4, that we could not recover 5° anomalies from close satellite at height of about 900 km, without using any a-priori information from terrestrial gravity data, i.e. when both the initial value and the weight matrix of the anomalies were considered to be zero. This was inspite of ensuring sufficient observations over the peripheral anomalies in Sec. 5.1.3, and inspite of increasing the density of satellite arcs from roughly 1/2 anomaly block size to 1/4 anomaly block size in Sec. 5.1.4.

We may therefore utilize the a-priori variance of 5° residual anomalies to form their weight matrix, as has been done in the case of the recovery of 2°.5 anomalies in the previous section. The investigations for the recovery of 5° anomalies from close satellite at height of 250 km in Sec. 4.2, show the optimum recovery with the inclusion of one additional anomaly all around the area of investigation in the estimation process. We may, however, also try the recovery with 2 additional anomalies all around the area of investigation, in view of the results of Sec. 5.2.5. Similarly, we may also experiment with the weights of anomalies outside the area of investigation, and thus not covered with observations, being lower than the weights for the anomalies covered by observations.

The variance of 52 5° equal area residual anomalies used in the simulation of observations in Sec. 3.4, was found to be 108 mgals^2. We may thus form the weight matrix of the anomalies as a diagonal matrix, with all elements on the diagonal being 1/108, i.e. uniform weights corresponding to the std. devn. of 10.4 mgals. We may also obtain another solution using a similar weight matrix, but where the weights for the anomalies outside the area of investigation correspond to the std. devn. of 20 mgals, i.e. varying weights. We report in Table 5.19, 3 solution using 15 arcs, and solving for 24 anomalies, i.e. one additional anomaly all around, with uniform weights (Case 1), and varying weights (Case 2). In Case 3, we still use 15 arcs, but solve for 40 anomalies, i.e. 2 additional anomalies all around, with varying weights. The initial value of all anomalies in all the 3 cases was kept as zero.

Table 5.19

Anom. Discrep. and Std. Devns. of 12 5° Equal Area Mean Anomalies
Using A-Priori Variance of Anomalies.
Summed Range Rate Obsns. at 10 sec. Time Interval for 15 Arcs
With Arc Spacing Roughly Half Anomaly Block Size.
Height of Close Satellite ≈ 900 km

Anom. No.	Case 1. 24 Anom Uniform Weight		Case 2. 24 Anom Varying Weight		Case 3. 40 Anom Varying Weight	
	Anom Discr	Std Devn	Anom Discr	Std Devn	Anom Discr	Std Devn
1	7.2	8.4	10.0	9.1	10.8	9.1
2	9.8	8.1	6.0	8.9	6.0	9.0
3	2.2	8.2	2.1	9.0	1.7	9.1
4	-3.8	7.5	-2.4	7.7	-2.5	7.8
5	-11.0	7.3	-9.5	7.6	-7.0	7.7
6	13.6	7.9	0.2	8.8	-0.7	8.9
7	-6.3	8.2	-10.7	9.1	-10.9	9.2
8	2.9	8.2	1.3	8.3	-0.8	8.3
9	4.5	7.3	7.7	7.5	7.6	7.6
10	-3.1	8.2	-3.8	8.9	-2.8	9.0
11	-13.1	8.2	-16.1	9.0	-16.1	9.1
12	6.8	7.4	7.7	8.5	8.1	8.7
R.M.S. value	8.0	7.9	7.9	8.6	7.8	8.6

Units are mgals.

The solutions in Cases 1 and 2 are comparable to Solution 900-5-2A reported in Tables 5.5 and 5.6, where the R.M.S. value of anomaly discrepancy was 17.5 mgals. We therefore notice the improvement in anomaly recovery, when we use the a-priori variance of anomalies to form their weight matrix. Secondly, we find from Table 5.19 that there is no noticeable difference in the solutions in the 3 cases. The improvement in anomaly recovery thus results from the diagonal weight matrix not being zero, but it is not material if the weights are uniform, or are lower for the anomalies not covered with observations. Also, unlike Sec. 5.2.5, it is adequate to consider one additional anomaly all around the area of investigation. This was also found when two other solutions were tried analogous to Cases 2 and 3, but using 28 arcs, i.e. with arc spacing of 1/4th anomaly block size, the R.M.S. value of the anomaly discrepancy being 7.5 and 7.4 mgals respectively.

We may thus consider the optimum model for the recovery of 5° anomalies from close satellite at a height of about 900 km, being Case 2 of Table 5.19, where we utilize the a-priori variance of the anomalies. The arc spacing is then 1/2 anomaly block size, as more arcs to give a spacing of 1/4 anomaly block size do not cause a proportionately large improvement. Only one additional anomaly all around the area of investigation is included in view of the investigations in Sec. 4.2; but lower weights are assigned to anomalies not covered by observations, in view of the investigations in Sec. 5.2.5.

We have to now recall that the along-arc observations being at time interval of 10 seconds, were 3 times more closely spaced than the spacing between the arcs, which was about half anomaly block size. If we were not considering combination solution, we would have multiplied the std. devns of the recovered anomalies by $\sqrt{3}$. We could have also got the same results if we had multiplied the weight matrix of observations by 1/3, and then we do not scale the std. devns. of recovered anomalies. Accordingly, when considering the combination solution, we may multiply the first term of the normals in equation (2.42) by 1/3 before adding the weight matrix P_x based on the a-priori variance of anomalies. Case 2 of Table 5.22 was then run again with this modification.

We will call this as Solution 900-5-2C, 900 km being the height of the close satellite, 5 for size of anomaly blocks being recovered, 2 for including one additional anomaly all around the area of investigation, and suffix C to indicate a 'combination' solution. The statistics for examining the 'goodness' of anomaly recovery in Solution 900-5-2C are given in Table 5.20.

Table 5.20

Statistics for 5° Anomaly Recovery in Solution 900-5-2C.
Summed Range Rate Obsns. at 10 sec. Time Interval for 15 Arcs

No. of anomalies recovered	24
No. of anomalies of interest	12
A-priori std. devn. of anomalies of interest (mgals)	10.4
A-priori std. devn. of anomalies not covered by obsns (mgals)	20
R.M.S. value of anomaly discrepancy (mgals)	8.5
R.M.S. value of expected anomalies (mgals)	13.7
R.M.S. value of recovered anomalies (mgals)	8.5
Correln. coeff. (ρ) of recovered anom. with expected anom.	0.81
Mean correln. coeff. of adjacent recovered anom. (E.W. direction)	-0.18
Mean correln. coeff. of adjacent recovered anom. (N.S. direction)	-0.18
R.M.S. value of std. devn. of recovered anom. (mgals)	9.0

6. USE OF REAL DATA AND CONCLUSIONS

6.1 Use of Real Data

An effort was made throughout this study to use data, which would be similar to the real data, likely to be available later. This is particularly true for the data in Sec. 4.1 and 5.1, with the close satellite at height of about 900 km, which is likely to correspond closely to the Geos-C/ATS-6 configuration. The geometry, and the density of the across-arc and along-arc observations, and the nominal satellite Keplerian elements used in this study correspond closely to the proposed values.

The use of real data would obviously bypass the discussion in Sec. 3.4 about the extent of anomalies for simulation of observations, as it would sense the global effect of the gravity anomalies at the satellite altitude. The summed range rate measurements would, however, require preprocessing, primarily for the refraction effects for the ground ATS-6 tracking station to the ATS-6 relay satellite. As the relay satellite is nominally geostationary, and the signal path through the ionosphere and troposphere remains nearly the same for various observations in a satellite arc, the refraction corrections are likely to be well determined. The transponder delays of the satellites are not likely to cause any significant errors within the range of their calibration uncertainties of a few microseconds.

The initial state vector of the satellites for starting integration for individual arcs could not be determined in this study, as the observations were simulated for periods of 5 to 20 minutes only. The starting coordinates have thus to be obtained for each arc from an optimum combination of various tracking data (Martin, 1969; Martin, 1971; Kahn et al; 1972). It may be possible to refine these estimates further, by considering the summed range rate data over the entire usable period of the arc, over which the close satellite may be tracked by the relay satellite, say, over a 40 minutes arc. These final estimates may then be held fixed, as in this study, for the portion of the arc used over the area of investigation. This approach needs further investigation.

The subdivision of a 10° equal area block into component blocks of various sizes has been described in Sec. 3.1. In this study, the residual mean anomalies over a block of a given size, were estimated as a correction vector to an initial zero value vector. After obtaining these estimates of residual anomalies from the satellite to satellite tracking data, it may be desired to combine these with the estimates obtained from the terrestrial gravity data. The combined estimate may be obtained directly as indicated in equation (2.41) in Sec. 2.2.1. The terrestrial estimates of the residual anomalies may be obtained according to the scheme described in Sec. 3.3. Finally to convert

the residual anomalies, $\Delta g'$, into gravity anomalies, Δg_T, with respect to a given reference ellipsoid through a specified gravity formula as in equations (3.7) and (3.8) in Sec. 3.2, we may compute the gravity anomaly Δg_{PC}, implied by the accepted set of potential coefficients as in equation (3.3), and then obtain Δg_T from equation (3.1).

6.2 Computer Run Timings

The main computer program used in this study was the November, 1972 version of the Geodyn program (Chin, Goad and Martin, 1972), which was modified to accept gravity anomalies. These modifications have been described separately (Karki, 1973; Hajela, 1974). The Geodyn program was primarily used in data simulation mode for obtaining normals, and for the computation of the solution vector. A few supporting programs were also written separately, as described in Sec. 2.3.3. All information in this Section pertains to the IBM 360/175 Computer.

The computer runs, which took the most time, were for simulating observations using gravity anomalies, in addition to the (12,12) potential coefficients. For the close satellite at height of 900 km, with integration step size of 1 minute, it took about 54 seconds per arc of about 20 minutes duration, with data interval as 30 seconds. For the same satellite, it still took about 43 seconds per arc of about 5 minutes duration, with data interval as 10 seconds. For the close satellite at height of 250 km, with integration step size of 30 seconds, it took about 47 seconds per arc of about 5 minutes duration, with data interval as 10 seconds. If we were to simulate observations without using gravity anomalies, it took only about 8 seconds per arc of about 20 minutes duration for the close satellite at height of 900 km, in contrast to 54 seconds per arc, when gravity anomalies were also used.

The computer runs for obtaining the normal equations depended primarily on the number of anomalies to be estimated. For 92 and 40 anomalies to be estimated, it was respectively about 32 and 22 seconds per arc. Other computer runs for obtaining individual arc normals from summed normals for several arcs; or to combine normals for several arcs from individual arc normals, would take little time, about 5 seconds or less for the whole run. It would take similar time to reduce the number of unknowns from the summed normals. The inversion of normals and the computation of solution vector, were likewise about 5 seconds or less, once the normals and constant vector were available on the magnetic tape.

The core storage requirement for the Geodyn program in the data reduction mode is about 360K, when no gravity anomalies are input to the program. Additional storage of about 1.5 K is required for each gravity anomaly input to the program. Further information may be seen in the Geodyn program documentation (1972).

6.3 Summary of Results

The results of anomaly recovery for the preferred solutions in Chapters 4 and 5, have been summarized in Tables 6.1 and 6.2 respectively. The solutions for anomaly recovery extracted from Chapter 4, did not use any a-priori information about gravity anomalies, i.e. their initial value was taken as a zero vector, and their weight matrix was also taken as zero. The solutions for anomaly recovery extracted from Chapter 5, assumed the initial value of gravity anomalies as a zero vector, but the weight matrix was taken as a diagonal matrix, with weights as the reciprocal of a-priori variance of the gravity anomalies. The weights were the same for all anomalies covered with observations, and a lower weight for all anomalies not covered with observations.

Table 6.1

Summary of Results for Anomaly Recovery from Strong Signal
Summed Range Rate Obsns. with Std. Devn. 0.08 cm/sec. for Integration Interval of 10 Sec.
Simulated Obsns. without Observational Errors. Zero Weight Matrix for Anomalies.

Approximate height of close satellite (km)	900	250
Size of equal area mean anomaly block	10°	5°
Latitudinal extent of the area of investigation	70° 10°S-60°N	20° 20°N-40°N
Longitudinal extent of the area of investigation (approx.)	60° 240°-300° E	25° 250°-275° E
No. of anomalies of interest, covered by obsns.	37	12
No. of anomalies estimated	64	24
No. of anomaly blocks all around the area of investigation, not covered by obsns.	1	1
Spacing of satellite arcs in terms of anomaly block size	1/2	1/2
Longitudinal spacing of satellite arcs (approx.)	6°	3°
No. of satellite arcs used in the solution	14	12
R.M.S. value of expected anomalies (mgals)	5.4	13.7
R.M.S. value of recovered anomalies (mgals)	5.5	13.9
Correln. coeff. of recovered anom. with expected anom.	0.998	0.986
R.M.S. value of anomaly discrepancy (mgals)	0.3	2.3
Mean value of anomaly discrepancy (mgals)	-0.1	-0.2
Minimum value of anomaly discrepancy (mgals)	-0.7	-5.0
Maximum value of anomaly discrepancy (mgals)	0.8	3.6
Time interval of observations along an arc	1 min.	10 sec.
R.M.S. value of std. devn. of recovered anomalies (mgals)	5.2*	3.4
R.M.S. value of std. devn., corrected for integration interval of observations	2.0	3.4
Ratio of along-arc to across-arc spacing of observations	1	3
R.M.S. value of std. devn. of recovered anoms., corrected for integration interval and along-arc spacing of obsns	2.0	5.9
Average correln. coeff. between adjacent recovered anom. (E.W. direction)	-0.32	-0.26
Average correln. coeff. between adjacent recovered anom. (N.S. direction)	-0.44	-0.41
Results tabulated in Chapter 4	Soln. 10-2 Tables 4.11, 4.13; Figure 4.9 Also see Table 4.18	Soln. 250-5-2 4.16, 4.17 Figure 4.15

*R.M.S. value for 31 anomalies, after leaving out 6 anomalies on the south and west edges of the area, not well covered with observations (see remarks after Table 4.13 in Sec. 4.1.9).

Table 6.2

Summary of Results for Anomaly Recovery from Weak Signal
Summed Range Rate Obsns. with Std. Devn. 0.08cm/sec for Integration Interval of 10 Sec.
Simulated Observations without Observational Errors.
Diagonal Weight Matrix for Anomalies Using A-Priori Variance

Approximate height of close satellite (km)	250	900
Size of equal area mean anomaly block	$2^\circ.5$	5°
Latitudinal extent of the area of investigation	15° $22^\circ - 37^\circ$ N	20° $20^\circ - 40^\circ$ N
Longitudinal extent of the area of investigation (approx.)	13° $257^\circ - 270^\circ$ E	25° $250^\circ - 275^\circ$ E
No. of anomalies of interest, covered by obsns.	20	12
No. of anomalies estimated	56	24
No. of anomaly blocks all around the area of investigation, not covered by obsns.	2	1
A-priori std. devn. for weight matrix, for anomalies covered with obsns. (mgals)	17.5	10.4
A-priori std. devn. for weight matrix, for anomalies not covered with obsns. (mgals)	30	20
Spacing of satellite arcs in terms of anomaly block size	1/2	1/2
Longitudinal spacing of satellite arcs (approx.)	$1\frac{1}{2}^\circ$	3°
No. of satellite arcs used in the solution	20	15
R.M.S. value of expected anomalies (mgals)	18.3	13.7
R.M.S. value of recovered anomalies (mgals)	15.5	8.5
Correln. coeff. of recovered anom. with expected anom.	0.92	0.81
R.M.S. value of anomaly discrepancy (mgals)	8.5	8.5
Mean value of anomaly discrepancy (mgals)	-1.0	-0.4
Minimum value of anomaly discrepancy (mgals)	-18.0	-17.9
Maximum value of anomaly discrepancy (mgals)	10.3	12.1
Time interval of observations along an arc	10 sec.	10 sec.
Ratio of along-arc to across-arc spacing of observations	1	3
R.M.S. value of std. devn. of recovered anom. corrected for spacing of observations*	11.1	9.0
Average correln. coeff. between adjacent recovered anom. (E.W. direction)	-0.23	-0.18
Average correln. coeff. between adjacent recovered anom. (N.S. direction)	-0.39	-0.18
Results tabulated in Chapter 5	Soln. 2.5-3C Tables 5.16, 5.17	Soln. 900-5-2C Table 5.20

* See discussion before Table 5.20 in Sec. 5.3.

We may recall here the criteria used for judging the 'goodness' of anomaly recovery. For simulated observations, not burdened with observational errors, the R.M.S. value of anomaly discrepancy should be small, say 1/2 to 1/3 times the R.M.S. value of the expected anomalies. The R.M.S.value of recovered anomalies should be comparable to the R.M.S. value of the expected anomalies, with a high value, say, about 0.9, of the correlation coefficient between the recovered and expected anomalies. The R.M.S. value of the std. devns. of the recovered anomalies should be comparable to, or less than, the std. devn. of the expected anomalies, which may be obtained as the R.M.S. value of the expected anomalies. The correlation coefficients between adjacent recovered anomalies, both in the east-west and in the north-south directions, should be small, say less than 0.5.

We may also mention, in brief, the main conclusions about the observational data. The optimum number of satellite arcs to be used in the solution, are those, which achieve a spacing of about half of the anomaly block size desired to be recovered. This spacing refers to adjacent ascending, or descending, arcs. The satellite arcs should be uniformly spaced, and located symmetrically with respect to the area of investigation, considering both the ascending and descending arcs. It is necessary that the peripheral anomaly blocks are nearly as well covered with observations, as the central anomalies. The optimum shape of the area of investigation would thus depend on the inclination of the satellite. For satellites with inclination between $30^\circ - 60^\circ$, the shape of the area of investigation should be nearly a rhombus, with its diagonals in the east-west and in the north-south direction. The latitudinal extent of the area should not exceed about 40°, and should preferably lie wholly over either the equatorial region, or the mid-latitude region.

The observations should not extend beyond the area of investigation. If the spacing of observations along an arc is more dense than the spacing of observations between adjacent arcs, say n times, then the std. devns. of the recovered anomalies should be multiplied by a factor of $\sqrt{n}$. Alternatively, the scaling of the std. devns. of the recovered anomalies may also be achieved by multiplying the weight matrix of the observations by a factor of 1/n.

An additional anomaly all around the area of investigation should be estimated along with the anomalies covered by observations. However these anomalies not covered with observations, would not be recovered; and information should be extracted from the solution for only those anomalies covered by the observations. Only one additional anomaly all around the area of investigation is to be included in the solution for the recovery of 10° and 5° anomalies; but for smaller blocks like $2^\circ.5$, 2 additional anomalies all around the area of investigation, are to be included in the solution.

The anomaly recovery improves, if instead of taking the weight matrix of anomalies to be zero, we use a diagonal weight matrix with the same weight for all anomalies covered by observations, as the reciprocal of a-priori variance of the gravity anomalies. The weight for all anomalies not covered with observations,

is also same, but is lower than the weight for the anomalies covered by observations. The anomalies could not be recovered with weak signal, as discussed in Chapter 5, without using this information about the a-priori variance of the gravity anomalies.

Summed range observations are not sensitive enough, as compared to the summed range rate observations, for the recovery of gravity anomalies. For the recovery of residual anomalies in regional, or local, areas, no constraints should be imposed on the recovered anomalies to satisfy any specified values of the spherical harmonic coefficients.

Finally, we may compare the results of Schwarz (1970) with those obtained in the present study. These results cannot be compared rigorously because of the differences in the configuration of satellites, in the recovered parameters and in the size of blocks. The 'uncertainties' in the recovered values of density parameters by Schwarz may however, be related to the std. devns. of the recovered anomalies in this study, by first multiplying by a factor of 2π; and then by a factor of 16 to account for the std. devn. of summed range rate observations used by Schwarz being .005 cm/sec as compared to .08 cm/sec in this study for the integration interval of 10 seconds.

Schwarz (Solution 8.1) obtained an uncertainty of 0.6 to 1.8 mgals in the recovered values of $2^\circ \times 2^\circ$ density parameters, with the close satellite at height of 200 km tracked by a geosynchronous relay satellite. This is then equivalent to 60 to 180 mgals ($= 0.6$ to $1.8 \times 2\pi \times 16$) for comparison with the std. devns. of recovered $2^\circ.5$ equal area anomalies in this study from close satellite at height of 250 km. In Solution 5.1, using 2 low satellites in nearly same orbit at height of about 200 km, his uncertainty is equivalent to 80 to 240 mgals. The correlation coefficients in these 2 solutions were about -0.8 in the east-west direction and about -0.6 in the north-south direction. As the spacing between arcs used by Schwarz was roughly the same as block size, instead of 1/2 block size, his results can be perhaps compared with the solution for 9 arcs in Table 5.13 in this study, with the R.M.S. value of std. devns. of recovered anomalies being $80/\sqrt{2} = 112$ mgals. The final results obtained in Solution 2.5-30 in this study have been summarized in Table 6.2, which gives the R.M.S. value of std. devn. of recovered anomalies as 11 mgals, and the correlation coefficients in the east-west direction as -0.2, and in the north-south direction as -0.4. The spacing of arcs in this solution was 1/2 anomaly block size and the a-priori variance of anomalies was used in forming their weight matrix.

For $5^\circ \times 5^\circ$ density parameters, using 2 low satellites at height of about 300 km, Schwarz's uncertainty (Solution 3.1) is equivalent to 10 to 30 mgals. The correlation coefficients were about -0.6 in the east-west direction and 0.4 in the north-south direction. These results can be perhaps compared with the solution for 6 arcs in Sec. 4.2.2 for the recovery of 5°

equal area mean anomalies using a close satellite with height of 250 km. As this was considered inadequate spacing of arcs, the R.M.S. value of the std. devns. was not given but it was $7.9\sqrt{6}$ 19 mgals. For 12 arcs, i.e. with arc spacing of about 1/2 anomaly block size, the particulars for Solution 250-5-2 have been summarized in Table 6.1, which gives the R.M.S. value of std. devn. of recovered anomalies as 6 mgals, and the correlation coefficients in the east-west direction as -0.3, and in the north-south direction as -0.4.

Again, for $5^{\circ} \times 5^{\circ}$ density parameters, using 2 low satellites at height of about 700 km, Schwarz's uncertainty (Solution 1.4) is equivalent to 60 to 400 mgals. The correlation coefficients were about -0.8 in the east-west direction, and -0.2 to 0.2 in the north-south direction. These results are comparable with the solution for 8 arcs in Sec. 5.1.2 for the recovery of 5° anomalies using a close satellite with height of about 900 km. The R.M.S. value of the std. devns. was $190\sqrt{6} = 465$ mgals. The final results obtained in Solution 900-5-2C in this study have been summarized in Table 6.2, which gives the R.M.S. value of std. devn. of recovered anomalies as 9 mgals, and the correlation coefficients in the east-west and in the north-south directions as -0.2 mgals. The spacing of arcs in this solution was 1/2 anomaly block size and the a-priori variance of anomalies was used in forming their weight matrix.

We thus find that there are 2 noticeable differences in this study and that of Schwarz. The spacing between the arcs considered by Schwarz was roughly the same as the size of block in which density parameters were being estimated, while the optimum spacing of arcs was found to be 1/2 block size in this study. Secondly, Schwarz does not allow for the possibility of using a-priori knowledge of the variance of the parameters being recovered, to form a weight matrix for them. It was found in this study that there was a remarkable improvement in the anomaly recovery of $2^{\circ}.5$ anomalies from close satellite at height of 250 km, and of 5° anomalies from close satellite at height of 900 km, i.e. when the signal was weak, if the knowledge of the a-priori variance of anomalies was used to form their weight matrix.

6.4 Suggestions for Further Study

During the recovery of anomalies discussed in Chapter 4, no use was made of any a-priori information from the terrestrial data for these gravity anomalies. The recovery of anomalies was entirely from the information in the signal from satellite data, i.e. the summed range rate observations. In Chapter 5, the signal from satellite data alone was not sufficient to recover the anomalies. We then utilized the a-priori information about variance of these anomalies to assign a non-zero weight matrix for them. This weight matrix was diagonal and the weights assigned were the same for a set of anomalies. The initial value of all the anomalies was still kept as a zero vector. We thus did not utilize the a-priori estimates of these gravity anom-

alies from terrestrial observations, nor did we assign different weights to the anomaly estimates. Further study should be made for the optimum utilization of these terrestrial estimates of anomalies, and their std. devns., for getting a revised estimate, incorporating all available information from satellite and terrestrial observations. Rapp (1973b) has already reported the results of recovering 15° anomalies using optical satellite data, and a-priori terrestrial estimates of 15° anomalies and their std. devns. A study may now be made for the recovery of anomalies in smaller size, say 10° and 5° equal area blocks, by utilizing summed range rate observations from the Geos-C/ATS-6 tracking, and a-priori terrestrial estimates of these 10° and 5° anomalies.

Further study is also needed to obtain the starting coordinates of the close and realy satellites, for a short arc of the close satellite of less than one revolution, to fit the observations over a short time span of 5 to 20 minutes. This has already been indicated in Sec. 6.1. The accuracy with which these starting coordinates can be determined, and the effect of the uncertainty in this determination on the computed value of the summed range rate, needs to be investigated. The uncertainty in this computed value would affect the misclosure from the observed value, and this erroneous value would be propogated into the correction vector of the parameters of interest.

We have considered in this study the residual gravity anomalies referred to a set of potential coefficients complete up to degree and order 12. The purpose of using a potential field of higher order was to reduce the magnitude of the residual anomalies. However, as noted in Sec. 3.2 (Tables 3.1 and 3.2), this reduction was not substantial. It may be investigated if it would be better to define the earth's normal gravitational potential by utilizing a still larger set of potential coefficients, or some other representation, which would still retain the computational convenience of potential coefficients in generating the orbits (Kaula, 1970; Lundquist and Giacaglia, 1972), and the residual anomalies are then defined with respect to this new representation.

The shape of the area of investigation was discussed in Sec. 4.2. However, the extent of the area of investigation for the recovery of 5° and $2^{\circ}.5$ anomalies in Sec. 4.2 and Chapter 5, was chosen rather arbitrarily for the computational convenience of being covered by a limited number of satellite arcs. We did discuss in Sec. 4.1.9, the desirability of the area of investigation being separate for equatorial regions and mid-latitude regions, and accordingly limited to about 40° in latitudinal extent. It may further be investigated if there is any optimum extent of the area, which would yield a balance between computational effort and accuracy of anomaly recovery, for the case of summed range rate observations. This investigation may follow the report of Argentiero, Kahn and Garza-Robles (1974), where the discussion pertains to the recovery of gravity anomalies from altimeter data.

The formation of $2^{\circ}.5$ and 5° equal area blocks, as component blocks of 10° equal area blocks, has been discussed in Sec. 3.1, and the estimation of residual gravity anomalies in these blocks from terrestrial data in Sec. 3.3. We, however, note that this scheme results in the $2^{\circ}.5$ blocks being considerably unequal in area. This then leads to a non-homogeneous distribution of the number of observations over neighboring $2^{\circ}.5$ blocks, as discussed in the end of Sec. 5.2.2. The variation in the area of $2^{\circ}.5$ blocks was a result of these being meaned from the 25 1° equal area blocks, which were the smallest blocks in which the gravity anomaly was estimated or predicted within a 5° block, as discussed in Sec. 3.3. A new subdivision scheme of 5° blocks into $2^{\circ}.5$ and 1° blocks may be investigated, which would retain the advantages of the present scheme, but reduce the large variation in the area of neighboring $2^{\circ}.5$ blocks.

BIBLIOGRAPHY

Argentiero, P., Kahn, W.D., Garza-Robles, R. Strategies for Estimating the Marine Geoid from Altimeter Data, Goddard Space Flight Center, Greenbelt, Maryland. April, 1974.

Arnold, K. Determination of Gravity Anomalies by Satellite Geodesy; in The Use of Artificial Satellites for Geodesy; AGU Monograph No. 15, 1972.

Chin, M.M., Goad, C.C., and Martin T.V. Geodyn System Description, Vol. I, II, III. Wolf Research and Development Corporation, Riverdale, Maryland. September, 1972.

Cigarski, G.A., Velez, C.E. Cowell Orbit Generator Error and Time Analysis Program. Goddard Space Flight Center, Maryland. August, 1967.

Comfort, G.C. Direct Mapping of Gravity Anomalies by Using Doppler Tracking Between A Satellite Pair. J. Geophys. Res., 78, 6845-6851, 1973.

Desrochers, G.A. A Study of the Aliasing Effect on Gravitational Potential Coefficients as Determined from Gravity Data. Department of Geodetic Science Report No. 160. The Ohio State University, Columbus. December, 1971.

Geodyn System Description, Volume I. (See Chin, Goad and Martin, 1972).

Hajela, D.P. Quadrature Errors in the Partial Derivatives Required for the Direct Recovery of Gravity Anomalies from Satellite Observations. Department of Geodetic Science Report No. 189, The Ohio State University, Columbus. December, 1972.

Hajela, D.P. The Computatin of 15° and 10° Equal Area Block Terrestrial Free Air Gravity Anomalies. Department of Geodetic Science Report No. 194. The Ohio State University, Columbus. February, 1973.

Hajela, D.P. Modifications to Geodyn Program for Estimation of Gravity Anomalies. Unpublished. July, 1974.

Heiskanen, W.A. and Moritz, H. Physical Geodesy. W.H. Freeman and Company. San Francisco. 1967.

Hirvonen, R.A., and Moritz, H. Practical Computation of Gravity at High Altitudes. Report No. 27, Inst. Geod. Phot. Cart., The Ohio State University, Columbus, 1963.

Kahn, W.D., Bryan, J.W., Felsentreger, T.L., Wagner, C.A. Geos-C/ ATS-F Tracking and Gravimetry Experiment. Goddard Space Flight Center, Maryland. November, 1972.

Karki, P. The Use of Geodyn Program for Gravity Anomaly Recovery. Unpublished. May, 1973.

Kaula, W.M. Theory of Satellite Geodesy. Blaisdell Publishing Company, Mass. 1966.

Kaula, W.M. (Editor). The Terrestrial Environment: Solid Earth and Ocean Physics. Report of a Study at Williamstown, Mass. August, 1969.

Kaula, W.M. The Appropriate Representation of the Gravity Field for Satellite Geodesy. Proceedings 4th Symposium on Mathematical Geodesy, pp. 57-65. Com. Geod. Ital., Bologna, 1970.

Kaula, W.M. Error Analysis of Earth Physics Satellite Systems, Final Report, Part I. University of California, Los Angeles. October, 1972.

Koch, K.R. and Morrison, F. A Simple Layer Model of the Geopotential from a Combination of Satellite and Gravity Data. J. Geophys. Res., 75, 1483-1492, 1970.

Koch, K.R. and Witte, B.U. Earth's Gravity Field Represented by a Simple Layer Potential from Doppler Tracking of Satellites. J. Geophys. Res., 76, 8471-8479, 1971.

Lange, B.O., DeBra, D.B., Kaula, W.M. Final Technical Report on a Preliminary Design of a Drag-Free Satellite and its Application to Geodesy. Stanford University Center for Systems Research, Guidance and Control Laboratory, May, 1969.

Lundquist, C.A. and Giacaglia, G.E.O. Geopotential Representation with Sampling Functions; in The Use of Artificial Satellites for Geodesy; AGU Monograph No. 15, 1972.

Martin, C.F. Accuracy of Satellite Orbits Obtainable by Synchronous Satellite Tracking - C.3.1. Wolf Research and Development Corporation, Riverdale, Maryland. 1969.

Martin, C.F. Optimum Usage of Ground Stations for Geos-C Orbit Determination. Wolf Research and Development Corporation, Riverdale, Maryland. October, 1971.

Martin, C.F. Geodyn Modifications for Satellite to Satellite Tracking and Surface Density Layer Estimation. Wolf Research and Development Corporation, Riverdale, Maryland. February, 1972a.

Martin, T.V. Geodyn System Operations Description, Volume III. Wolf Research and Development Corporation, Riverdale, Maryland. February, 1972b.

Mikhail, E.M. Paramaeter Constraints on Least Squares. Photogrammetric Engineering, 36(12): 1277-91, 1970.

Moritz, H. A General Theory of Gravity Processing. Department of Geodetic Science Report No. 122. The Ohio State University, Columbus. May, 1969.

Mueller, I.I. Introduction to Satellite Geodesy. Frederick Ungar Publishing Company, New York. 1964.

Mueller I.I. Spherical and Practical Astronomy as Applied to Geodesy. Frederick Ungar Publishing Company, New York. 1969.

NASA. Geos-C Mission Proposal Briefing Information, Wallops Island, Virginia. December, 1972.

NASA. Geos-C Mission Plan. Wallops Island, Virginia. May, 1974.

Obenson, G.T. Direct Evaluation of the Earth's Gravity Anomaly Field from Orbital Analysis of Artificial Earth Satellites. Department of Geodetic Science Report No. 129. The Ohio State University, Columbus. March, 1970.

Rapp, R.H. The Direct Combination of Satellite and Gravimetric Data for Mean Anomaly Determination. Department of Geodetic Science Report No. 131. The Ohio State University, Columbus. January, 1971a.

Rapp, R.H. Equal Area Blocks. Bulletin Geodesique, No. 99, pp. 113-125, March, 1971b.

Rapp, R.H. Implementation Suggestions for the Direct Combination of Satellite and Gravimetric Data. Department of Geodetic Science Report No. 167. The Ohio State University, Columbus. December, 1971c.

Rapp, R.H. The Formation and Analysis of a 5° Equal Area Block Terrestrial Gravity Field. Department of Geodetic Science Report No. 178. The Ohio State University, Columbus. June, 1972.

Rapp, R.H. Numerical Results from the Combination of Gravimetric and Satellite Data Using the Principles of Least Squares Collocation. Department of Geodetic Science Report No. 200. The Ohio State University, Columbus. March, 1973a.

Rapp, R.H. Results from the Direct Combination of Satellite and Gravimetric Data. Paper presented at the First International Symposium in the Use of Artificial Satellites for Geodesy and Geodynamics. May 14-21, 1973b.

Rapp, R.H. Lectures on Advanced Gravimetric Geodesy. Unpublished Class Notes. The Ohio State University, Columbus. December, 1973c.

Robinson, J.V. Optimum Integration Interval for Use in Orbit Computations with the NWL-9 Gravitational Parameter Set. NWL Technical Report TR-2478. September, 1970.

Schwarz, C.R. Gravity Field Refinement by Satellite to Satellite Doppler Tracking. Department of Geodetic Science Report No. 147. The Ohio State University, Columbus. December, 1970.

Snowden, J.M. and Rapp, R.H. Two Fortran IV Computer Programs for the Combination of Gravimetric and Satellite Data. Department of Geodetic Science Report No. 116. The Ohio State University, Columbus. November, 1968.

Tscherning, C.C. and Rapp, R.H. Closed Covariance Expressions for Gravity Anomalies, Geoid Undulations, and Deflections of the Vertical Implied by Anomaly Degree Variance Models. Department of Geodetic Science Report No. 208. The Ohio State University, Columbus. May, 1974.

Uotila, U.A. Introduction to Adjustment Computations with Matrices. Unpublished Notes. Department of Geodetic Science. The Ohio State University, Columbus. 1967.

Velez, C.E. Local Error Control and Its Effects on the Optimization of Orbital Integration. NASA Technical Note C-4542. June, 1968.

Vonbun, F.O. Geodetic Satellite Mission and Geos-C Spacecraft. Space Research XI, pp. 457-467, Akademie-Verlag, Berlin, 1971.